HITUBES PROJECT

DESIGN AND INTEGRITY ASSESSMENT OF HIGH STRENGTH TUBULAR STRUCTURES FOR EXTREME LOADING CONDITIONS

Deliverables 4.1, 4.2, 4.3 & 4.4

D4.1: Materials and fracture-mechanic properties including loading rate and corrosion
D4.2: Test data on welded tubular connections
D4.3: Performance of advanced post-treatment welding techniques
D4.4: Test data on bolted tubular connections

Authors

Sergio Rivera, Ricardo Alvarez, Ricardo Lezcano
Eva Johansson, Nuria Fuertes
Helena Guvaia, Carlos Maia
Jean-Pierre Jaspart, Jean-François Demonceau, Long Van Hoang, Ly Dong Phuong Lam
Spyros Karamanos , Philip Perdikaris, Aglaia Pournara, Charis Papatheocharis, George Varelis

Contributing Partners

Fundacion ITMA, Spain
Korrosions Och Metallforskningsinstitutet AB, Sweden
Instituto de Soldadura e Qualidade, Portugal
Université de Liège, Belgium
University of Thessaly, Greece

Table of Contents

D4.1 Materials and fracture-mechanic properties including loading rate and corrosion- Deliverable D4.1

D.4.1.1. Materials and fracture-mechanic properties

D.4.1.1.1 Macroscopic examination

Macroscopic examination is used to reveal the macroscopic features of a welded joint, usually by examination of transverse sections. This is done by visual/optical examination of the prepared surface, after etching.

The test specimens were prepared and etched in accordance with EN 1321 on one side, to clearly reveal the fusion line, the heat affected zone (HAZ) and the build up of the runs. The macroscopic examination included the unaffected parent metal and a macro-reproduction (Photo) was taken per procedure test.

The acceptance levels are given in EN 15614-1: a welding procedure is qualified if the imperfections are within the specified limits of quality level B in EN 25817 except for imperfection types as follows: excess weld metal, excess convexity excess throat thickness and excessive penetration for which level C (less stringent than level B) shall apply.
The photo macrographs are presented below:

Figure 4.1.1a Butt welds

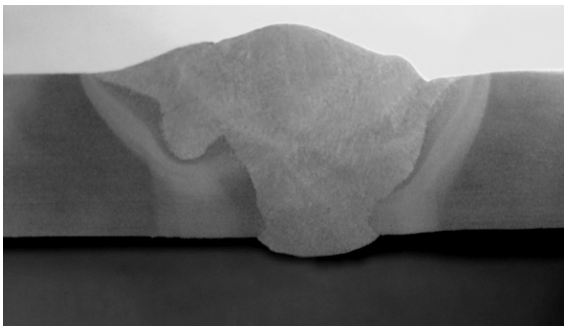

Over matching condition

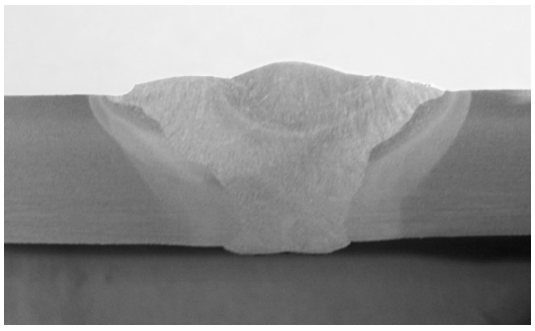

Under matching condition

Figure 4.1.1b X-joint (overmatching)

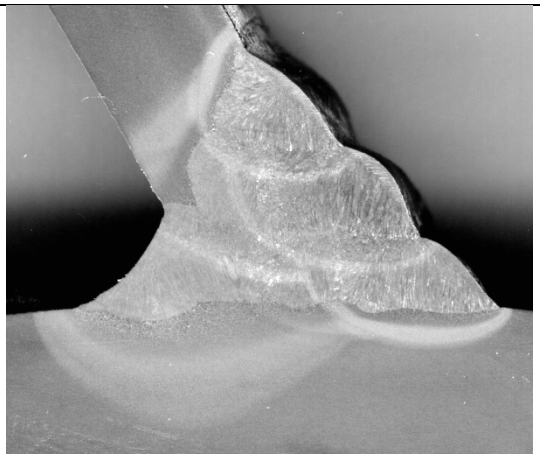

Specimen extracted from location “D”*

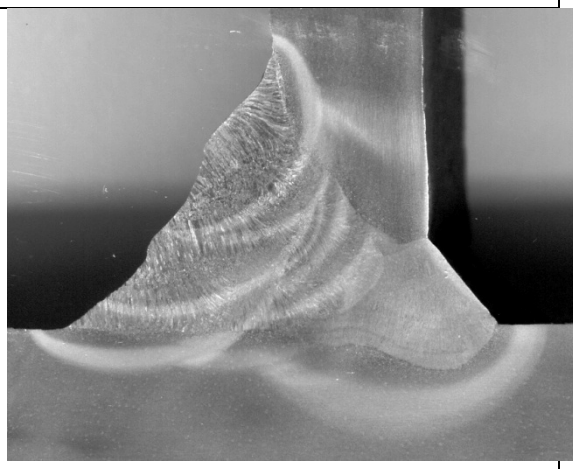

Specimen extracted from location “E”*

Figure 4.1.1c K-joint (overmatching)

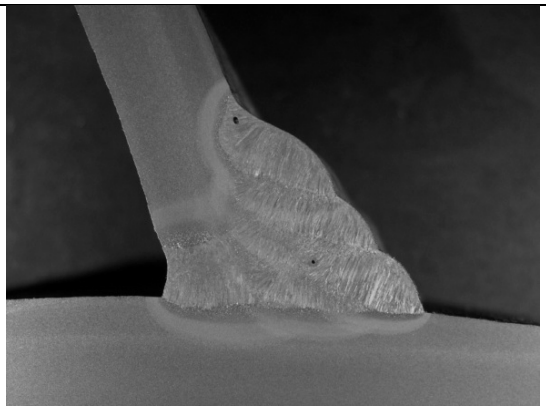

Specimen extracted from location “C”*

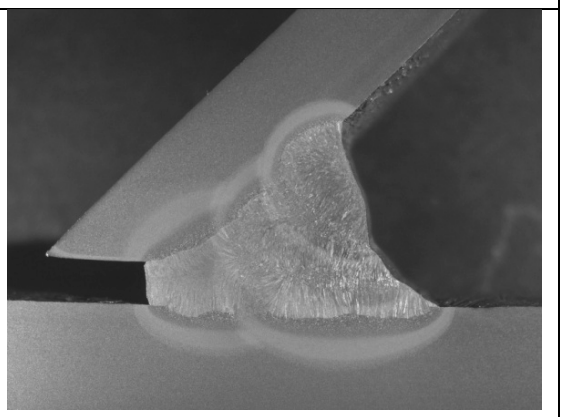

Specimen extracted from location “A”*

*See the Mid-term report page168.

Figure 4.1.1d Flanged connection

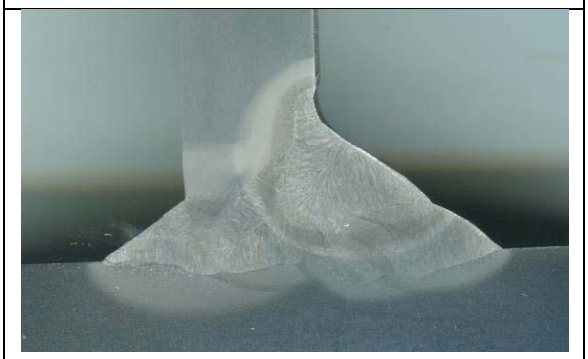

Specimen extracted from location “F”*

* See the Mid-term report page169.

D.4.1.1.2 Hardness tests

Hardness tests are used to define hardened or softened regions due to welding. Vickers hardness testing with a load of HV10 was performed in accordance with EN 1043-1. Hardness measurements were taken in the weld, the heat affected zones and the parent metal in order to evaluate the range of hardness values across the welded joint.

The acceptance levels of hardness are given in EN 15614-1: TS 590 steel is quenched and tempered steel in group 3 according to technical report ISO/TR 15608, so the maximum acceptable hardness value is 450 HV10, in the non-heat treated condition. The hardness test results are shown in the following figures.

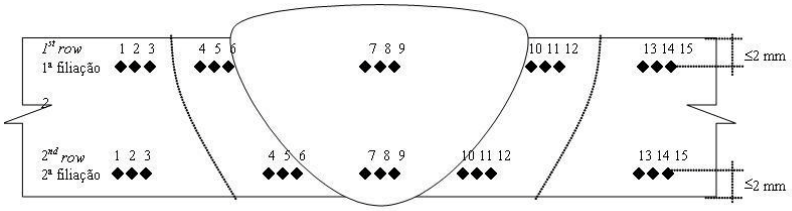

Rows of indentations

Localização *Location*	**Indentação** *Indentation*	**1ª Filiação** *1st row*	**2ª Filiação** *2 nd row*
MB/*PM*	1	306	263
	2	306	269
	3	315	270
ZTA/*HAZ*	4	275	251
	5	297	255
	6	290	260
MF/*WM*	7	319	273
	8	317	281
	9	319	275
ZTA/*HAZ*	10	292	260
	11	271	260
	12	271	255
MB/*PM*	13	302	268
	14	301	263
	15	302	260

HV10 hardness values

Figure 4.1.2a Butt weld overmatching

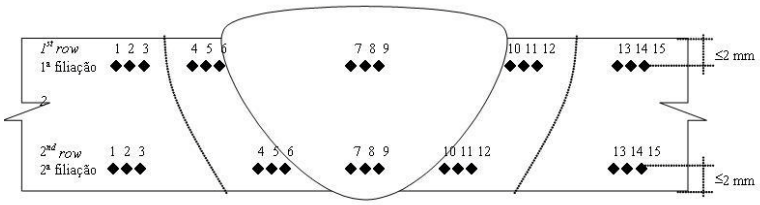

Rows of indentations

Localização *Location*	**Indentação** *Indentation*	**1ª Filiação** *1st row*	**2ª Filiação** *2 nd row*
MB/*PM*	1	299	280
	2	306	276
	3	301	267
ZTA/*HAZ*	4	281	259
	5	284	269
	6	278	263
MF/*WM*	7	308	249
	8	301	254
	9	302	248
ZTA/*HAZ*	10	272	271
	11	267	270
	12	266	264
MB/*PM*	13	284	273
	14	289	271
	15	294	272

HV10 hardness values

Figure 4.1.2b Butt weld undermatching

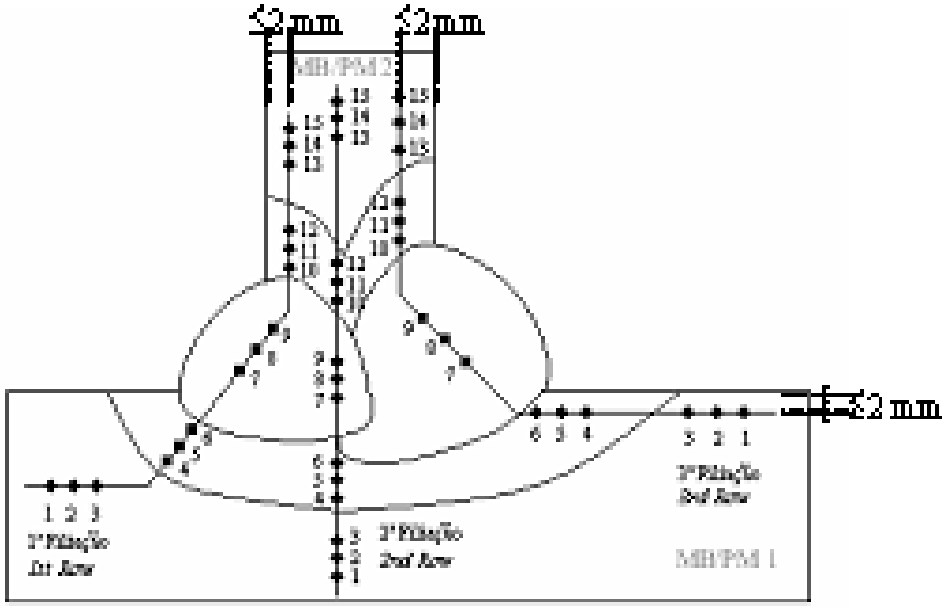

Rows of indentations

Localização *Location*	Indentação *Indentation*	1ª Filiação *1st row*	2ª Filiação *2 nd row*	3ª Filiação *3 rd row*
MB/*PM*	1	313	279	301
	2	305	289	308
	3	309	288	298
ZTA/*HAZ*	4	432	279	275
	5	414	294	258
	6	372	252	253
MF/*WM*	7	423	430	285
	8	412	387	287
	9	416	309	292
ZTA/*HAZ*	10	403	329	316
	11	334	273	320
	12	331	294	305
MB/*PM*	13	297	291	279
	14	301	288	280
	15	298	285	280

HV10 hardness values

Figure 4.1.2c X-joint overmatching (specimen extracted from location ‘E’)

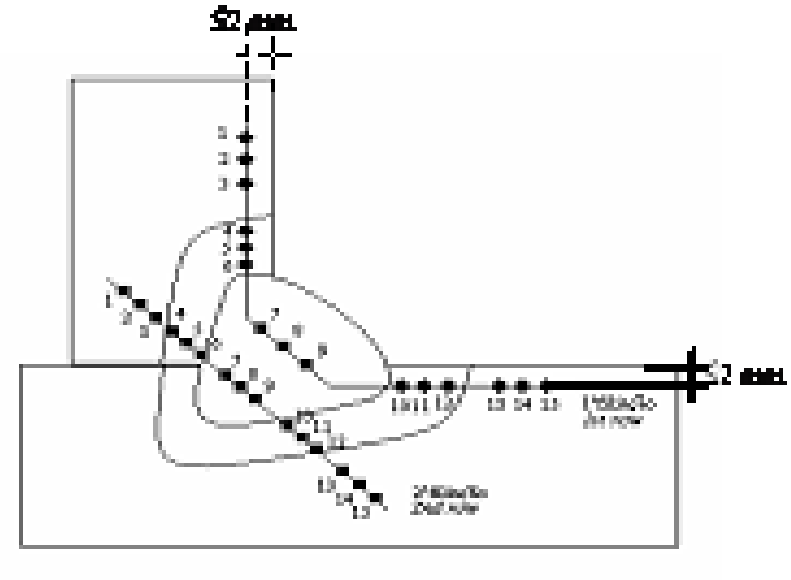

Rows of indentations

Localização *Location*	Indentação *Indentation*	1ª Filiação *1st row*	2ª Filiação *2 nd row*
MB/*PM*	1	280	273
	2	285	274
	3	294	278
ZTA/*HAZ*	4	331	271
	5	346	288
	6	350	281
MF/*WM*	7	381	284
	8	379	283
	9	368	290
ZTA/*HAZ*	10	320	313
	11	327	309
	12	277	262
MB/*PM*	13	305	269
	14	302	277
	15	304	283

HV10 hardness values

Figure 4.1.2d K-joint overmatching (specimen extracted from location ‘A’)

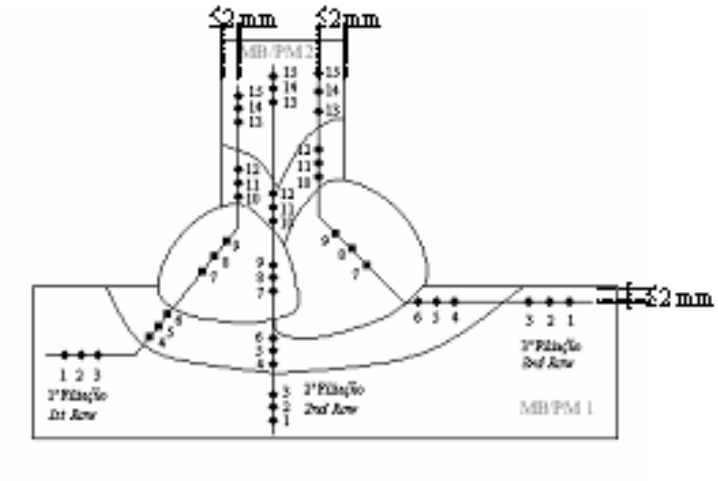

Rows of indentations

Localização *Location*	Indentação *Indentation*	1ª Filiação *1st row*	2ª Filiação *2 nd row*	3ª Filiação *3 rd row*
MB/*PM*	1	293	279	330
	2	289	286	326
	3	283	286	329
ZTA/*HAZ*	4	266	289	297
	5	277	292	331
	6	278	337	334
MF/*WM*	7	221	231	219
	8	221	237	213
	9	227	238	204
ZTA/*HAZ*	10	258	205	298
	11	265	201	293
	12	263	192	285
MB/*PM*	13	171	185	157
	14	170	179	160
	15	171	174	156

HV10 hardness values

Figure 4.1.2e Flanged connection (specimen extracted from location ‘F’)

Both macroscopic examination and hardness tests have been found to comply with EN 15614-1, which specifies how a welding specification is qualified by welding procedure tests.

D.4.1.1.3 Fatigue tests on the welds of the base metal

These tests were performed in order to get the fatigue curve for the welds in the mismatching conditions. The specimen geometry is described in Figure 4.1.3.

TEST, MACHINE AND SPECIMEN DATA	Material designation: TS590 overmatching, TS590 undermatching, S355 overmatching, S355 undermatching.
	Machining: Following annex I of testing standard ASTM E466. The specimen edges have been mechanically rounded by hand polishing to a radius of 3 mm.
	Type of machine: Servo hydraulic testing machine INSTRON 8504.
	Software: INSTRON FASTRACK 2 SAX Single Axis.
	Waveform: Sine — Load ratio: R=0.1 — Run-out: $2E^6$cycles
	Test temperature: 23ºC — Specimens tested: 12 per condition, except S355 overmatching (11 specimens)
	Failure criteria: Total rupture of the specimen

Nominal dimensions of reduced sections (not considering weld over thickness)

Width – 25.00 mm

Thickness – 12.50 mm

Figure 4.1.3: Specimen Geometry

The fatigue endurance limit, that is the value of stress for an estimated life of $2 \cdot 10^6$ cycles was calculated for each base material and compared with the values for the mismatched welds. The results can be seen in Table 4.1.1 and Figure 4.1.4.

Table 4.1.1 Fatigue endurance limit of base materials and welds

	Fatigue endurance limit (Stress at $2 \cdot 10^6$ cycles)
TS590 base material	693
TS590 overmatching	98
TS590 undermatching	135
S355 base material	432
S355 overmatching	167
S355 undermatching	116

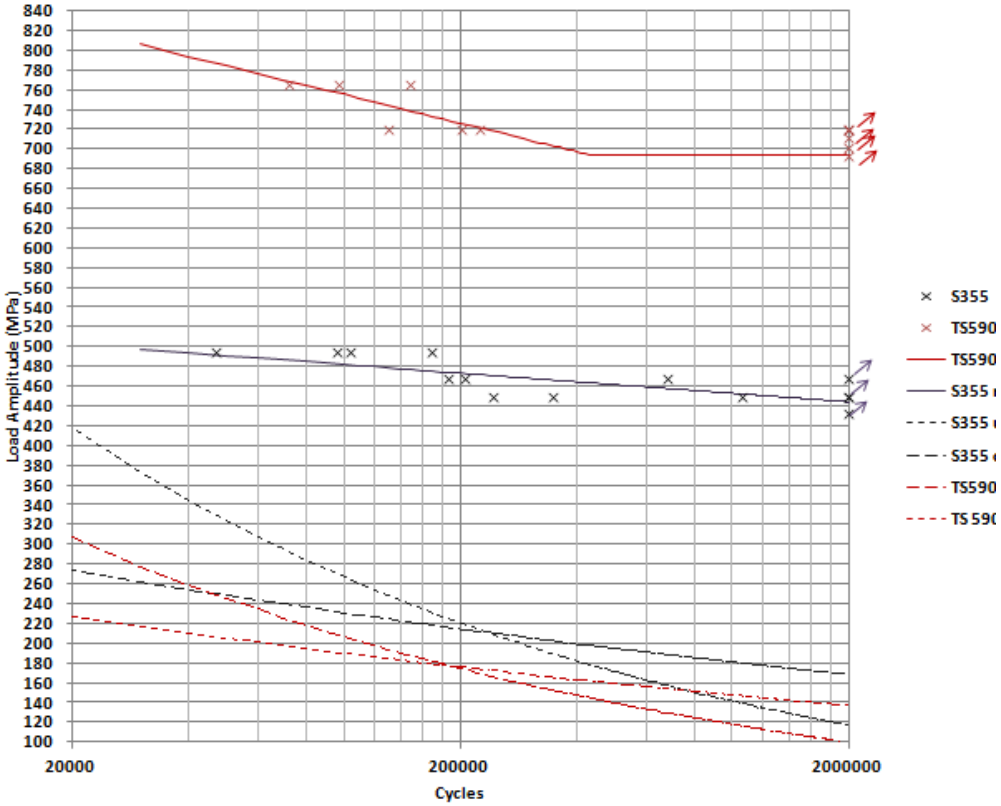

Figure 4.1.4. Comparison of the S-N curves of base material and mismatched welds.

D.4.1.1.4 Tensile tests at high rate loading

The tensile test behavior of the both base materials (TS590 and S355) was evaluated at different strain rates. Four different levels were selected according to the information reported by the coordinator of the project (10^0 s^{-1}, 10^{-1} s^{-1}, 10^{-2} s^{-1}, 10^{-3} s^{-1}). The tests were performed in cylindrical specimens with a nominal diameter of 5 mm and a reduced length section of 35 mm. A clip-on gage extensometer of 25 mm of initial length and 12.5 mm of spam was placed. The equipment used was an Instron 8801 servo-hydraulic testing machine with a 100 kN capacity load cell. The results are shown in the Figures 4.1.5 and 4.1.6 and as a resume in the Table 4.1.2. In the tests performed to the two values of higher rate (10^0 s^{-1}, 10^{-1} s^{-1}), an initial transition state occurs in the machine up to the nominal rate is reached. This happens in a short time of a few milliseconds, but it is enough to reach the yield stress of the material. This phenomenon can be seen in the Figure 4.1.7. A recalculation of the values of strain rate is included in the results table. It must be noted that this corrected value should be taken into account instead of the nominal value in the calibration of the models for this rates.

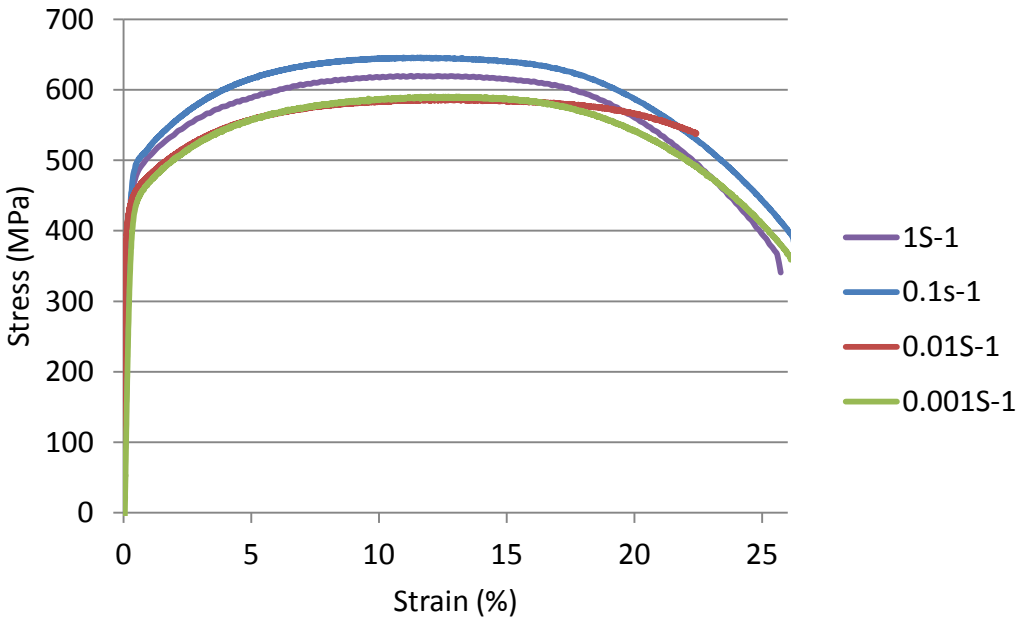

Figure 4.1.5. Stress-Strain behavior of S355 base material

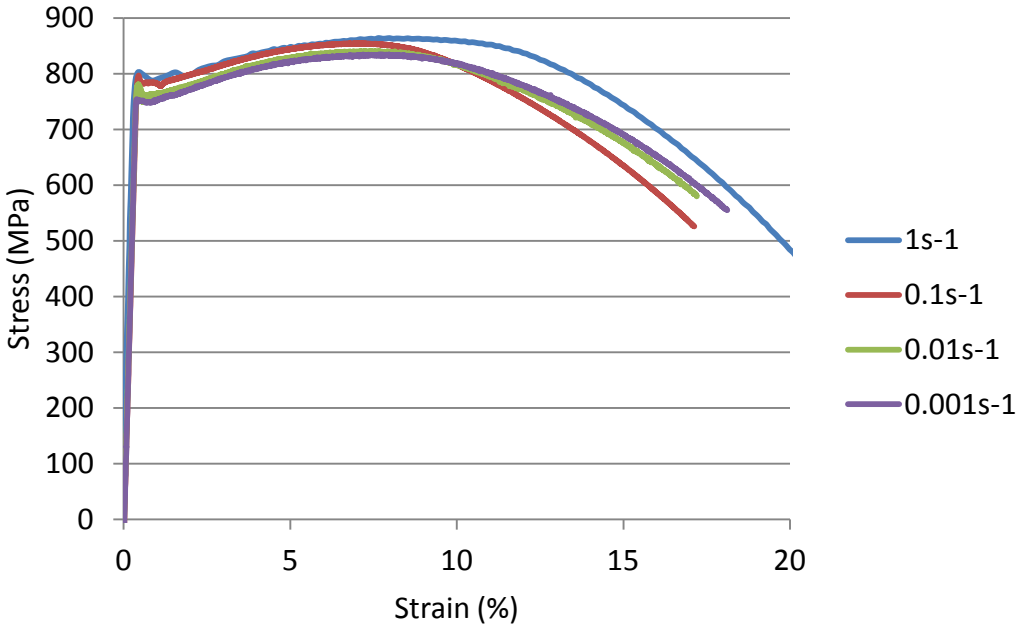

Figure 4.1.6. Stress-Strain behavior of TS590 base material

Table 4.1.2 Tensile test data

TS590

Yield stress rate (s^{-1})	Nominal rate (s^{-1})	Yield stress (MPa)	Tensile strength (MPa)	Elongation (%)
0.18	1	803	864	20.5
0.05	0.1	796	854	18
0.01	0.01	781	840	19.5
0.001	0.001	745	835	19

S355

Yield stress rate (s^{-1})	Nominal rate (s^{-1})	Yield stress (MPa)	Tensile strenght (MPa)	Elongation (%)
0.28	1	475	620	26
0.06	0.1	482	645	26.5
0.01	0.01	440	586	29
0.001	0.001	425	590	26

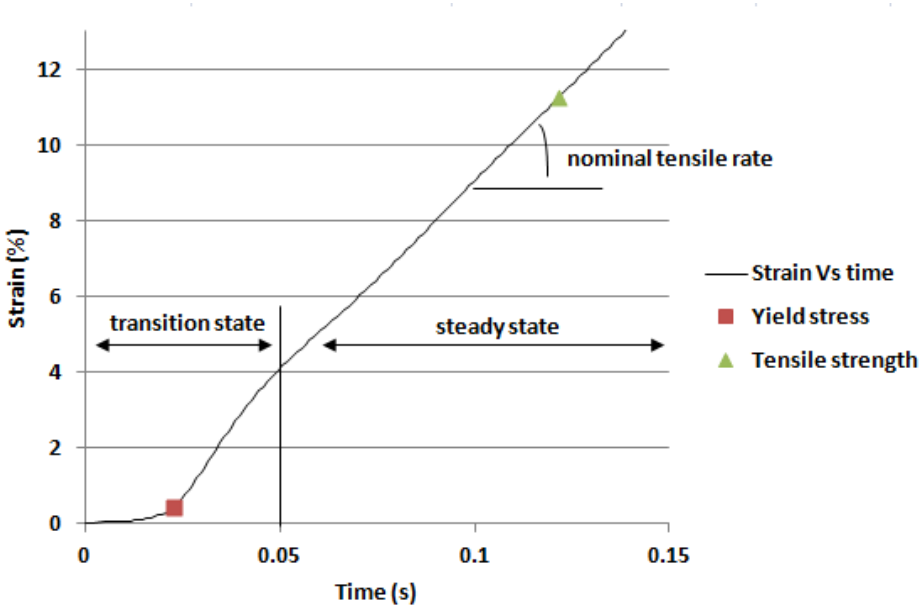

Figure 4.1.7. Strain rate during the tensile zone (transition state) and rest of the test (steady state)

The fatigue curves corresponding to the welds penalize the fatigue endurance limit with respect to the fatigue curves of the base material. This can be due to the geometry of the specimen (cylindrical in the base material and prismatic in the welds) and specially to the welding condition, as it was noted in the last report.

D.4.1.2 Corrosion tests on base metal welds

D.4.1.2.1 Corrosion rate measurements

General corrosion is a type of corrosion that is more or less uniformly distributed over the entire exposed metal surface. General corrosion proceeds at approximately the same corrosion rate over the exposed metal surface. Carbon steels corrode uniformly when exposed to open offshore atmospheres and natural sea waters, leading to the rusty appearance. The corrosion protection occurs by the formation of passive iron oxide (γ-Fe2O3 and Fe3O4) surface layers.

Two different materials were tested, TS590 and S355. The specimens were cut from the weld metal and base metal. Prior to the tests, the samples were wet ground with 600-grade SiC paper and rinsed with de-ionized water and ethanol, dried and exposed to air for approximately 24 hours. The exposed surface area of each specimen was approximately 100 mm^2. The test was performed on duplicate samples, a total of 24 samples were tested.

Average of the corrosion rates are summarized in Table 4.1.3.

Table 4.1.3 Average of corrosion rates [mm/year] for TS590 and S355 base metal and weld metal.

	Environment	Air or N_2 bubble	Average corrosion rate **(mm/year)**	$\pm\frac{1}{n}\sum\left\|x-\bar{x}\right\|$
TS590	3.5% NaCl	Air bubble	0.14	0.018
TS590	3.5% NaCl	N_2 bubble	0.105	0.033
TS590	1% NaCl	N_2 bubble	0.06	0.007
S355	3.5% NaCl	Air bubble	0.168	0.01
S355	3.5% NaCl	N_2 bubble	0.11	0.034
S355	1% NaCl	N_2 bubble	0.085	0.020
TS590 weld	3.5% NaCl	Air bubble	0.18	0.045
TS590 weld	3.5% NaCl	N_2 bubble	0.13	0.058
TS590 weld	1% NaCl	N_2 bubble	0.12	0.078
S355 weld	3.5% NaCl	Air bubble	0.24	0.034
S355 weld	3.5% NaCl	N_2 bubble	0.20	0.038
S355 weld	1% NaCl	N_2 bubble	0.09	0.06

The corrosion rates of the TS590 and S355 weld metal in aerated and de-aerated sodium chloride solution with different NaCl concentrations at room temperature (~ 25 ºC) are shown in Figure 4.1.8. No apparent crevice or pitting corrosion was observed on the surface. The corrosion rate of the two steel grades, except for the weld, decreased when de-aerated solution was used.

The corrosion rate of S355 for base and weld metal is higher compared with the TS590 grade, particularly in presence of high concentration of the NaCl and de-oxygenated conditions. Slightly higher corrosion rate was achieved in 3.5 wt% NaCl compared to 1 wt.% NaCl. Furthermore, maximum corrosion rates for both materials were obtained in the presence of the oxygen. In 1 wt% NaCl solution, in the absence of oxygen, the corrosion rate of the weld metal of TS590 steel grade was higher than that of S355 weld, whereas the opposite was achieved for the base metal. However, these differences are not significant due to a large spread in data.

The corrosion rates for TS590 and S355 both for base and weld metal in aerated 3.5 wt% NaCl solution were higher than those obtained from tested specimens in de-aerated 3.5 wt% NaCl solution. In general the weld metal had higher corrosion rate compared to the base metal.

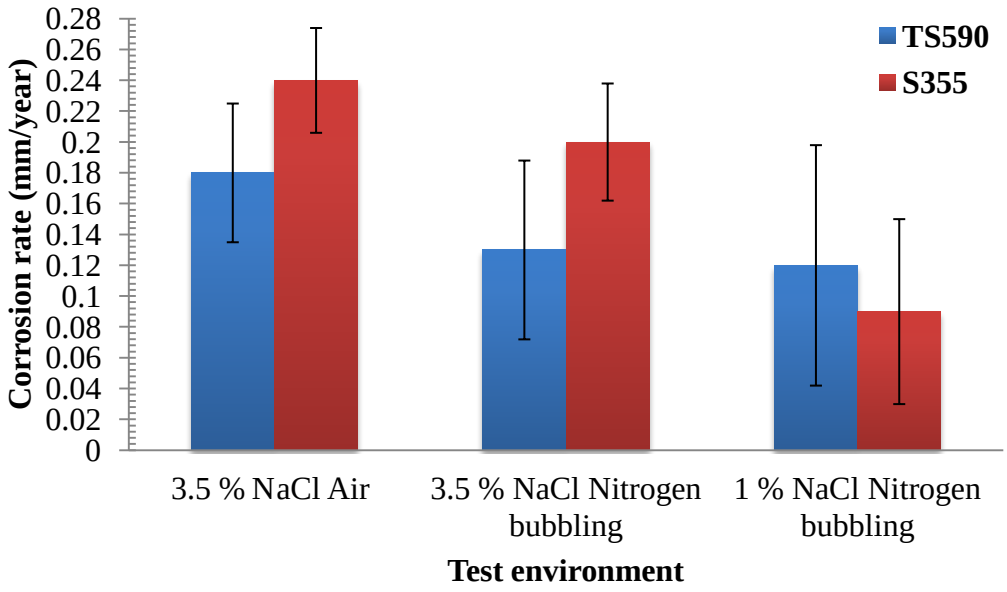

Figure 4.1.8 Corrosion rate of weld metal of TS590 and S355 in various corrosive environments

The results of this study show that the corrosion rate of TS590 and S355 is dependent on Cl^- concentration and oxygen content dissolved in the solution. Dissolved salts, such as NaCl (Na^+ and Cl^- ions), increase the solution conductivity and thus, enhance the corrosion rate of both base and weld metal of TS950 and S355 steel grade, see Figure 4.1.8. Due to the lack of passive layer, high strength low-alloyed steels are highly susceptible to uniform corrosion. The corrosion products (i.e. $Fe(OH)_2$) formed on the metal surface are porous, and thus, Cl^- ions can easily penetrate it and reach the bare surface of the sample. The chloride ions affect the metal surface uniformly and thus the metal uniformly corrodes.

Oxygen content dissolved in the solution also increases the corrosion rate of the steels. Higher corrosion rates (lowest R_P) were observed for the specimens tested in aerated condition compared with those tested in purged solutions with N_2-bubbling.

To conclude, base and weld metal of TS590 had a higher corrosion resistance compared to the corresponding of S355 in 3.5 wt% NaCl.

D.4.1.2.2 Slow strain rate tests (SSRT)

Samples from TS590 and S355 were longitudinally cut from weld metal, base metal and HAZ region. The SSRT specimens, with 3.00 mm in gauge diameter and 31 mm in gauge length (± 0.05) were machined from the two different kinds of weld configurations (i.e. K and X-joint). Figure 4.1.9 shows a photo of a SSRT tensile specimen. The length direction of the tensile sample was parallel to the longitudinal of the pipe. The samples' surfaces were abraded with 600-grith SiC abrasive paper.

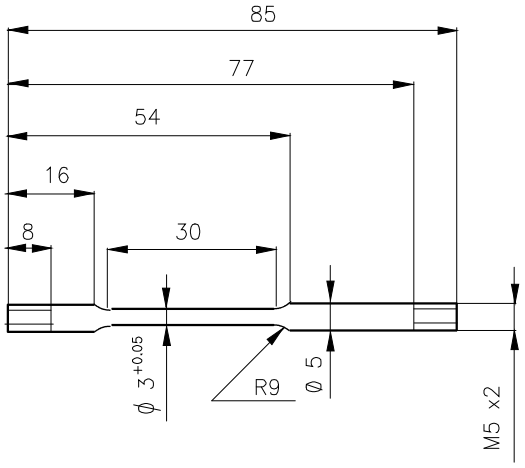

Figure 4.1.9 Dimensions of SSRT tensile specimen

The test results as stress-strain diagram are shown in Figures 4.1.10a-g.

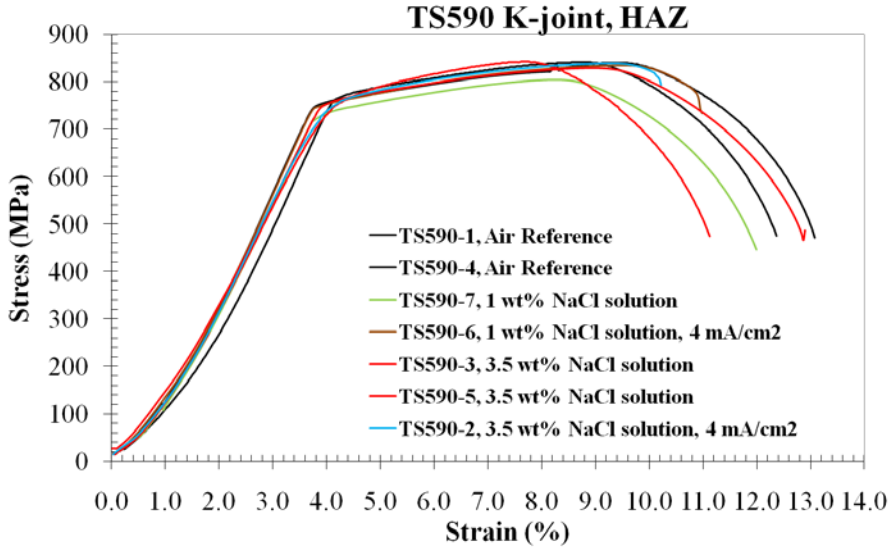

Figure A2.10a. Stress vs. strain curves of HAZ TS590 K-joint after SSRT tests performed in air, 1 wt% and 3.5 wt% NaCl solutions under OCP and cathodic polarization

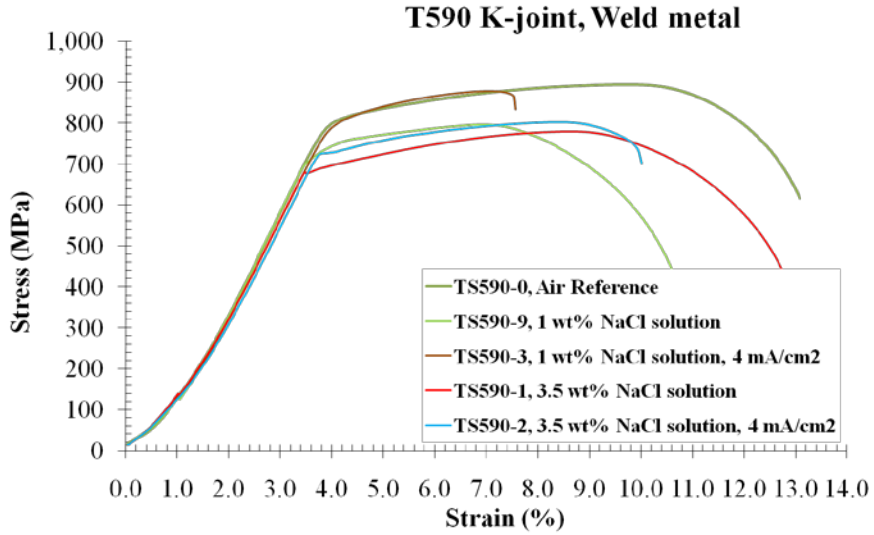

Figure 4.1.10b. Stress vs. strain curves of weld metal TS590 K-joint after SSRT tests performed in air, 1 wt% and 3.5 wt% NaCl solutions under OCP and cathodic polarization

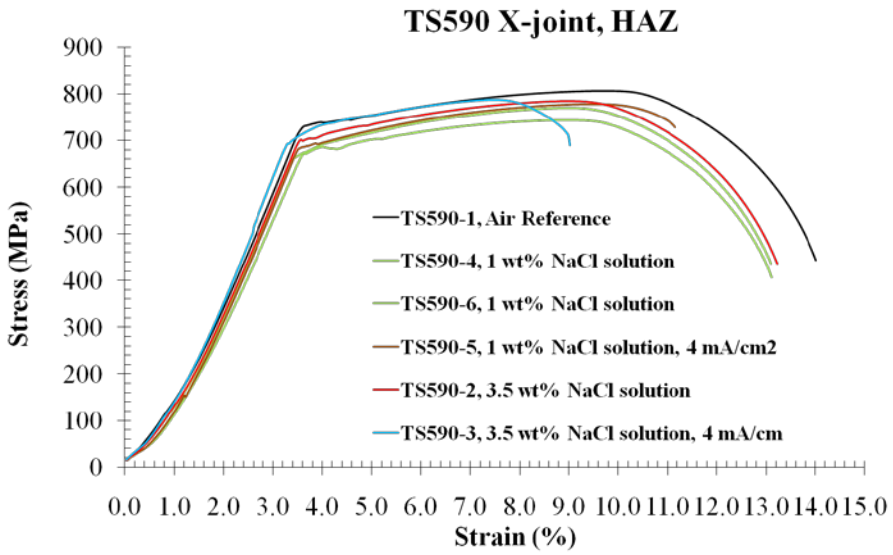

Figure 4.1.10c. Stress vs. strain curves of HAZ TS590 X-joint after SSRT tests performed in air, 1 wt% and 3.5 wt% NaCl solutions under OCP and cathodic polarization

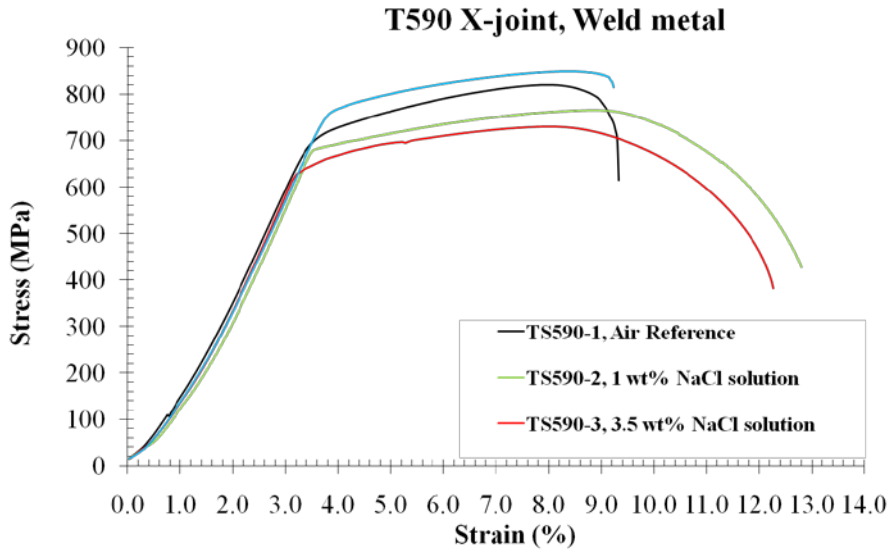

Figure 4.1.10d. Stress vs. strain curves of weld metal TS590 X-joint after SSRT tests performed in air, 1 wt% and 3.5 wt% NaCl solutions under OCP and cathodic polarization

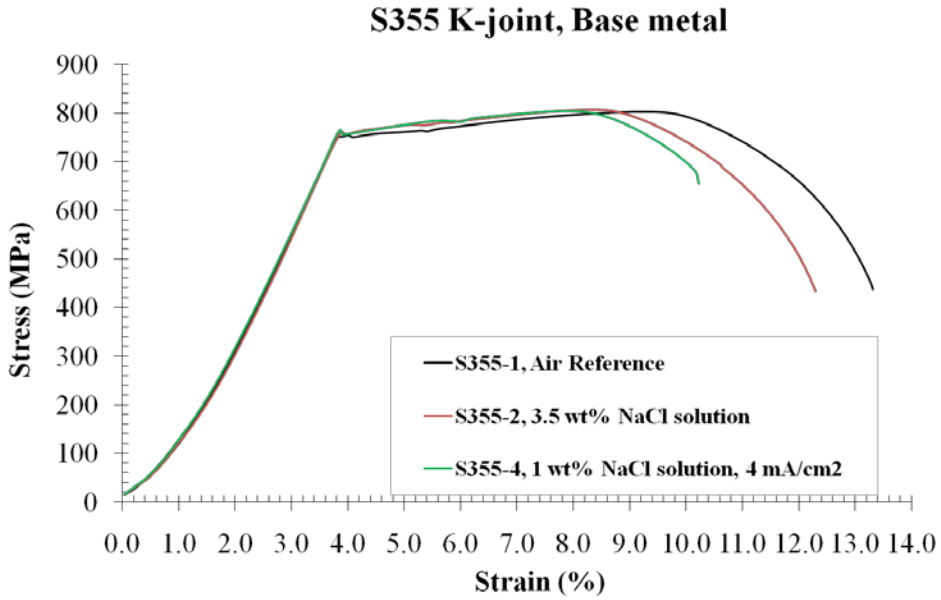

Figure 4.1.10e. Stress vs. strain curves of base metal S355 K-joint after SSRT tests performed in air, 1 wt% and 3.5 wt% NaCl solutions under OCP and cathodic polarization

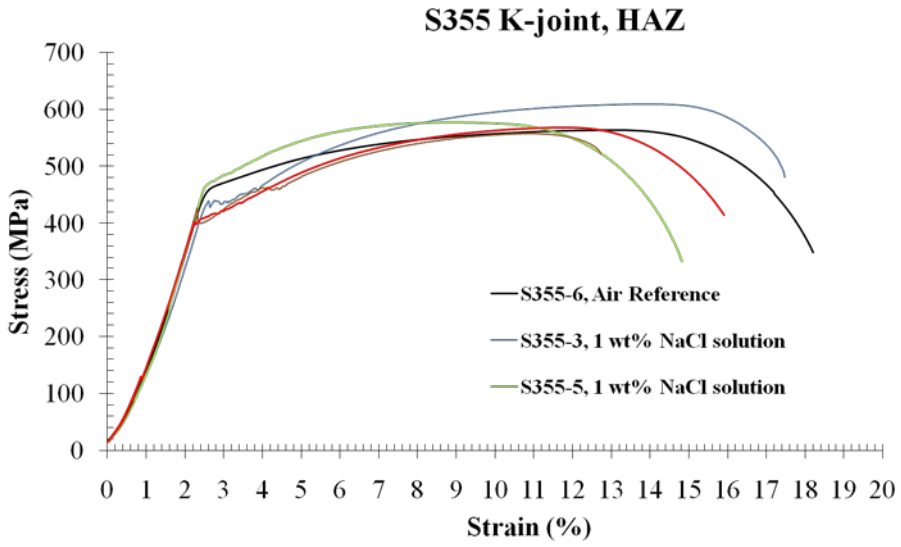

Figure 4.1.10f. Stress vs. strain curves of HAZ S355 K-joint after SSRT tests performed in air, 1 wt% and 3.5 wt% NaCl solutions under OCP and cathodic polarization

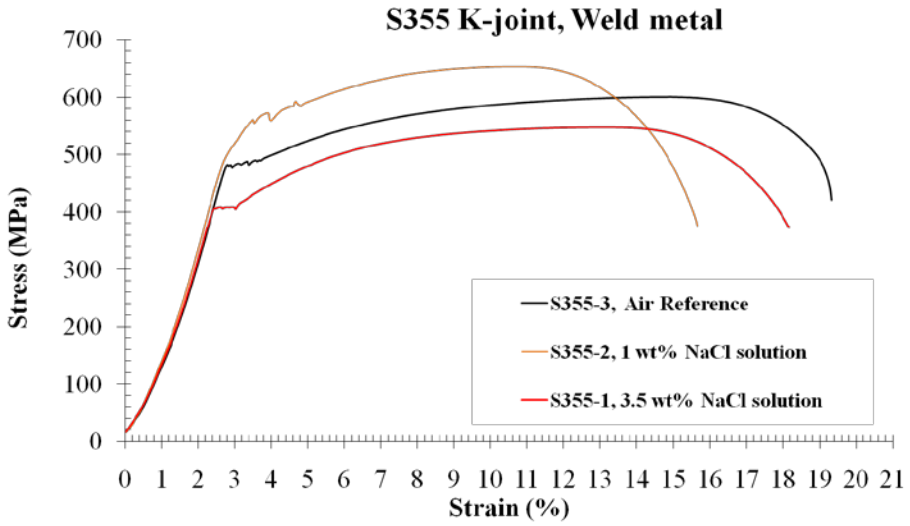

Figure 4.1.10g. Stress vs. strain curves of weld metal S355 K-joint after SSRT tests performed in air, 1 wt% and 3.5 wt% NaCl solutions under OCP and cathodic polarization

Mechanical properties such as EL%, yield stress (YS) and ultimate tensile strength (UTS) were calculated from the stress vs. strain curves and the results are presented in the following tables.

Table 4.1.4a. Mechanical properties of TS590, S355 and their welded joints

Steel grade	Test environment	1 wt% NaCl				
	samples	YS (MPa)	UTS (MPa)	TTF(hr)	EL (%)	RA (%)
TS590 K-joint	Base metal	770	812	35.38	10.35	78.85
	HAZ	740	804	32.08	9.40	75.45
	Weld metal	745	796	29.42	8.20	74.45
TS590 X-joint	HAZ	688	757	36.38	10.65	76.64
	Weld metal	700	765	35.58	10.50	73.40
S355 K-joint	Base metal	-	-	-	-	-
	HAZ	455	653	43.50	13.50	75.10
	Weld metal	458	593	44.88	13.30	71.50

Table 4.1.4b. Mechanical properties of TS590, S355 and their welded joints

Steel grade	Test environment	1 wt% NaCl 4 mA/cm^2				
	samples	YS (MPa)	UTS (MPa)	TTF(hr)	EL (%)	RA (%)
TS590 K-joint	Base metal	755	804	29.83	6.80	38.29
	HAZ	760	834	30.50	7.80	22.81
	Weld metal	820	877	21.00	3.30	15.26
TS590 X-joint	HAZ	695	778	31.00	7.20	32.01
	Weld metal	*	*	*	*	*
S355 K-joint	Base metal	765	803	28.42	6.60	66.74
	HAZ	430	558	35.33	9.20	36.48
	Weld metal	*	*	*	*	*

*No measurements: Not possible to make specimens due to curvature of joints

Table 4.1.4c. Mechanical properties of TS590, S355 and their welded joints

Steel grade	Test environment	3.5 wt% NaCl				
	samples	YS (MPa)	UTS (MPa)	TTF(hr)	EL (%)	RA (%)
TS590 K-joint	Base metal	780	822	35.17	10.00	76.31
	HAZ	770	835	33.58	9.25	74.05
	Weld metal	690	780	35.42	10.30	72.23
TS590 X-joint	HAZ	710	784	36.75	10.80	77.40
	Weld metal	670	731	34.08	10.00	75.41
S355 K-joint	Base metal	765	807	34.17	9.10	76.73
	HAZ	465	568	44.17	13.20	72.98
	Weld metal	410	547	50.50	14.60	65.99

Table 4.1.4d. Mechanical properties of TS590, S355 and their welded joints

Steel grade	Test environment	3.5 wt% NaCl 4 mA/cm^2				
	samples	YS (MPa)	UTS (MPa)	TTF(hr)	EL (%)	RA (%)
TS590 K-joint	Base metal	778	822	28.04	6.35	34.78
	HAZ	775	838	28.42	5.90	28.41
	Weld metal	730	801	27.83	6.30	25.11
TS590 X-joint	HAZ	730	788	25.08	5.30	38.33
	Weld metal	775	849	25.67	5.10	26.09
S355 K-joint	Base metal	-	-	-	-	-
	HAZ	*	*	*	*	*
	Weld metal	*	*	*	*	*

*No measurements: Not possible to make specimens due to curvature of joints

After SSRT, the side view images, reduction of area and time to failure were investigated in order to characterise different modes of fracture.

D.4.1.2.3 TS590 base metal and weld

Photos of the fractures of the cracked specimens of HAZ and weld metal of TS590 steel tested in different environments are shown in Figures 4.1.11a-b. It is clear that the materials tested in air, 1 wt% and 3.5 wt% NaCl solution under free corrosion potential almost showed the same behaviour. In other word, the fracture surface of samples consisted of a typical ductile behaviour with a cup-and-cone configuration. Considerable necking was seen for the samples tested in air, 1 wt% and 3.5 wt% NaCl solutions under free corrosion potential condition accompanied with high reduction in area (RA%). The samples tested under cathodic polarisation with 4 mA/cm^2 of current density did not show any non-uniform plastic deformation after the necking point. Accordingly, the brittle fractures appeared after the SSRT tests.

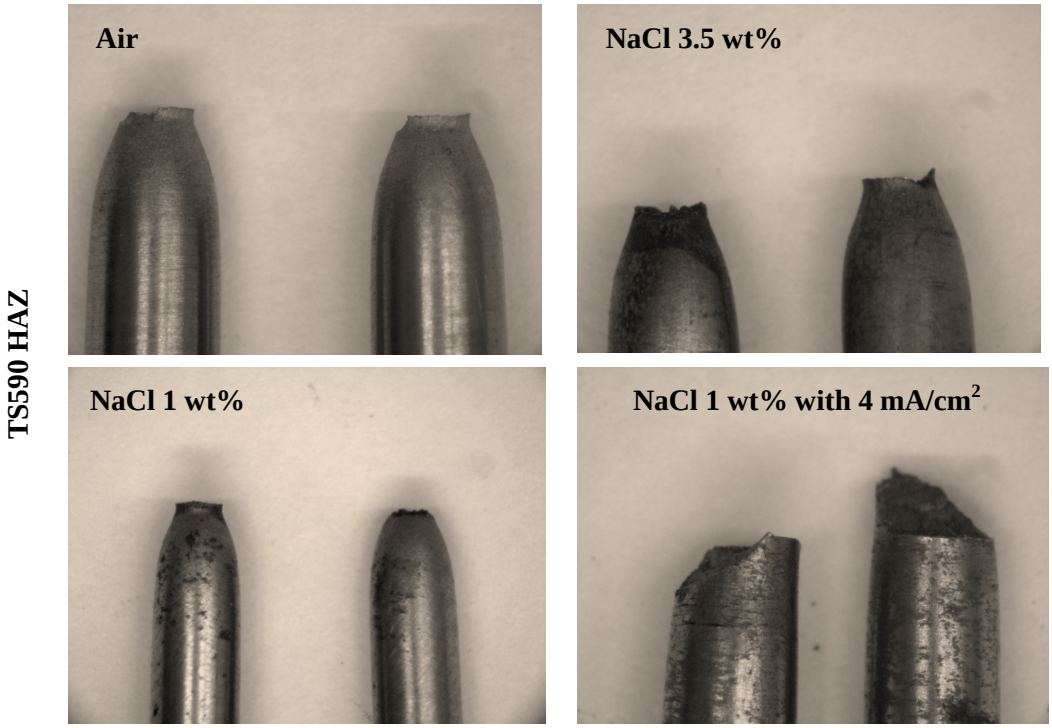

Figure 4.1.11a. Fractography corresponding to TS590 HAZ tested in Air; 3.5 wt% NaCl (OCP); 1 wt% NaCl (OCP) and 1 wt% NaCl under cathodic protection

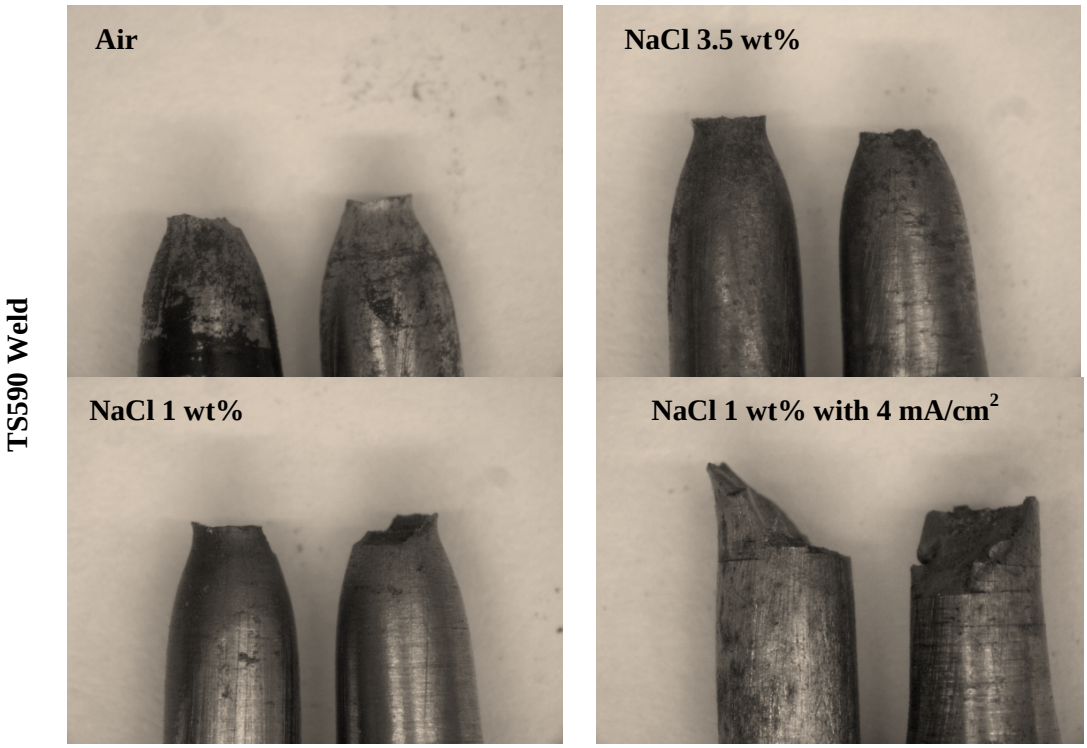

Figure 4.1.11b. Fractography corresponding to TS590 weld metal tested in Air; 3.5 wt% NaCl (OCP); 1 wt% NaCl (OCP) and 1 wt% NaCl under cathodic protection

D.4.1.2.3.1 K-joint

D.4.1.2.3.1.1 Reduction in area

Figure 4.1.12 shows the RA% of base steel, welded metal and HAZ for TS590 after SSRT testing under open circuit potential condition. The RA% of the base metal for fractured samples in air, 1 wt% and 3.5 wt% NaCl were measured to be 75.7%, 78.9% and 76.3% respectively, which was larger than all RA%

achieved with HAZ and weld metal. The results showed no significant different between the tested samples in the different environments.

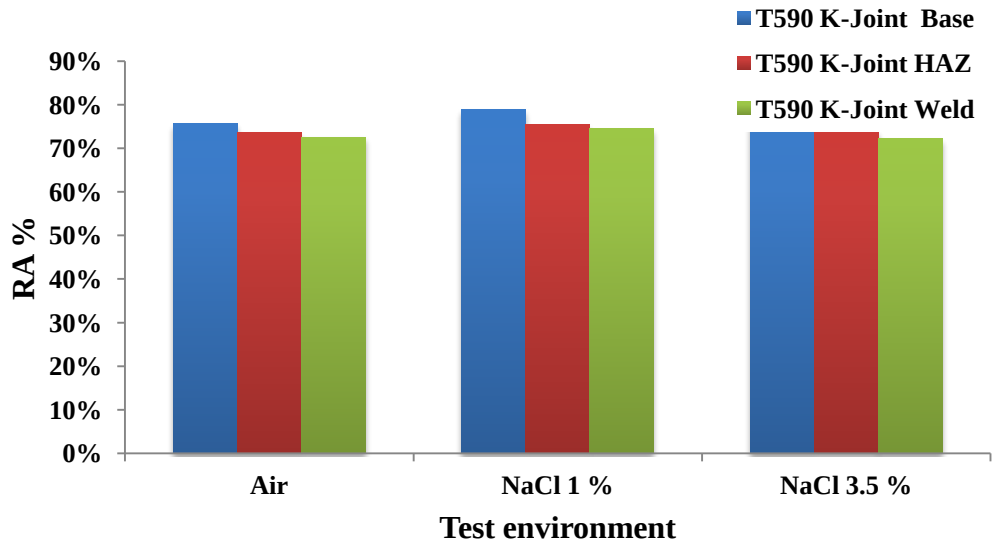

Figure 4.1.12. RA% of base steel, welded metal and HAZ of TS590 K-joint pipeline steel

Figure 4.1.13 shows the RA% of tested TS590 steel grade in air, 1 wt% and 3.5 wt% NaCl solutions with cathodic polarisation of 4 mA/cm^2. The loss of RA% was as high as 38 % for base metal, 23% for HAZ and 15% for weld metal. The results show that when cathodic polarisation is applied, the weld metal and HAZ have about the same brittle sensitivity in 1 wt% NaCl solution while the base metal had a higher RA%, and thus, a better resistance to hydrogen embrittlement and a more ductile fracture. Overall, it can be said that the weld metal revealed the highest susceptibility to hydrogen assisted stress corrosion cracking. Although further increase of NaCl increases the RA% for weld metal and HAZ and to some extent decreases for base metal. It indicates that the HAZ and weld metal in 1 wt% NaCl solution showed more susceptibility to hydrogen embrittlement compared to 3.5 wt% NaCl solution.

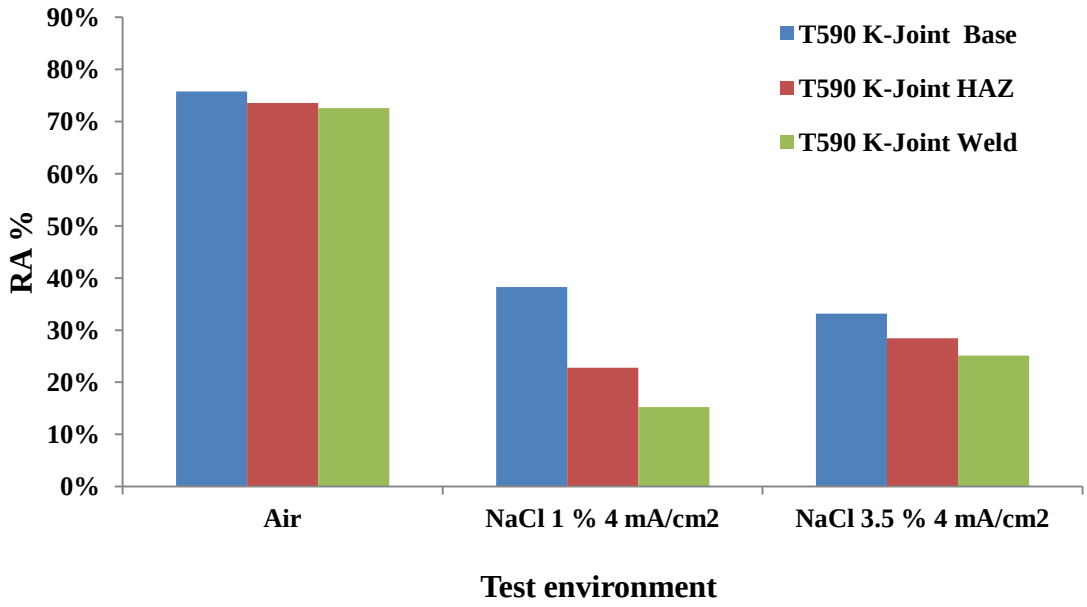

Figure 4.1.13. RA% of polarized base steel, welded metal and HAZ TS590 K-joint pipeline steel using 4 mA/cm^2 current density during SSRT testing

D.4.1.2.3.1.2 Time to failure

The time to failure can also be taken into account as a measure of susceptibility to SCC. Figure 4.1.14 clarifies the relative time to failure vs. test environment of TS590 K-joint of base metal, HAZ and weld metal tested specimens, in two different types of sodium chloride solution under free corrosion potential and applied cathodic polarisation.

Good correlation was observed between time to failure, relative hydrogen degradation and SCC parameters. In other words, the failed specimens under cathodic polarisation showed significant decrease in time to failure. It is clearly observed that the weld metal showed more susceptibility to SCC comparing to base steel and HAZ. However, the time to failure is longer for HAZ and weld in 3.5 wt% NaCl solution under free potential than in 1 wt% NaCl solution which is difficult to explain.

The tests under cathodic polarisation with applied 4 mA/cm^2, revealed that the time to failure of steel and weld severely decreased in 1 wt% NaCl and 3.5 wt% water solution compared to free potential tests. The weld metal susceptibility to HE tested in 3.5 wt% NaCl solution using 4 mA/cm^2 current density decreased compared to tested samples in 1 wt% NaCl solution. A large decrease (i.e. ~ 50%) observed for relative time to failure of weld metal tested in 1 wt% NaCl solution confirmed this claim.

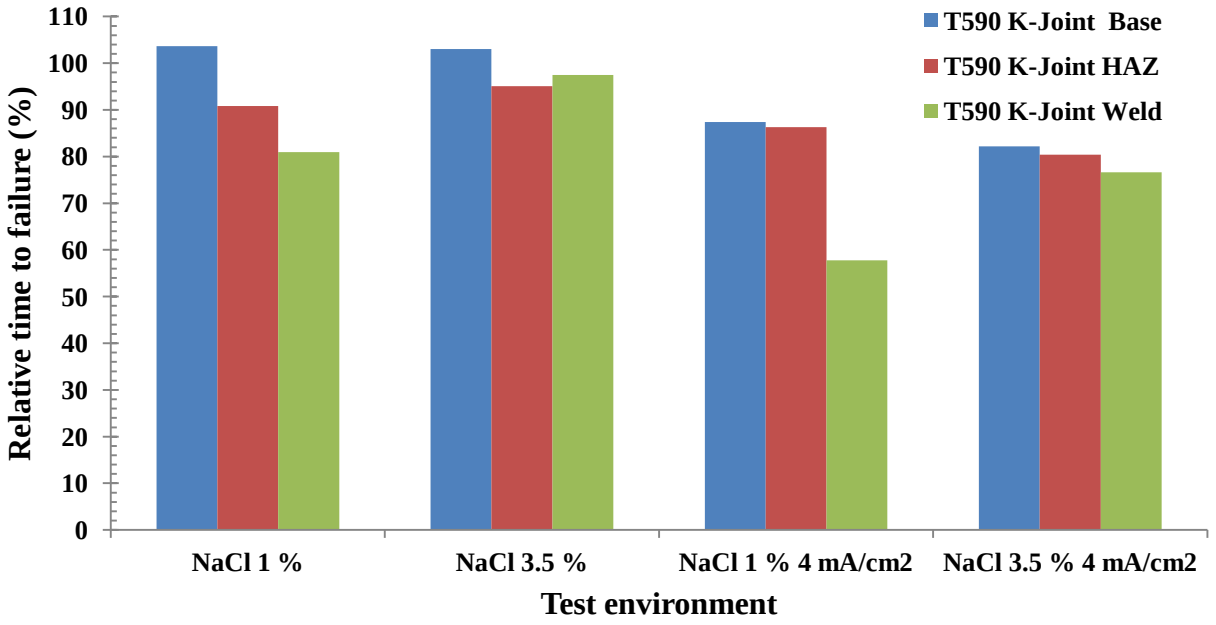

Figure 4.1.14. Relative time to failure vs. test solution of TS590 K-joint under free potential and cathodic polarization

D.4.1.2.3.2 X-joint

D.4.1.2.3.2.1 Reduction in area

After SSRT, large reduction in cross-sectional of area was observed for the weld's specimen tested in air, as shown in Figure 4.1.15. It can be clearly seen that the corrosive aqueous solution with 1 wt% and 3.5 wt% sodium chloride solution had no effective impact on the materials susceptibility to SCC for base metal and HAZ. However, it seems that the obtained result from weld metal tested in air is not logical.

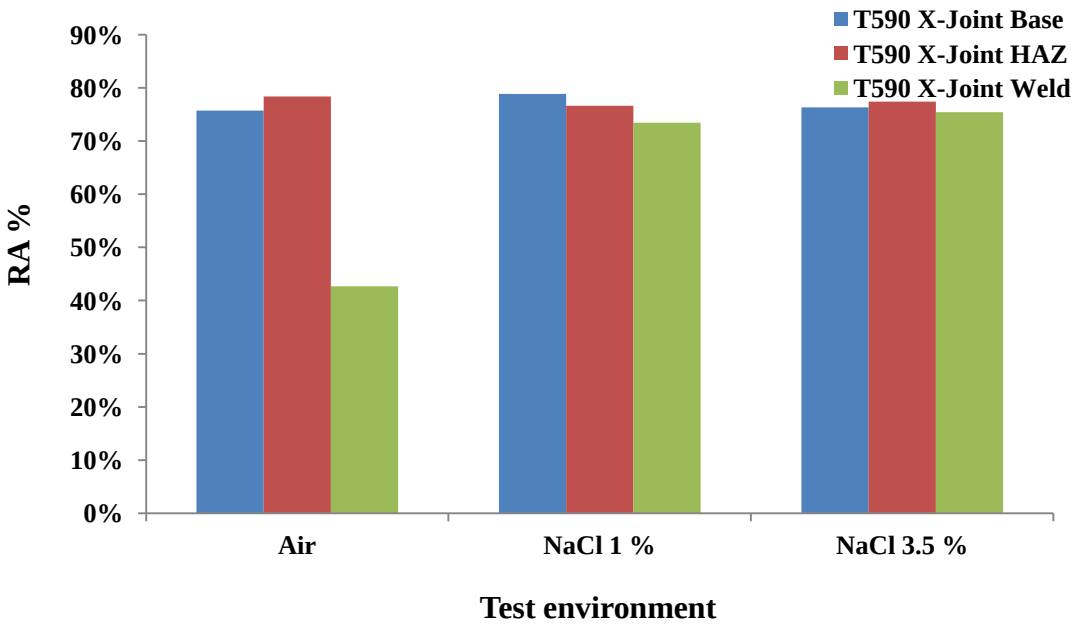

Figure 4.1.15. RA% of base steel, welded metal and HAZ of TS590 X-joint pipeline steel

The measured RA%-values in different sodium chloride concentration solution under cathodic polarisation with 4 mA/cm^2 current density are shown in Figure 4.1.16 It is obvious that the cathodic polarisation drastically decrease the reduction in area of all tested samples prepared from base metal and its welded joint. Based on the obtained results, the minimum RA% among the tested samples was observed for weld metal. It indicates that the weld metal is more susceptible to SCC (i.e. hydrogen embrittlement) compare to the base steel and HAZ.

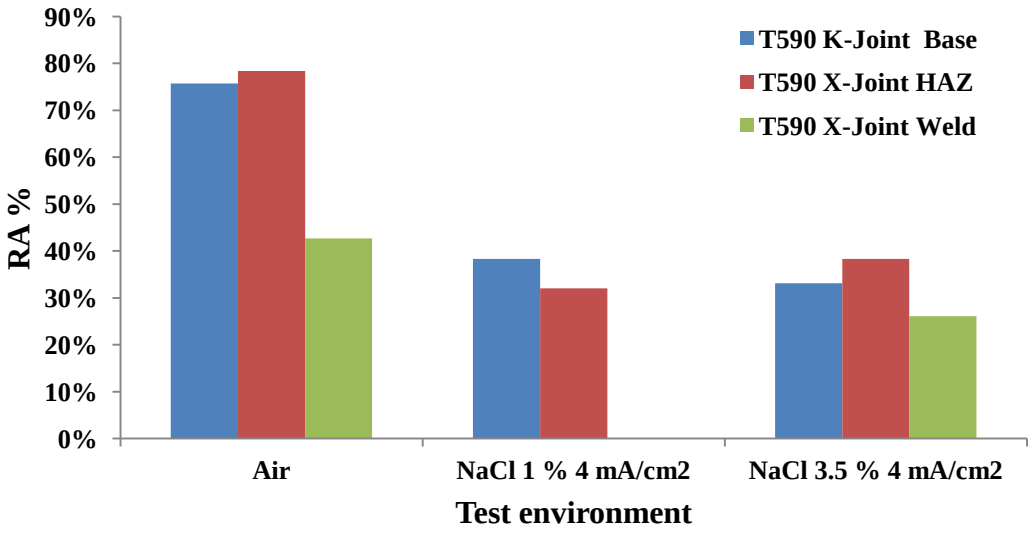

Figure 4.1.16. RA% of polarized base steel, welded metal and HAZ TS590 X-joint pipeline steel using 4 mA/cm^2 current density during SSRT testing

D.4.1.2.3.2.2 Time to failure

The relative time to failure bar charts for tested samples in four different environments is shown in Figure 4.1.17. There were three types of samples in each test environment; base metal, HAZ and weld metal. It is seen that all samples had almost the same relative time to failure in 1 wt% and 3.5 wt% NaCl solutions under free corrosion potential. However, a considerable decline of relative time to failure was observed for weld and HAZ tested samples under cathodic polarisation due to the hydrogen absorption process.

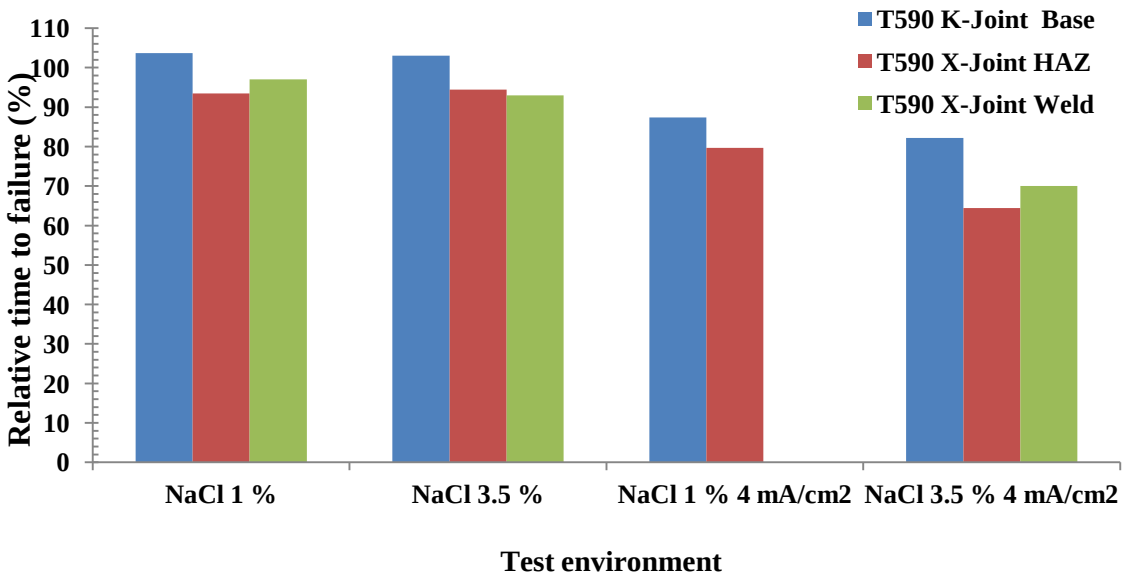

Figure 4.1.17. Relative time to failure vs. test solution of TS590 X-joint under free corrosion potential and cathodic polarisation

D.4.1.2.3.3 Fractography

Examples of characteristic fractures of the base metal and its welded joint of TS590 K-joint tested in air, 1 wt% and 3.5 wt% NaCl solutions after SSRT test are presented in Figures 4.1.18-4.1.20.

D.4.1.2.3.3.1 Air

When a ductile fracture occurs, a typical cup-and-cone surface is observed with three different textures: fibrous zone (central region), radial marks and shear lips. The slant shear region of failed surface is clearly observed in Figure 4.1.18 a, b, c. The fibrous region and radial marks are clearly distinguished from each other with a clear boundary as shown in Figure 4.1.18 a, b. The presence of the radial marks implies that cracks were initiated in the periphery and propagated in radial direction towards the centre of the tensile specimen as shown in Figure 4.1.18 a, b.

All the examined steels presented a mixture of ductile and brittle fracture. The SEM micrographs indicated a similar type of fracture mode for base metal and HAZ. The fracture surface consisted of a mixture of microvoids coalescence (MVC), typically observed in a ductile fracture and cleavage which is a common mechanism of brittle transgranular fracture. Transgranular fracture takes places through tear of the crystals along crystallographic planes in radial marks region. Large voids nucleated from the metallic inclusions were also detected, as shown in Figure 4.1.18 a', b'. The weld metal suffered from a mixture of brittle-ductile fracture i.e. initially brittle, then ductile, Figure 4.1.18 c. The MVC was observed and no cleavage was detected. In these cases, the obtained data from SEM are in good agreement with the calculated relative time to failure, RA% and EL% after SSRT test.

Environment: Air

sample

Base metal

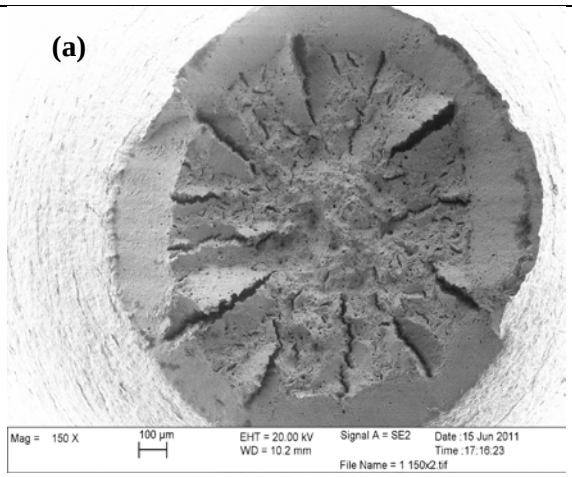

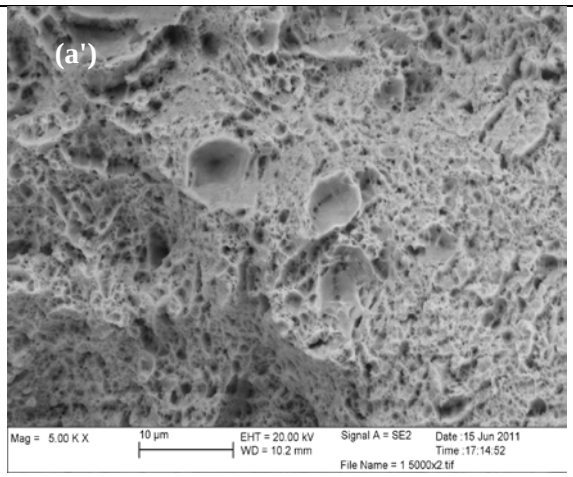

150x 5000x

HAZ

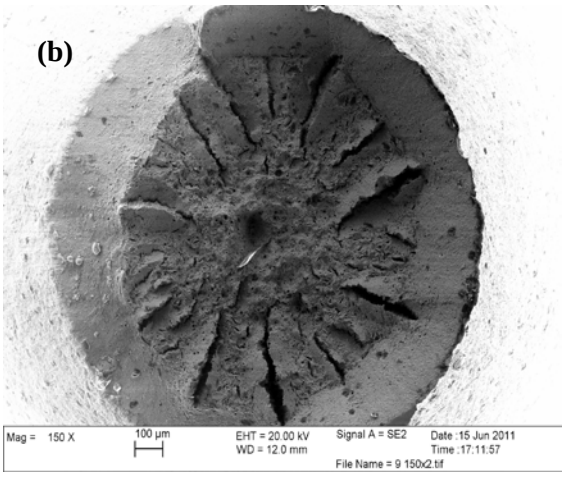

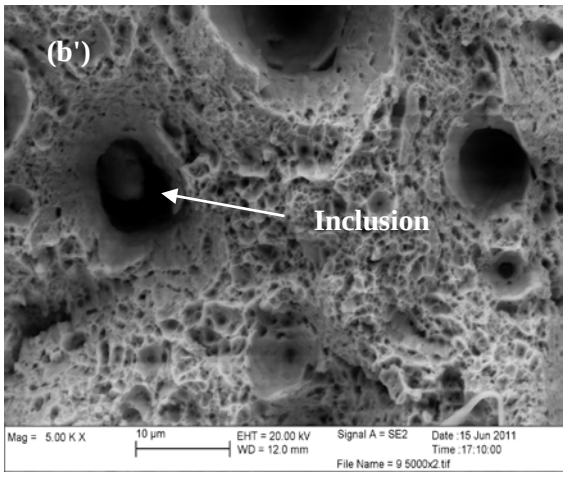

150x 5000x

Weld metal

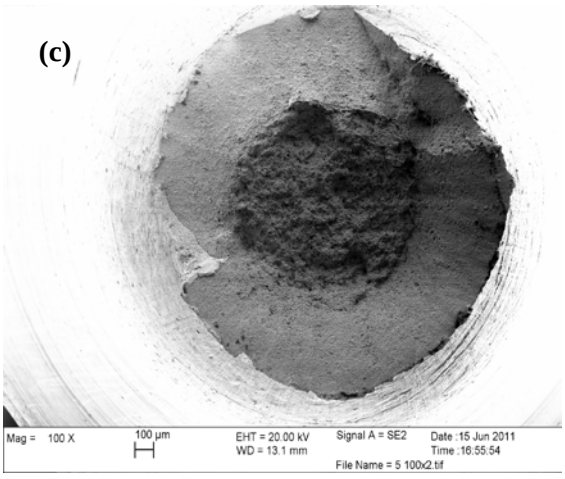

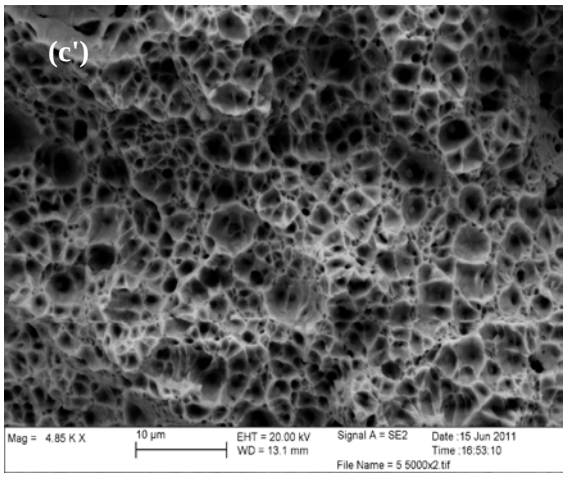

100x 5000x

Figure 4.1.18. SEM images showing the fracture surfaces of the base metal, HAZ and weld of TS590 after SSRT testing in air

D.4.1.2.3.3.2 NaCl 1 wt%

The micrographs fracture surface of the base TS590 steel and its welded joint after SSRT testing in 1 wt% NaCl solution are illustrated in Figure 4.1.19. Corrosion products appeared on the fracture faces for steel TS590 performed in 1 wt% NaCl solution, Figure 4.1.19 a, a'. The surface fractures of base metal and HAZ samples investigated in 1 wt% NaCl consisted of quasi-cleavage and MVC. It can be seen that both base metal and HAZ had the same sensitivity to sodium chloride solution so that the cracks formation and propagation occur in the same region. The area of fibrous for both case has been slightly increased which shows enhanced ductility in 1 wt% NaCl solution. On the other hand, both for base and HAZ the shallower radial marks confirm this claim.

It was observed that the 1 wt% NaCl solution has influenced the weld metal susceptibility to SCC more than that of HAZ and parent metal. It can be confirmed by lower ductile area and lower reduction in area after fracture.

Environment	NaCl 1 wt%	
sample		
Base metal	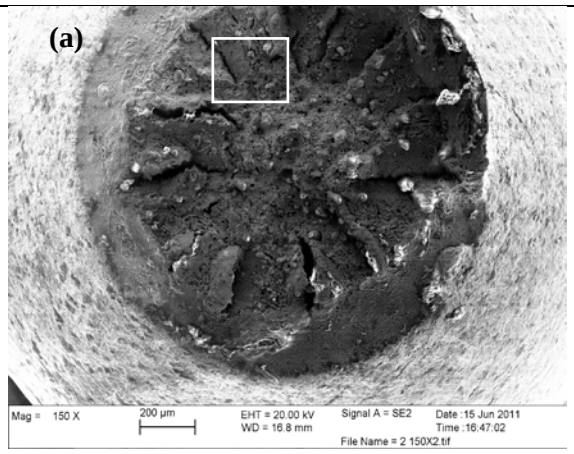	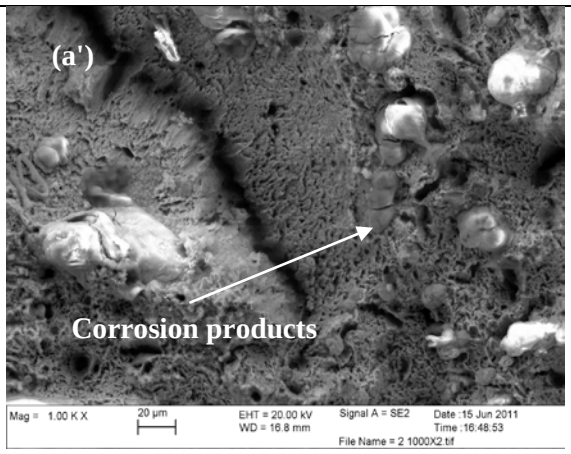
	150x	1000x
HAZ	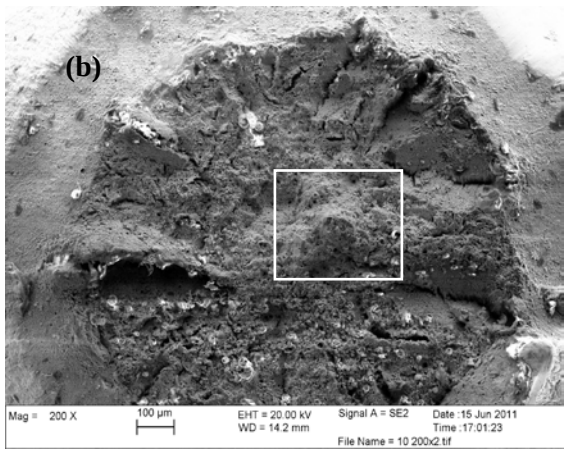	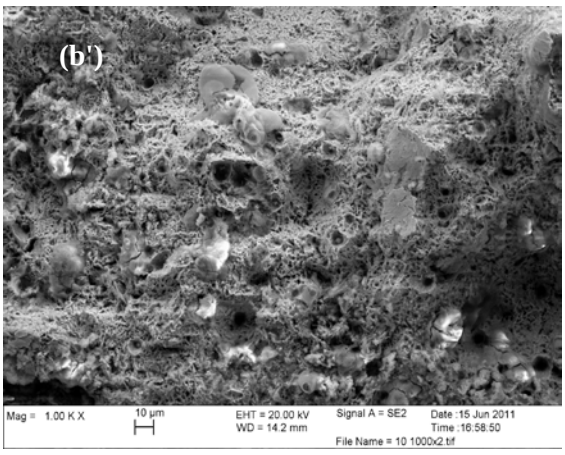
	200x	1000x
Weld metal	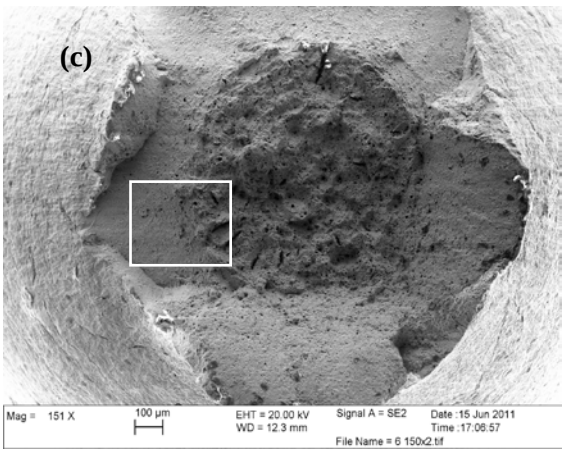	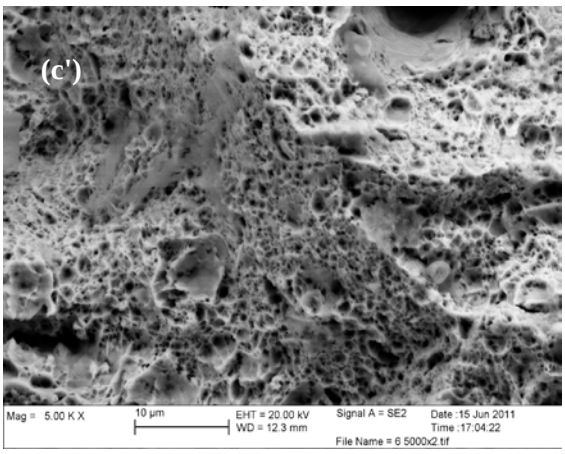
	150x	5000x

Figure 4.1.19. SEM images showing the fracture surfaces of the base metal, HAZ and weld of TS590 after SSRT in 1 wt% NaCl solution under OCP condition

D.4.1.2.3.3.3 NaCl 1 wt% solution with cathodic polarisation

After SSRT testing in 1 wt% NaCl with cathodic polarisation the failure fracture of the TS590 base material, HAZ and weld were investigated. The entire surface ruptures showed brittle failure when cathodic polarisation was applied. In other words, in hydrogen charged steels, brittle rupture occurred

under the influence of hydrogen. The fracture surface under cathodic polarisation in sodium chloride solution consists of intergranular as well as transgranular crack propagation, Figure 4.1.20 a, b, c. The base metal specimen showed a great number of cleavages on the fractured surface which formed in different crystallographic directions and planes as shown in Figure 4.1.20 a. The presence of the intergranular cracks (Figure 4.1.20 a') demonstrates the brittle rupture of the base metal accompanied with applied cathodic polarisation. In this perspective, the material did not show any plastic deformation after necking and immediately started to be broken.

From the SEM images, it can be seen that the SCC susceptibility of the weld metal is higher than that of base metal and HAZ in 1 wt% NaCl solution with applied 4 mA/cm^2 current density. This claim was confirmed by no significant reduction in area. Almost all specimens suffered from hydrogen influence. In hydrogen embrittlement mechanism, the ruptures are occurred at the initial cracks, which lead to a flat surface appearance after the failure. No consequential RA% was observed for the weld metal tested specimen under cathodic polarisation as revealed in Figure 4.1.20 c. The fracture surface indicates cleavage face (Figure 4.1.20 c'), which is a typical feature of brittle fracture.

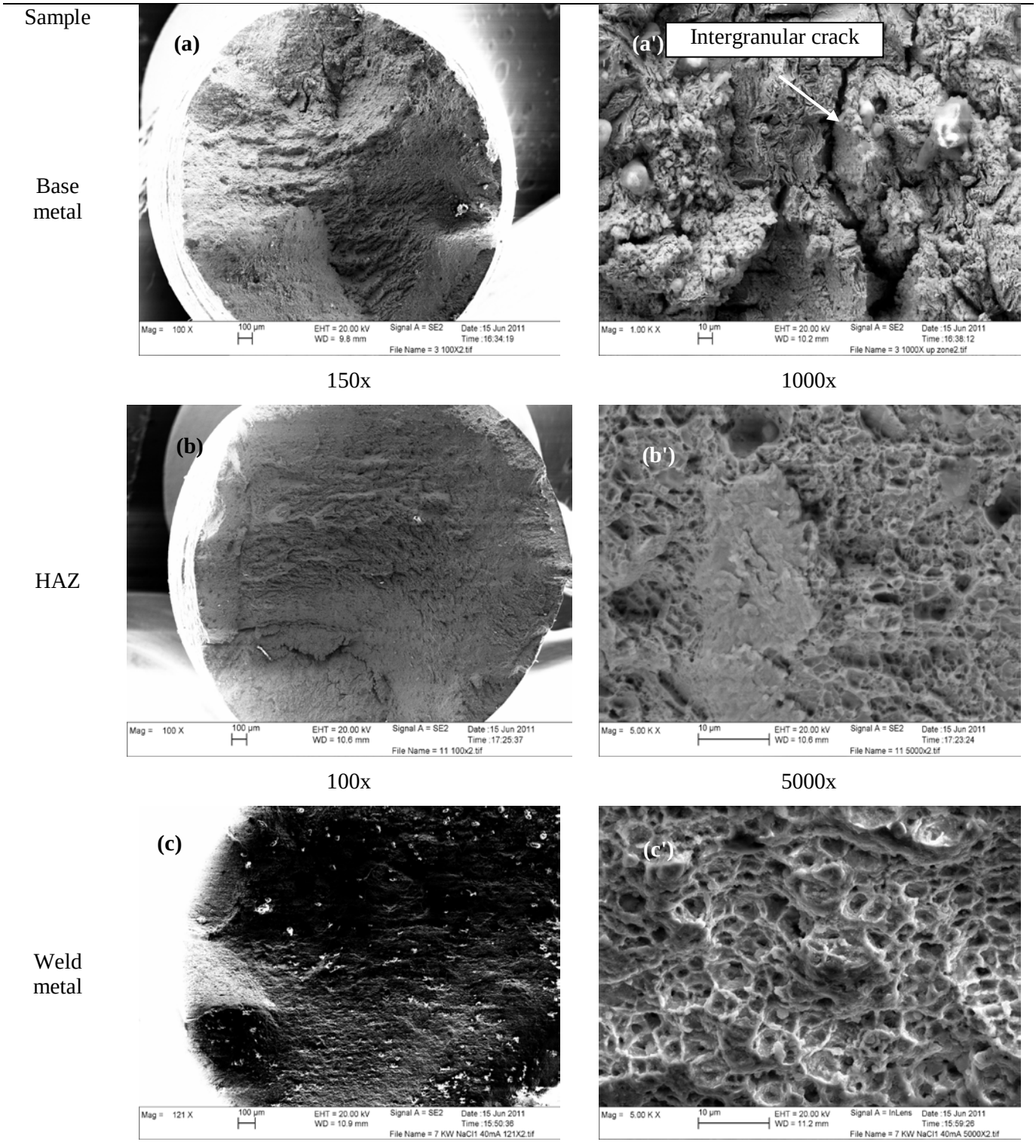

Figure 4.1.20. SEM images showing the fracture surfaces of the base metal, HAZ and weld of TS590 after SSRT testing in 1 wt% NaCl solution applying 4 mA/cm^2 current density for cathodic polarisation

D.4.1.2.4 S355 base metal and weld

D.4.1.2.4.1 Reduction of area

Figure 4.1.21 illustrates the RA% of the S355 ordinary steel grade tested in air, 1 wt% and 3.5 wt% NaCl solutions under open circuit potential condition. The weld metal had lower RA% than the base

and HAZ in all tested environments. Base metal and HAZ had equal RA% under applied tensile stress in air and in 3.5 wt% NaCl solution. No measurement was performed for base metal in 1 wt%. The results show a lower RA% for weld metal and HAZ in 3.5 wt% NaCl than in 1 wt% NaCl. From this point of view, it is showed that the cracks will always initiate from weld metal. Furthermore, for HAZ and weld metal, the study showed no significant difference between RA% in air and in 1 wt% NaCl solution.

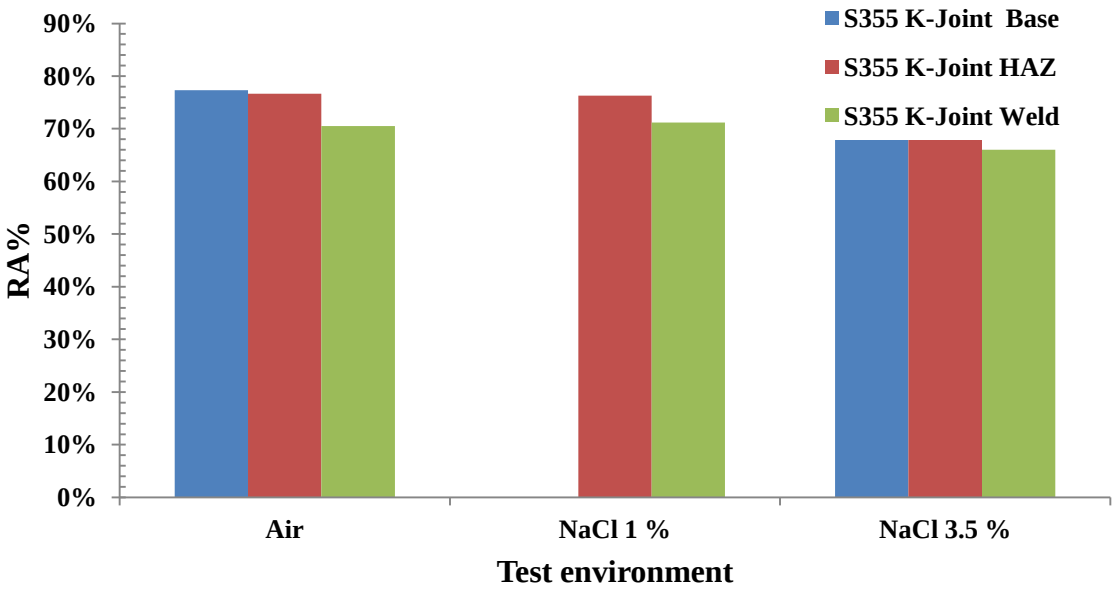

Figure 4.1.21. RA% of base steel, welded metal and HAZ of S355 K-joint pipeline ordinary steel

Results from measurements in air and 1 wt % NaCl solution with cathodic polarisation are shown in Figure 4.1.22. The results show a considerable lower RA% for both base and HAZ with cathodic polarisation in 1 wt% NaCl solution compare to air. The applied 4 mA/cm^2 current density increased the susceptibility to hydrogen embrittlement for base metal and HAZ. The base metal showed a higher RA% i.e. less sensitive towards SCC than the HAZ with cathodic polarisation.

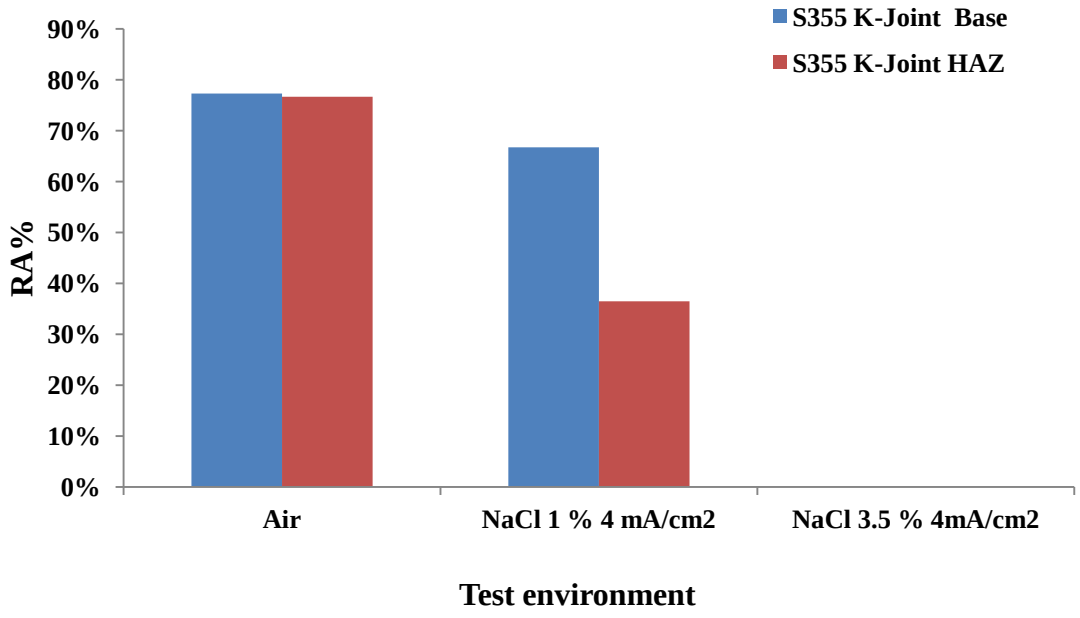

Figure 4.1.22. RA% of polarized base steel and HAZ S355 ordinary steel grade using 4 mA/cm^2 current density during SSRT testing

D.4.1.2.4.2 Time to failure

Analyzing the load vs. time curves after SSRT test, it is presented that applied 4 mA/cm^2 of current density dramatically resulted in decrease of time to failure, shown in Figure 4.1.23. However, only slight decrease was observed in time to failure at free potential comparing to the value obtained from performed test in air.

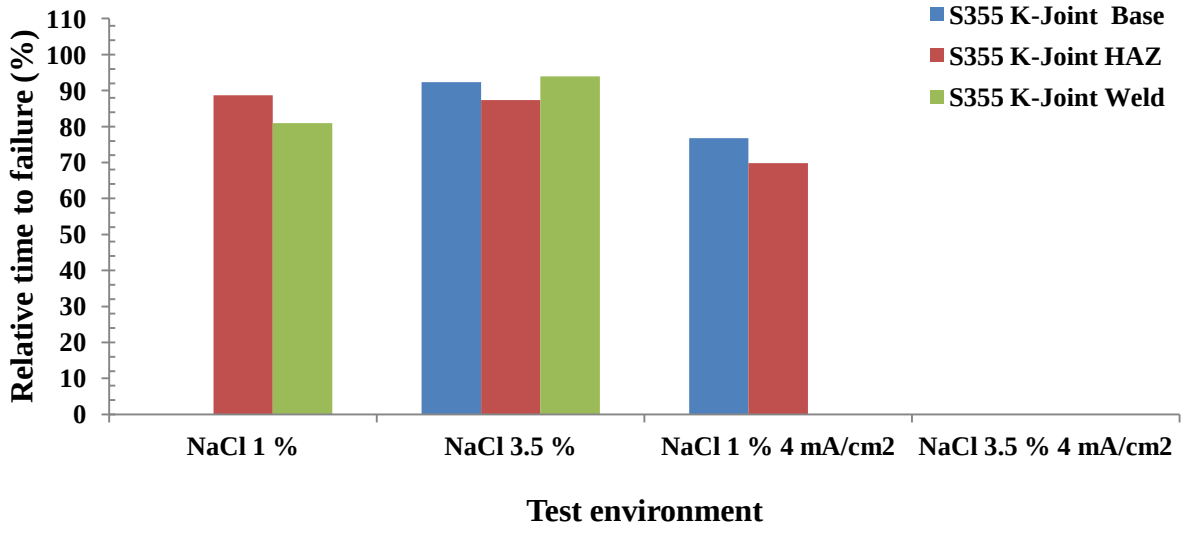

Figure 4.1.23. Relative time to failure vs. test solution of S355 K-joint under free potential and cathodic polarisation

So far, following main conclusions can be drawn regarding the susceptibility of TS590 and S355 steels grade to general corrosion, stress corrosion cracking and hydrogen assisted stress corrosion cracking:

- The weld metal and HAZ of TS590 had higher susceptibility to hydrogen assisted stress corrosion cracking compare to base metal, confirmed by small reduction in area (RA%) and time to failure.
- Cathodic polarisation with using 4 mA/cm^2 increased the susceptibility to hydrogen assisted stress corrosion cracking for base metal and HAZ of S355 steel.

D.4.2. Test data on welded tubular connections

D.4.2.1 General

This experimental investigation consists of ten (10) tests on overmatch-welded tubular connections of which the brace has a nominal cross-section CHS 193.7x10 and the chord CHS 355x12. The material is high-strength steel (TS590) with nominal yield stress of 735 MPa. For the experimental study of the behavior of high-strength steel welded tubular connections under out-of-plane (OPB) and in-plane (IPB) bending, eight (8) specimens were tested, four (4) for each type of loading. In addition, two (2) specimens were tested under cyclic axial loading. Two (2) weld types have been considered, denoted as weld type A (lower weld metal strength) and weld type B (higher weld metal strength). The joint welds have been performed according to the provisions of AWS D1.1/D1.1M:2004.

D.4.2.2 Test set-up and Instrumentation

To conduct the tests special hinges and grips were manufactured in order to carry out 4-point bending tests for the OPB specimens and 3-point bending tests for the IPB specimens (see Figure 4.2.1). For the OPB tests, the specimens were supported using a double-hinge 'roller' system (see Figure 4.2.1) with ball joint hinges and the load was applied to the brace through a steel cross-beam with a system of two special ball-joint hinges and appropriate wooden grips (see Figure 4.2.2). For supporting the IPB specimens, the same double-hinge 'roller' system was used, while the load was applied through an actuator which was bolted to the top of the chord (see Figure 4.2.1). For the axial tests, one end of the specimens' brace has been hinged to the bottom beam of the testing frame and the other end to a lever-arm steel beam.

Regarding the instrumentation setup for these tests, wire position transducers were used to measure load-point displacements, DCDT's for measuring support displacements and a number of strain gages were placed at critical locations. Especially, uniaxial 5-element strip strain gages were placed on the chord for measuring strains in the region near the weld toe. The gages were at a distance of 3 mm, with the first one being 5 mm away from the weld toe. For the OPB tests the gages were placed in the hoop direction of the chord (saddle) and for the IPB test in the meridional direction of the chord (crown) (see Figure 4.2.3).

(a) (b)

Figure 4.2.1: General view of the test set-up with the specimens for: (a) out-of-plane bending tests, (b) in-plane bending tests.

(a) (b)

Figure 4.2.2: (a) Double-hinge ‘roller’ and (b) beam/wooden grips system for OPB tests.

(a) (b)

Figure 4.2.3: Uniaxial 5-element strip strain gages at: (a) the hoop direction of the chord (saddle location), (b) the meridional direction of the chord (crown location).

D.4.2.3 Experimental results

The experimental set-up for OPB and IPB tests is shown in Figure 4.2.4. The experimental results are summarized in Table 4.2.1. The experimental procedure for each type of tests is described below.

Table 4.2.1: Test results.

type of specimen and loading type	weld type	type of loading	applied moment M_{max} (kNm) or axial load F_{max} (kN)	R	loading cycles to failure, N_f
OPB	A	monotonic	121.4	-	-
	B	monotonic	115.4	-	-
	A	cyclic	9.3 to 93.4	0.1	240
	B	cyclic	9.3 to 93.4	0.1	200
IPB	A	monotonic	267.8	-	-
	B	monotonic	251.5	-	-
	A	cyclic	21.3 to 213.1	0.1	976
	B	cyclic	21.3 to 213.1	0.1	669
Axial	A	cyclic	75 to 750	0.1	1,000 (*)
	B	cyclic	75 to 750	0.1	750 (*)

(*) approximate value corresponding to significant axial stiffness loss.

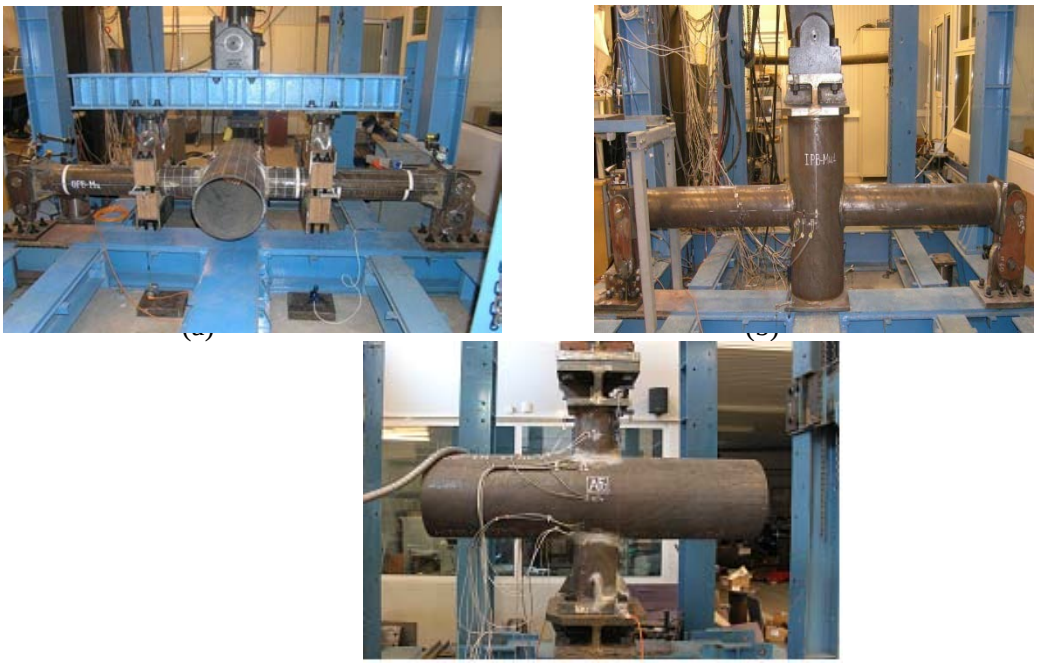

(c)

Figure 4.2.4: Test setup for tests: (a) out-of-plane bending, (b) in-plane bending, (c) axial loading.

(a) OPB tests: two specimens were subjected to monotonic loading, one for each weld type. The bending moment capacity M_{max} of the specimen with weld type A and that with weld type B is 121.4 kNm at a load-point displacement (LPD) of 107.5 mm and 115.4 kNm at a LPD=78.5 mm, respectively. Both specimens failed at the chord saddle region of the weld toe of the joint (see deformed specimen in Figure 4.2.5). The other two of the OPB specimens were tested under low-cycle fatigue, one with weld type A and one with weld type B. After an initial applied bending moment of 100 kNm to both specimens, they were subjected to fatigue loading of 75% to 80% of the maximum monotonic load; M_{min}=9.3 kNm and M_{max}=93.4 kNm (load ratio, $R=M_{min}/M_{max}$=0.1) at a frequency of 0.1 Hz. The weld type A specimen failed after 240 loading cycles exhibiting a slightly higher fatigue resistance than the specimen with the weld type B which failed after 200 cycles (Figure 4.2.7). The behavior of the specimens subjected to monotonic and cyclic loading was rather similar. All specimens failed in the form of fracture at the chord saddle of the joint, near the weld toe (Figure 4.2.8). Moreover, it was observed that, under monotonic loading, the specimen with the lower strength of the weld (type A) showed about 5% higher flexural capacity and 37% higher load-point deflection than the one with the higher strength weld (type B) (see Figure 4.2.6). According to CIDECT 8, the predicted moment capacity of the OPB specimen under monotonic loading is about 113 kNm. The measured values were 7% and 2% higher for weld type A and B, respectively.

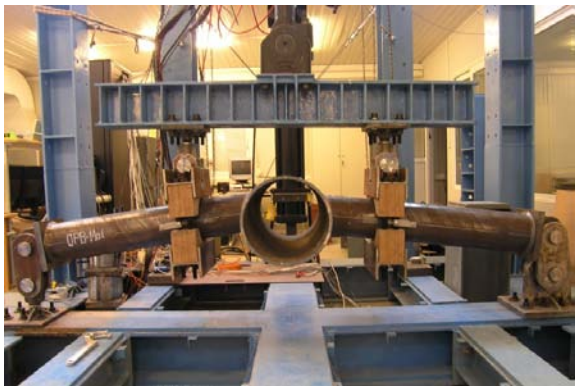

Figure 5: Deformed specimen; out-of-plane bending OPB,

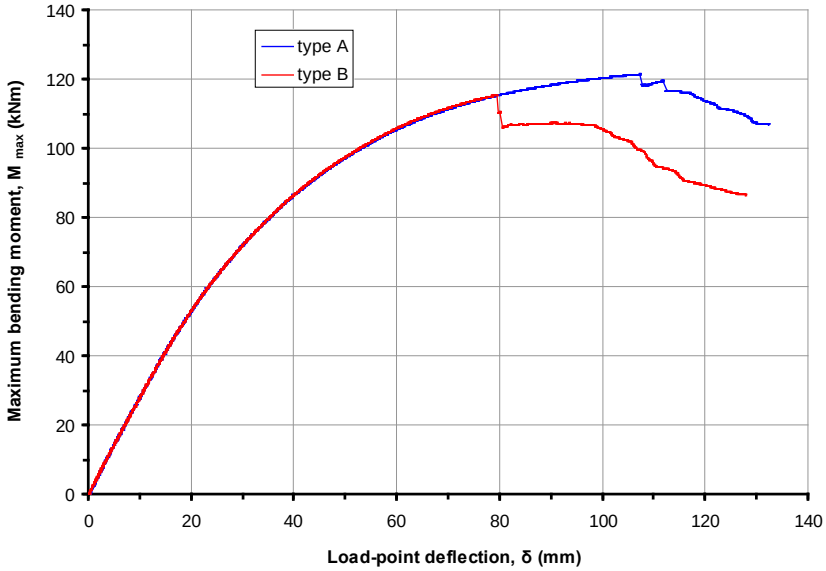

Figure 4.2.6: Load vs. displacement curves for the OPB specimens under monotonic loading.

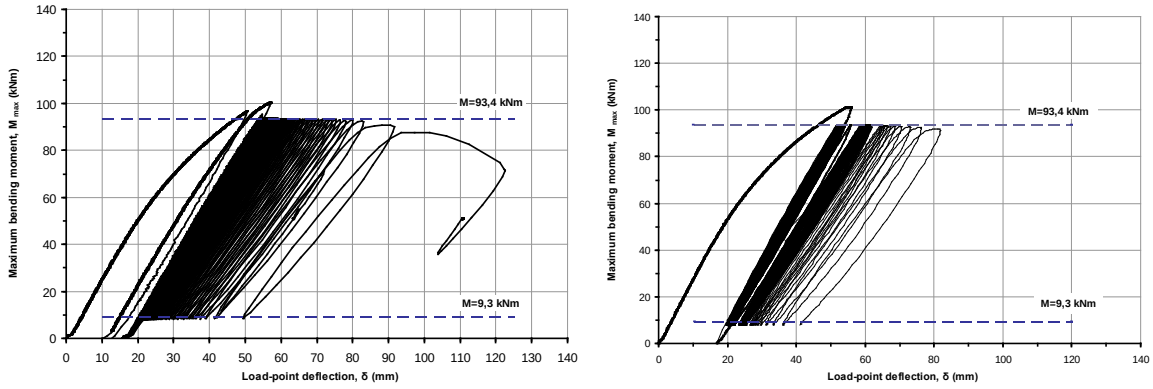

(a) (b)

Figure 4.2.7: Load vs. displacement curves for OPB specimens under cyclic loading: (a) type A weld, (b) type B weld.

(a) (b)

Figure 4.2.8: (a) OPB specimen at failure, (b) failure crack of OPB specimen.

(b) IPB tests: two specimens were subjected to monotonic loading, one for each weld type. The specimen with weld type A and weld type B failed under a M_{max}=267.8 kNm with a LPD=159.3 mm and a M_{max}=251.5 kNm with a LPD=111.5 mm, respectively. Failure occurred at the chord crown location of the weld toe of the joint (see deformed specimen in Figure 4.2.9). The specimen with the lower strength weld (type A) exhibited about 6% higher flexural capacity and 43% higher load-point

deflection than the one with the higher strength weld (type B) (see Figure 4.2.10), values which are similar to those for the OPB monotonic tests. According to the provisions of EN 1993-1-8, the predicted bending moment capacity of the joint under monotonic loading is about 202 kNm. The measured capacity was about 33% and 25% higher for weld type A and B, respectively.

The other two IPB specimens were tested under low-cycle fatigue, one with weld type A and one with weld type B. After an initial applied bending moment of 213.1 kNm to both IPB specimens, they were subjected to fatigue loading with a M_{min}=21.3 kNm and M_{max}=213.1 kNm (load ratio, $R=M_{min}/M_{max}=0.1$) at a frequency of 0.2 Hz. The specimen with weld type A failed after 976 loading cycles and that with weld type B after 669 cycles (see Figure 4.2.11). Both specimens failed due to fatigue at the chord crown region of the joint, at the same location as in the tests under monotonic loading. All specimens failed after forming a through-thickness crack in the chord along the circumference of the weld, starting at the chord's crown of the joint (Figure 4.2.12).

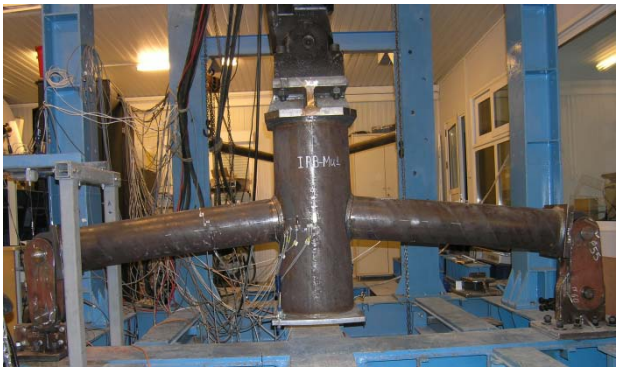

Figure 4.2.9: Deformed specimen; in-plane-bending IPB

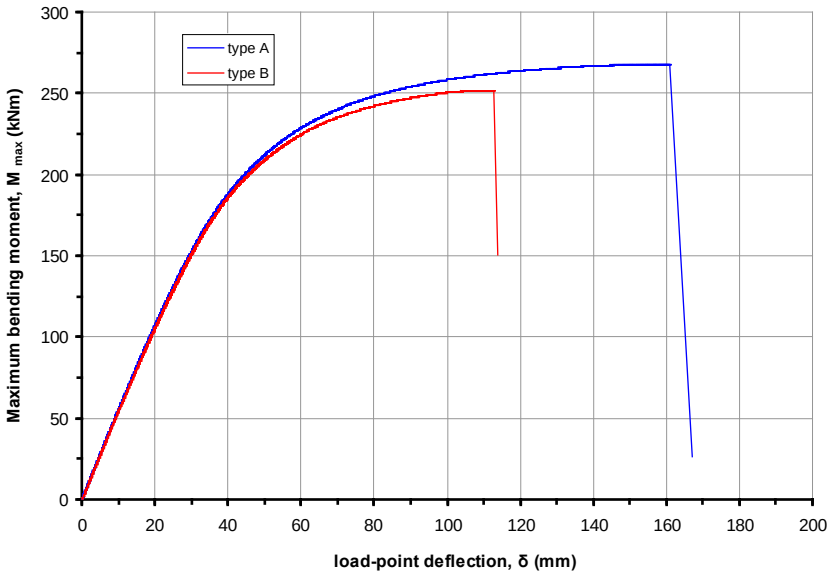

Figure 4.2.10: Load vs. displacement curves for the IPB specimens under monotonic loading.

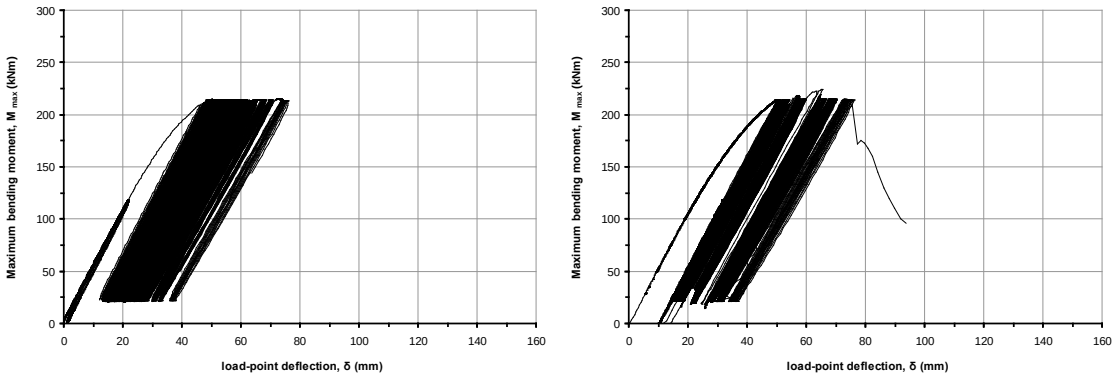

(a) (b)

Figure 4.2.11: Load vs. displacement curves for: (a) type A, (b) type B cyclic IPB tests.

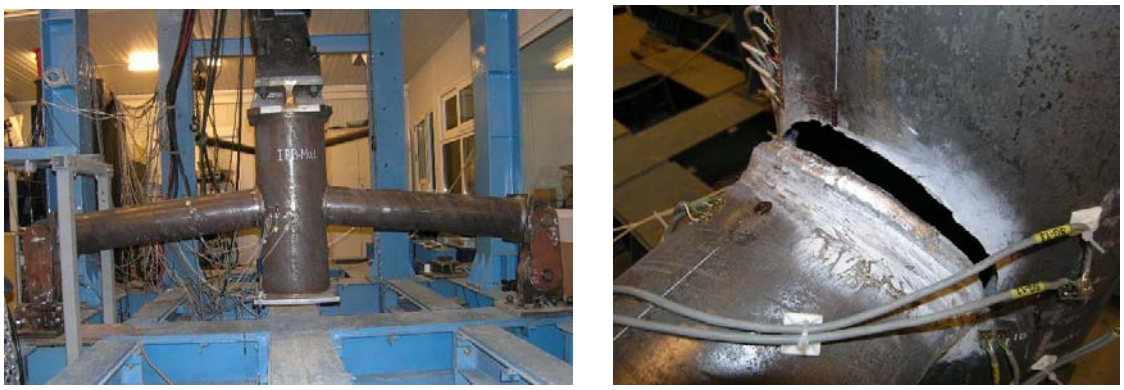

(a) (b)

Figure 4.2.12: (a) IPB specimen at failure, (b) failure crack of IPB specimen.

(c) Axial load tests: two X-joint specimens were subjected to low-cycle fatigue under cycling axial loading, one with weld type A and one with weld type B. The specimens were subjected to a cyclic tensile loading on the braces, with a maximum and minimum force equal to 750 kN and 75 kN respectively (load ratio, $R=F_{min}/F_{max}=0.1$). The load was applied through a level-arm system, as shown in Figure 4.2.4c, at a low frequency ranging between 0.01 and 0.03 Hz. Both specimens failed due to fatigue through-thickness crack at the chord saddle region of the joint. However, both specimens were able to sustain the applied load for more than 1,000 cycles. The initial range of axial deformation (elongation) of the specimens were measured equal to 7.3 mm and 7.6 mm (Figure 4.2.13). Furthermore, the evolution of range of axial deformation with respect to the number of cycles indicated that after a certain number of cycles N_f, the rate of increase becomes quite significant (Figure 4.2.13), and this can be considered as structural failure. From Figure 4.2.13, the value of N_f for weld type B can be considered approximately equal to 750 cycles, whereas weld type A specimen had a better behavior and the corresponding value is equal to about 1,000 cycles. The two curves of Figure 4.2.13 demonstrate clearly the superior behavior of weld type A. The response of the two specimens under cyclic loading is shown in Figure 4.2.14, and are compatible with the results of Figure 4.2.13. Finally, the through-thickness crack is shown in detail in Figures 4.2.15.

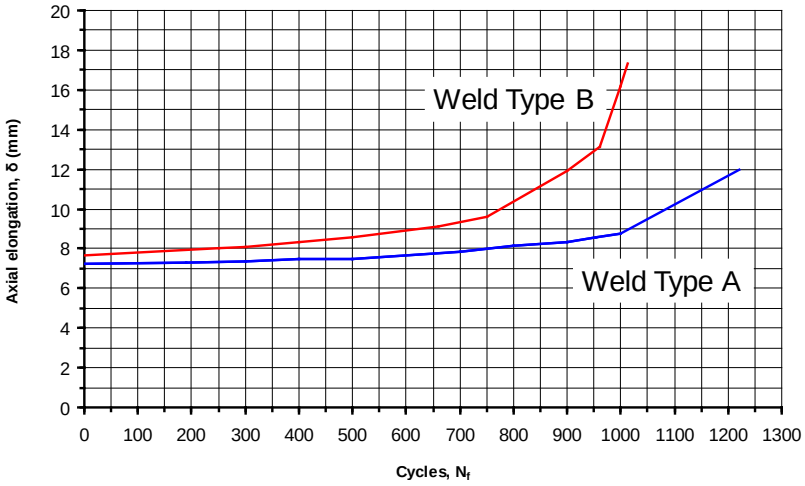

Figure 4.2.13: Axial loading specimen; evolution of axial deformation.

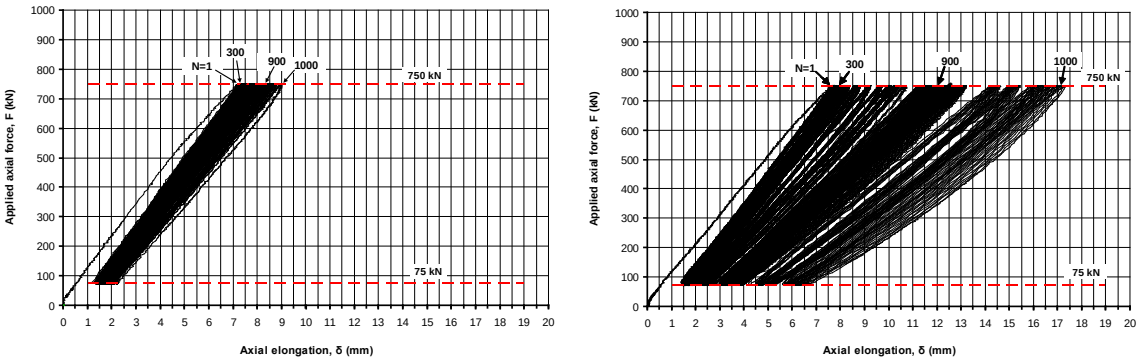

(a) (b)

Figure 4.2.14: Axial loading specimen; load-deformation curve for (a) weld type A, (b) weld type B.

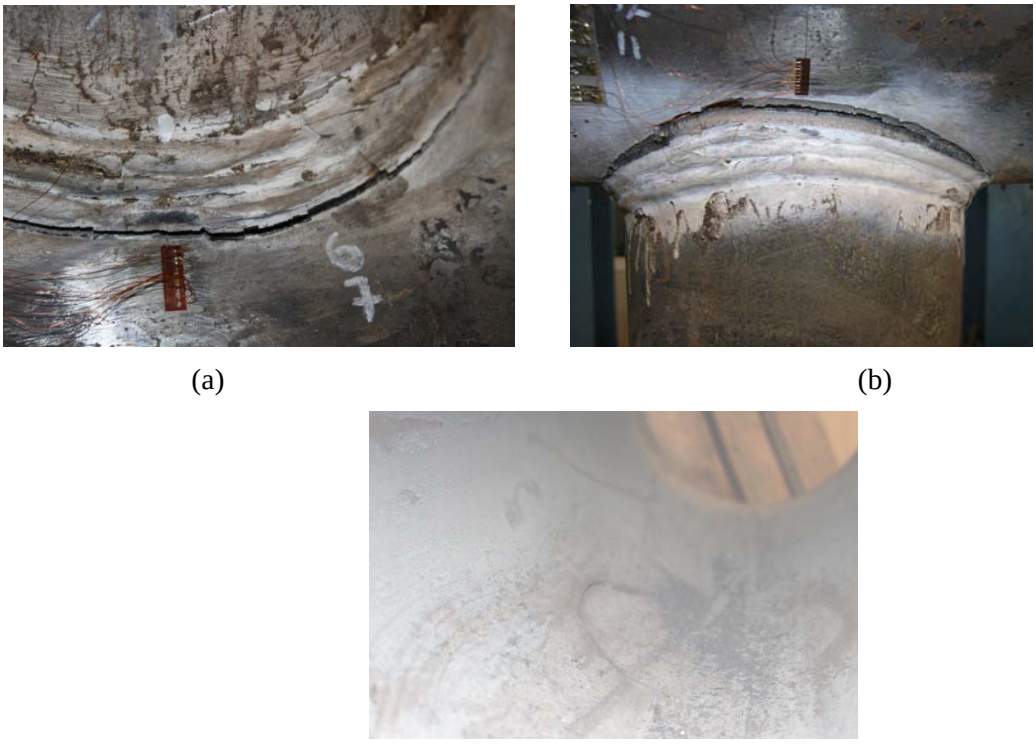

(a) (b)

(c)

Figure 4.2.15: Fatigue crack of axial loading specimen; (a) and (b) external view of crack at chord saddle, (c) internal view of through-thickness crack.

D4.3: Performance of advanced post-treatment welding techniques- Deliverable D4.3

With reference to the Work package 4- Task 4.3, high cycle fatigue tests were performed on ultrasonic peening specimens both in undermatching and overmatching welds. The welded tubes of the TS590 material can be seen in the Figures 4.3.1 and 4.3.2. The material was delivered in the undermatching and peening condition (Figure 4.3.1) and in the overmatching and peening condition (Figure 4.3.2). An indication of the filler metal has identified the matching condition of the tubes (G55 and G79 respectively). The peening treatment has been recognized visually after cleaning the welded surface.

Figure 4.3.1: TS590 tube in the undermatching and peening condition

Figure 4.3.2: TS590 tube in the overmatching and peening condition

D.4.3.1 Description of the axial fatigue test

Rectangular specimens were extracted from a longitudinal section of the welded tube with the reduced section of the specimen matching up with the weld. The specimen geometry is shown in Figure 4.3.3.

Figure 4.3.3a: Specimen geometry

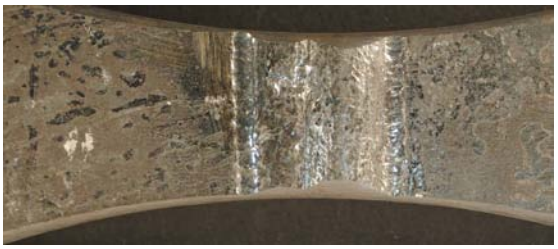

Figure 4.3.3b: Detail of the peening surface

The details of the test are listed below.

Material designation: TS590

Surface treatment: US Peening

Specimen geometry: See Figure 4.3.3

Condition: overmatching and undermatching

Machining: was performed following annex I of the testing standard ASTM E466. The specimen edges have been mechanically rounded by hand polishing to a radius of 3 mm.

Type of machine: Servo hydraulic testing machine INSTRON 8504

Software: INSTRON FASTRACK 2 SAX Single Axis

Waveform: Sine

Load ratio: R=0.1

Run-out: 2E6 cycles

Test temperature: 23ºC

Specimens tested: 12 per condition

Failure criteria: Total rupture of the specimen

Nominal dimensions of reduced sections (not considering weld over thickness):

Width – 25.00 mm, Thickness – 12.50 mm.

D.4.3.2 Test results

The fatigue tests on overmatching and undermatching peening specimen were performed.

Overmatching peening (OP)

The result is presented in Table 4.3.1.

Table 4.3.1: Test results for overmatching peening

Nº	Specimen	Max Stress [MPa]	Mean Stress [MPa]	Stress Amplitude [MPa]	Freq [Hz]	Cycles	Test finishing cause
1	OP1	300	165	270	25	47138	Total rupture
2	OP2	200	110	180	25	2000000	Run-out
3	OP3	300	165	270	25	28226	Total rupture
4	OP4	200	110	180	25	2000000	Run-out
5	OP5	250	137.5	225	25	23890	Total rupture
6	OP6	250	137.5	225	25	477346	Total rupture
7	OP7	275	151.25	247.5	25	171490	Total rupture
8	OP8	275	151.25	247.5	25	253782	Total rupture
9	OP9	200	110	180	25	628646	Total rupture
10	OP10	225	123.75	202.5	25	252098	Total rupture
11	OP11	250	137.5	225	25	782897	Total rupture
12	OP12	225	123.75	202.5	25	337346	Total rupture

Undermatching peening (UP)

The results are presented in Table 4.3.2.

Table 4.3.2: Test result for undermatching peening

Nº	Specimen	Max Stress [MPa]	Mean Stress [MPa]	Stress Amplitude [MPa]	Freq [Hz]	Cycles	Test finishing cause
1	UP1	500	275	450	15	16659	Total rupture
2	UP2	400	220	360	20	59144	Total rupture

3	UP3	300	165	270	25	261336	Total rupture
4	UP4	200	110	180	25	538680	Total rupture
5	UP5	100	55	90	30	2000000	Run-out
6	UP6	200	110	180	25	2000000	Run-out
7	UP7	250	137.5	225	25	753125	Total rupture
8	UP8	300	165	270	25	640880	Total rupture
9	UP9	250	137.5	225	25	766225	Total rupture
10	UP10	400	220	360	20	96485	Total rupture
11	UP11	200	110	180	25	2000000	Run-out
12	UP12	500	275	450	10	19070	Total rupture

The S-N diagram is represented in Figure 4.3.4.

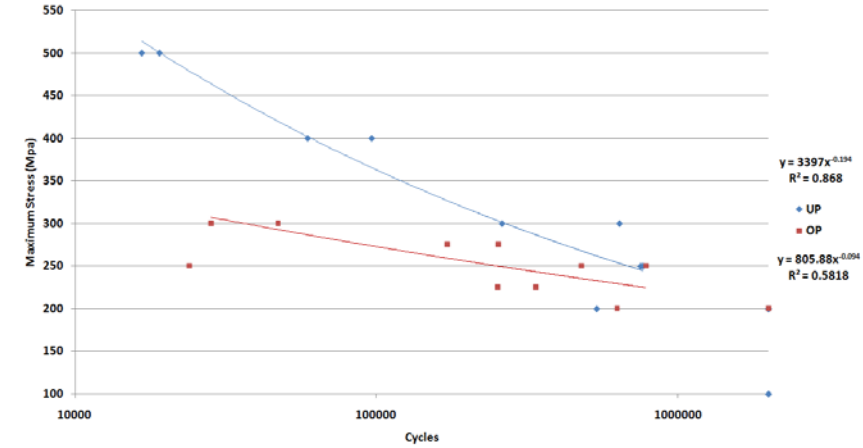

Figure 4.3.4: S-N diagram

D.4.3.3 Fractographic analysis

The fracture surface is shown in Figure 4.3.5. It was observed that the initiation of the fatigue occurs in all the specimens from the root fusion line.

Figure 4.3.5: Failure along the root fusion line for OP specimen

Figures 4.3.6 and 4.3.7 show the fracture surfaces for UP and OP specimens respectively. It can be noted that OP contains more defects like pores and lack of fusion. UP weld surfaces are smoother.

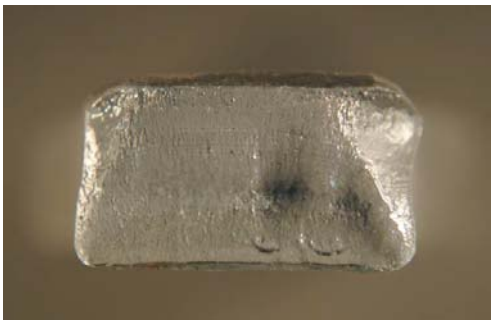

Figure 4.3.6 a UP1

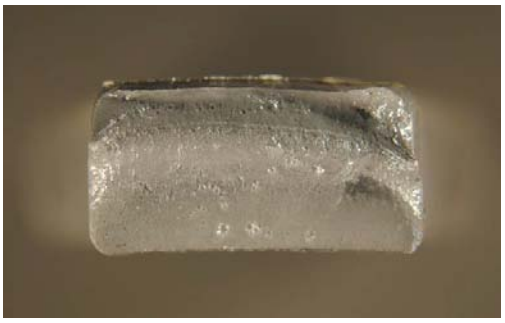

Figure 4.3.6 b UP2

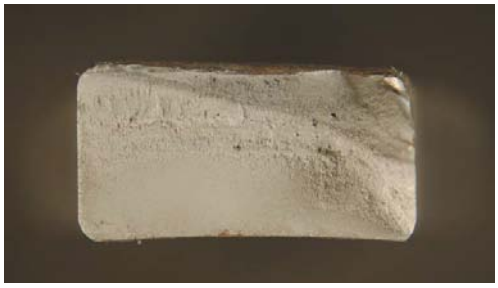

Figure 4.3.6 c UP3

Figure 4.3.6 d UP4

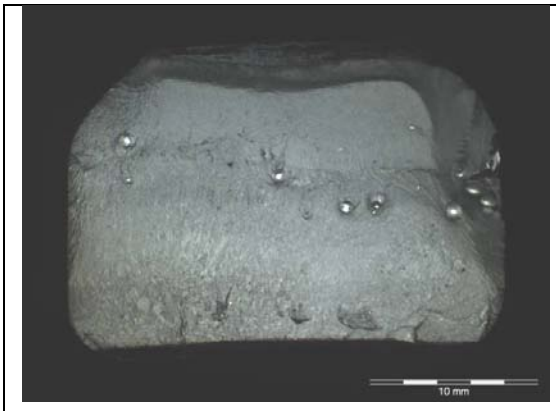

Figure 4.3.7 a OP1

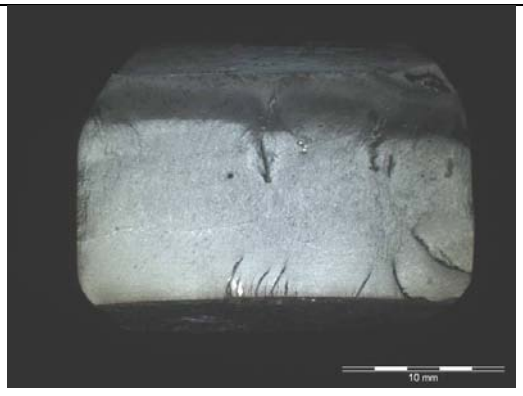

Figure 4.3.7 b OP2

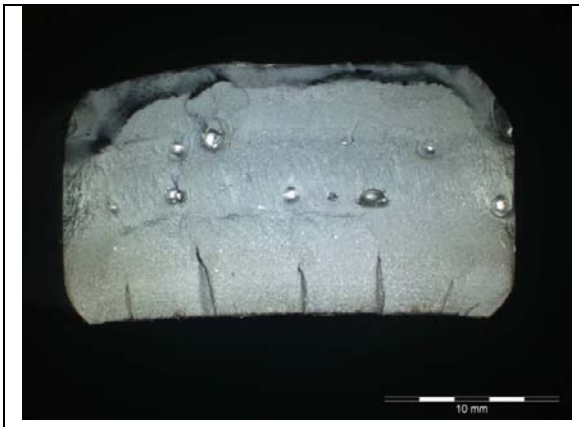

Figure 4.3.7c OP3

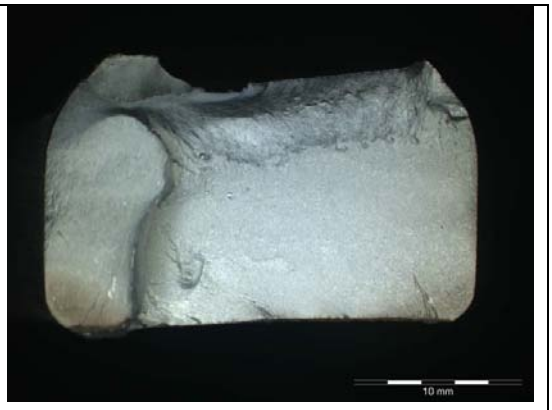

Figure 4.3.7 d OP4

The obtained results for S-N curves of undermatching peening (UP) and overmatching peening (OP) showed a better performance of the UP specimens at low stresses (indicating a longer nucleation stage of the fatigue process), although the final endurance fatigue limit can be considered the same for both welding conditions. All specimens broke starting in the root fusion line, and, avoiding those ruptures due to lack of fusion or welding defects (which are not being considered in the calculations), the fatigue grew into the HAZ until a final break.

D4.4: Test data on bolted tubular connections - Deliverable D4.4

The test data of various tests relevant to the bolted connections are gathered in Annexes as follows.

Detail of measurement of the initial out-of-plan of the flanges is presented in Annex 0.

Detail of results of the coupon tests is presented in Annex 1.

Detail of results of the tests on bolts is presented in Annex 2.

Detail of information of the tightening of the bolts is presented in Annex 3.

Results of the joint tests are presented in Annexes 4-11.

ANNEX 0: Data of the measurement of the out-of-plan of the flanges

Table 4.4.1

Spe.	Flange	Measurement value in mm at the points (Fig.15)											
		1	2	3	4	5	6	7	8	9	10	11	12
S1,S2	No measurement												
S3	1	1,79	2,99	3,28	2,39	3,88	2,92	1,39	2,88	3,10	2,87	3,65	3,03
	2	2,25	2,67	2,65	2,35	2,84	2,78	2,57	2,72	2,92	2,12	3,26	2,79
S4	1	1,98	2,11	2,07	1,57	1,72	1,59	1,22	1,39	1,57	1,30	1,63	1,59
	2	1,86	2,46	2,30	1,52	2,35	2,29	2,20	1,96	1,82	1,82	1,56	1,71
S5	1	1,84	0,82	1,62	2,03	1,30	1,89	1,93	0,95	1,94	2,47	1,37	1,98
	2	1,68	2,80	2,5	1,63	2,56	2,49	1,59	2,98	2,82	1,62	2,68	2,68
S6	1	4,37	3,65	3,38	2,48	2,92	3,25	2,56	2,65	2,38	1,97	3,47	4,44
	2	1,74	2,55	2,95	1,67	2,45	2,60	2,30	2,83	2,57	1,66	2,05	2,21

ANNEX 1: Data of the coupon tests

(extracted from the flange and the tubes) in French, *Summary of results:*

Table 4.4.2

Eprouvette n°	Fmax N	Pr.	a_0 mm	b_0 mm	R_{eH} MPa	$R_{p0.2}$ MPa	R_m MPa	m_E N/mm²	L_0 mm	A %	Dr mm	Commentaire
HT1	199553.91	L	11.31	20.05	-	823	880	205183	80	7.4	10	rupture ext.extensometre
HT2	201360.31	L	10.99	20.78	-	823	882	206320	80	8.8	2	rupture ext.extensometre
HT3	199858.13	L	11.39	19.95	-	819	880	202568	80	18.5	45	rupture int.extensometre
HP15_1	160021.06	P	14.67	19.89	415	393	-	200891	80	-	50	rupture int.extensometre
HP15_2	154483.78	P	14.7	19.32	413	400	-	200987	80	-	50	rupture int.extensometre
HL15_1	158021.33	L	14.51	19.97	395	387	-	210683	80	-	50	rupture int.extensometre
HL15_2	158813.08	L	14.61	20	407	390	-	213069	80	-	50	rupture int.extensometre
HP20_1	208075.33	P	19.74	19.94	395	381	-	211984	80	-	35	rupture int.extensometre
HP20_2	209158.19	P	19.82	19.99	389	372	528	210151	80	29.9	35	rupture int.extensometre
HL20_1	208677.14	L	19.62	19.99	410	397	-	205781	80	-	50	rupture int.extensometre
HL20_2	145327.63	L	19.65	18.8	393	379	393	199686	80	0.2	35	rupture int.extensometre
HL20_2b	192358.19	L	19.65	18.8	369	363	521	197866	80	31.8	50	rupture int.extensometre
HL20_3	169542.17	L	19.58	20.03	432	413	432	204392	80	0.2	50	rupture int.extensometre
HL20_3b	210192.94	L	19.58	20.03	-	372	536	198225	80	30.4	50	rupture int.extensometre
HL15_3	158904.59	L	14.66	20.03	393	377	541	200776	80	33.7	45	rupture int.extensometre
HP15_3	157758.64	P	14.71	19.89	406	373	539	201879	80	29.6	50	rupture int.extensometre
HP20_3	205742.52	P	19.58	20	390	361	525	208999	80	31.3	45	rupture int.extensometre

Load-deformation curves for the tests:

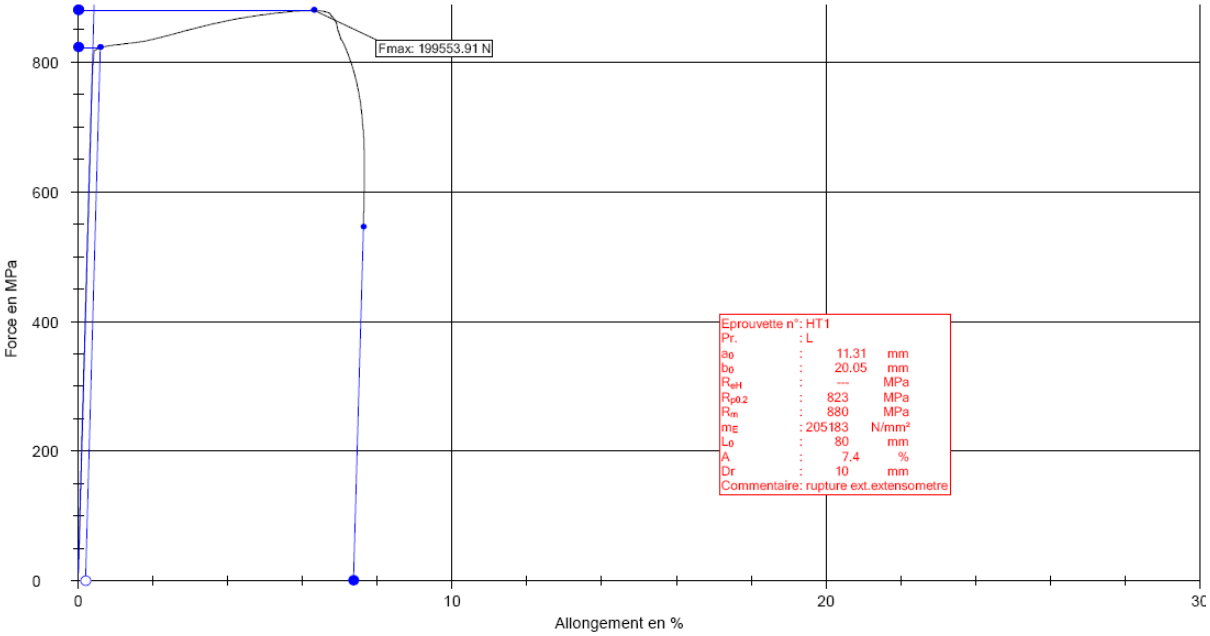

Figure 4.4.1

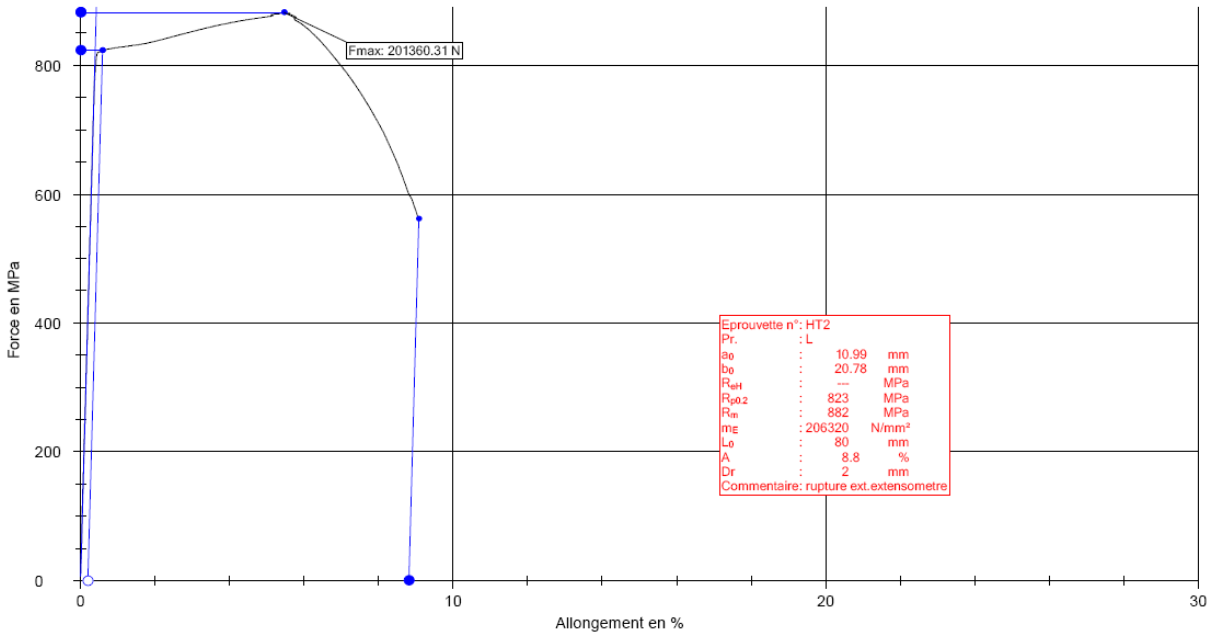

Figure 4.4.2

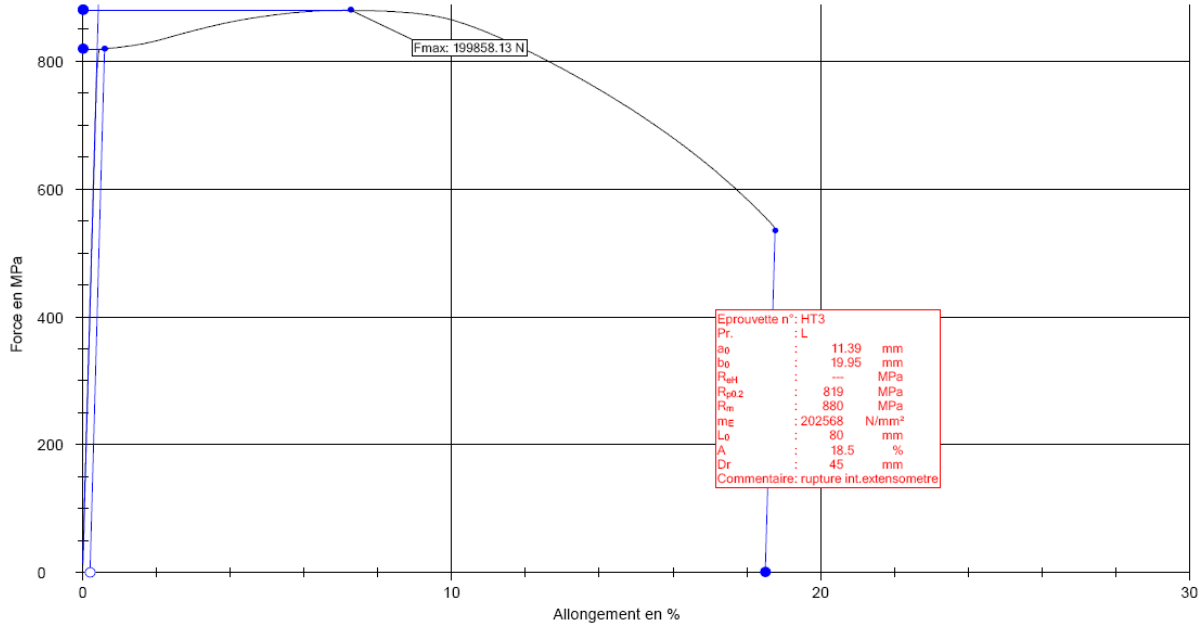

Figure 4.4.3

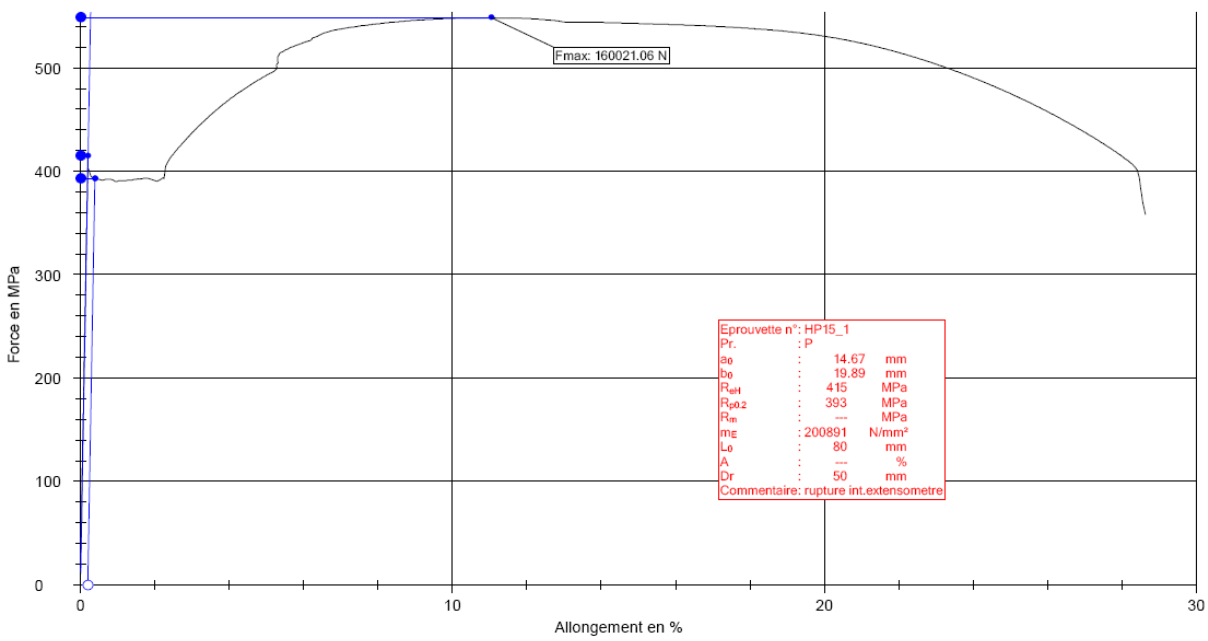

Figure 4.4.4

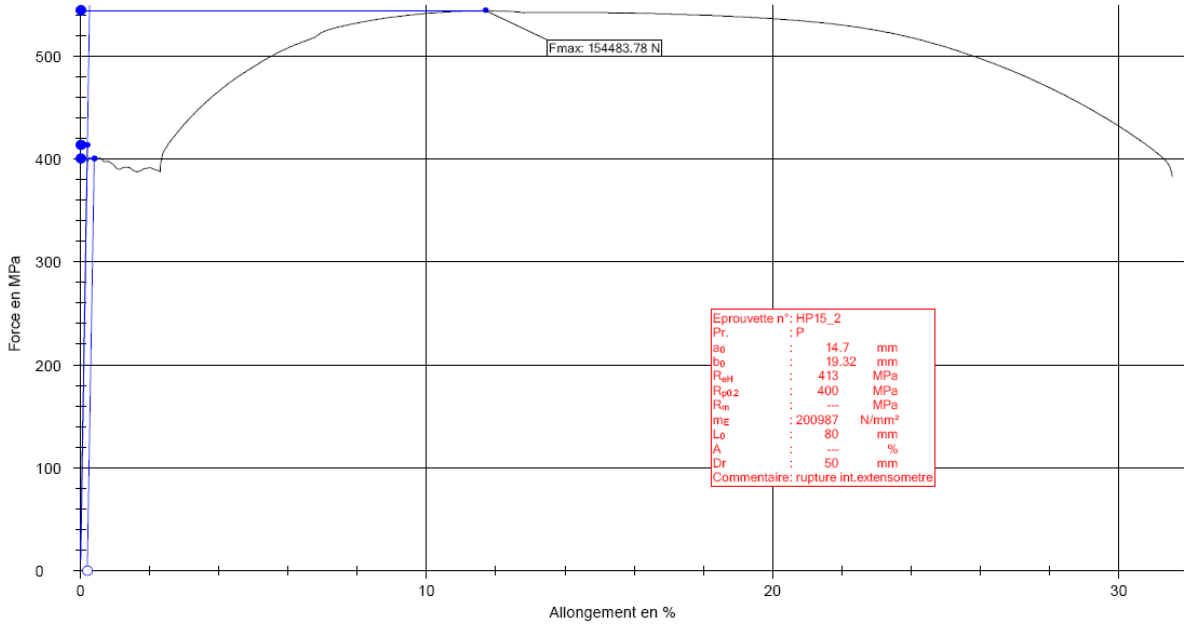

Figure 4.4.5

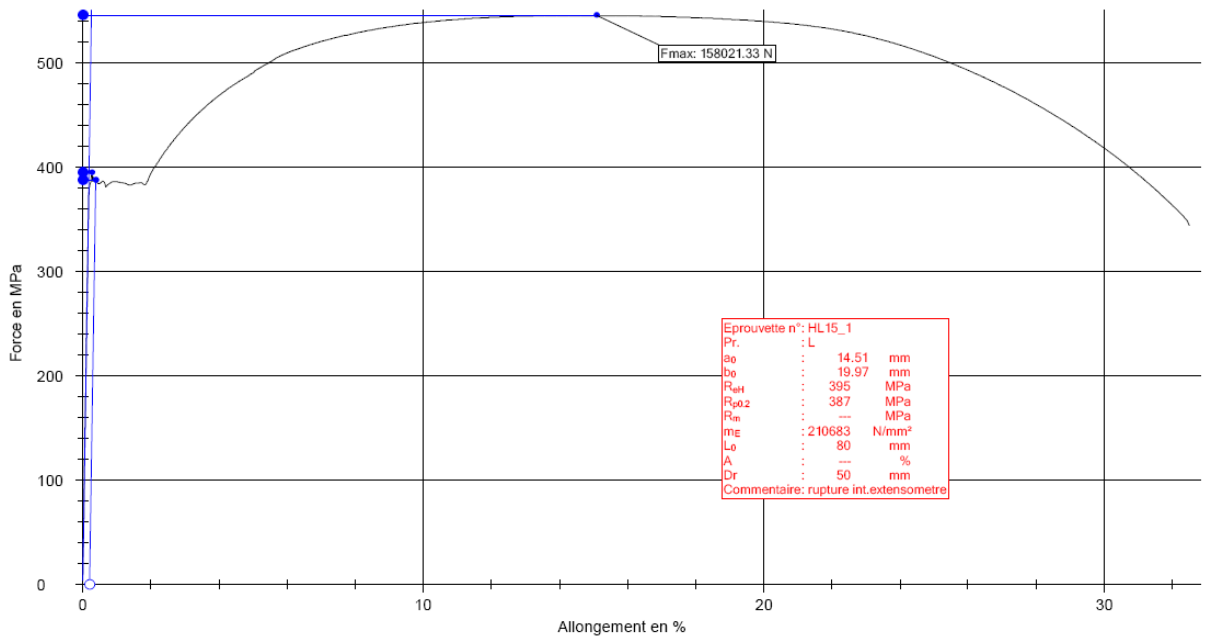

Figure 4.4.6

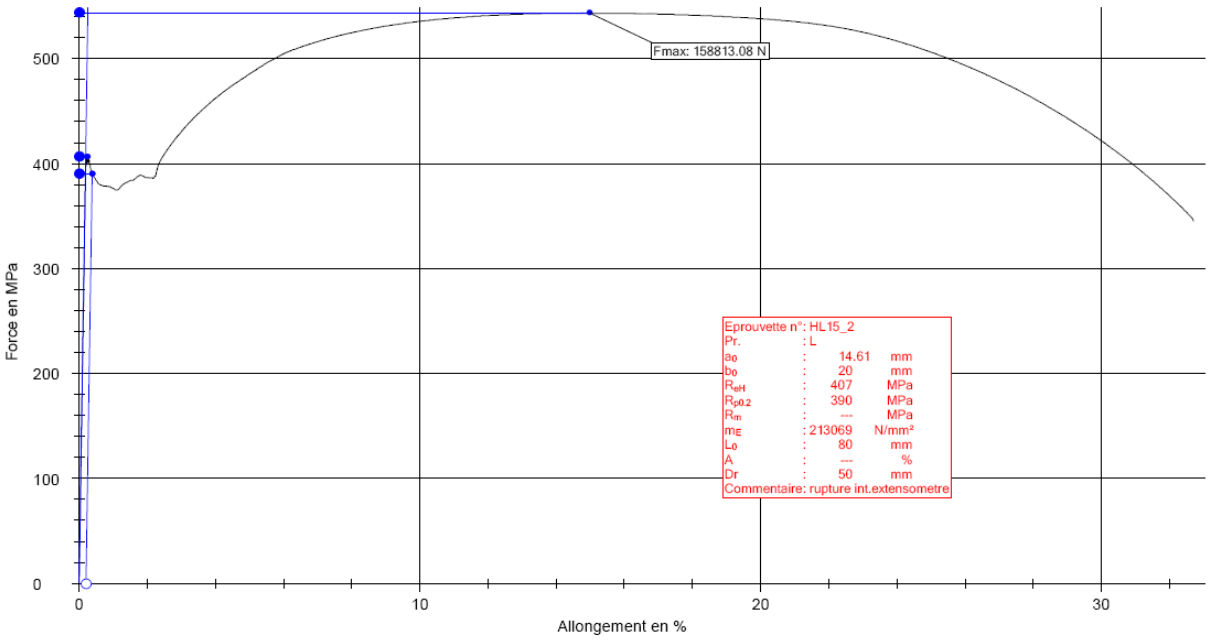

Figure 4.4.7

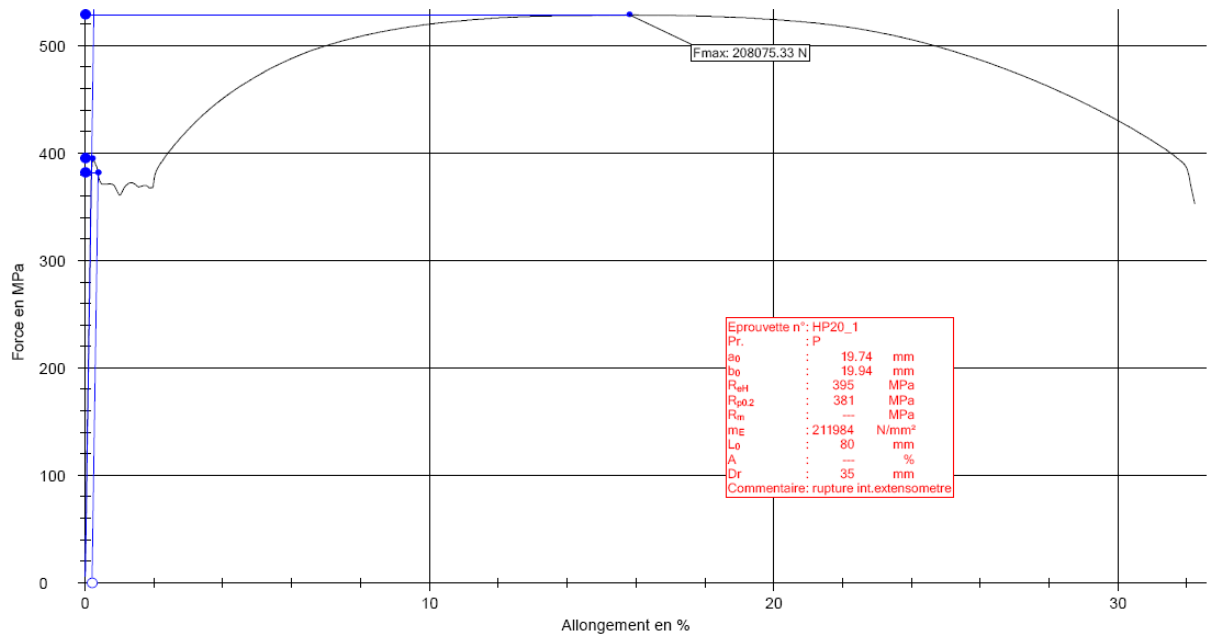

Figure 4.4.8

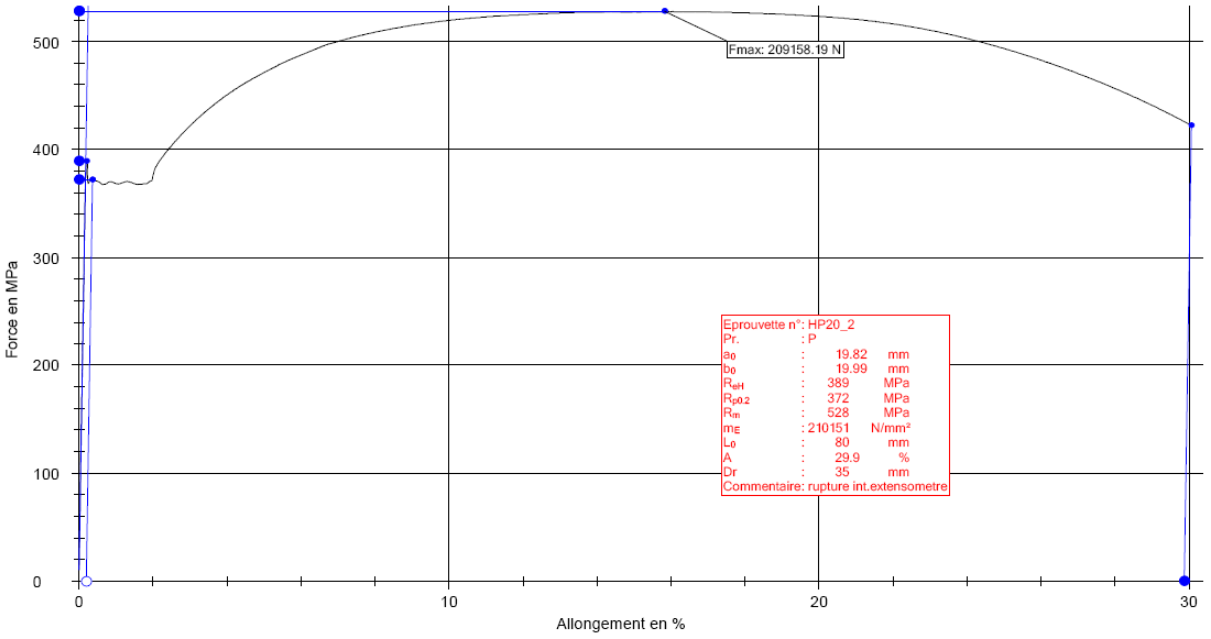

Figure 4.4.9

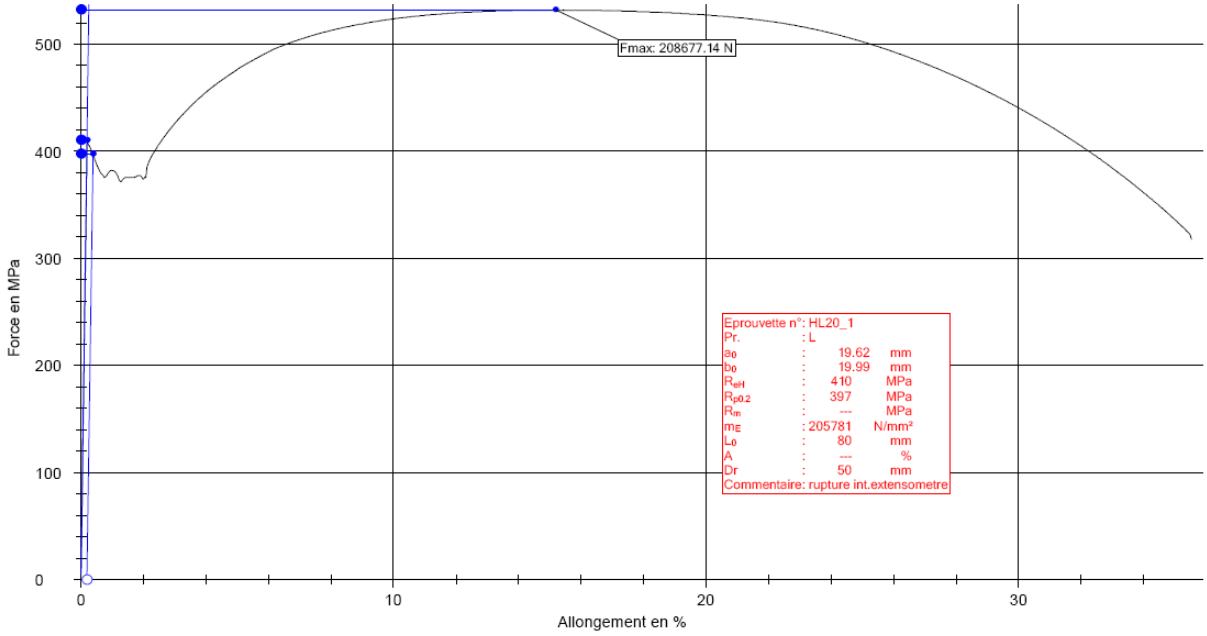

Figure 4.4.10

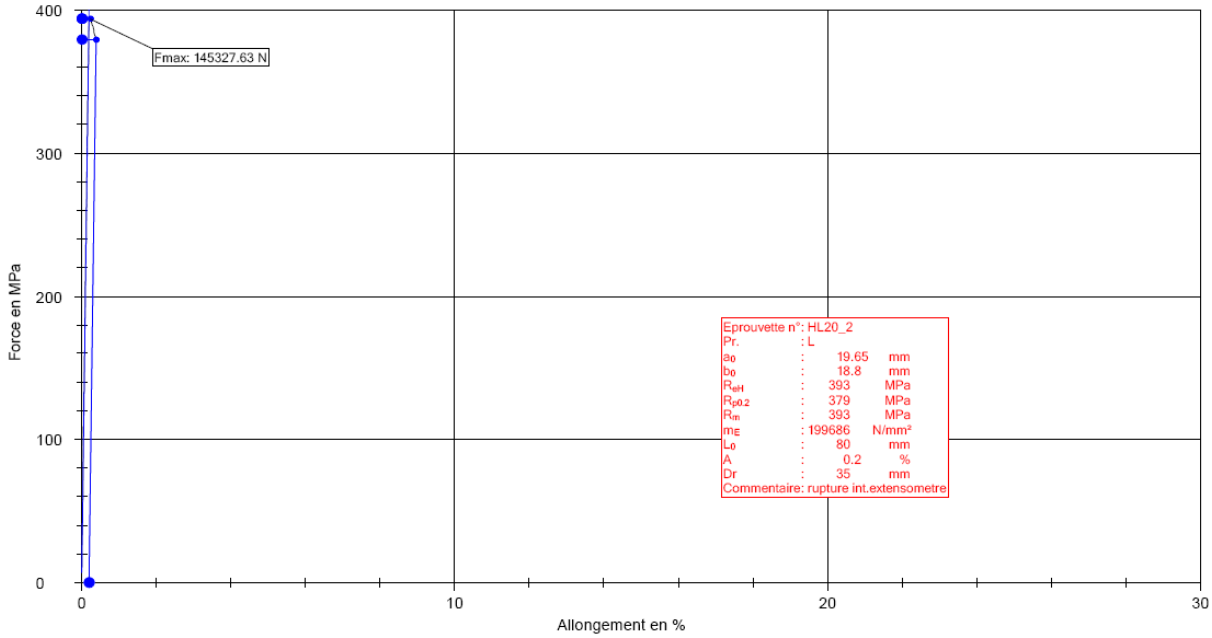

Figure 4.4.11

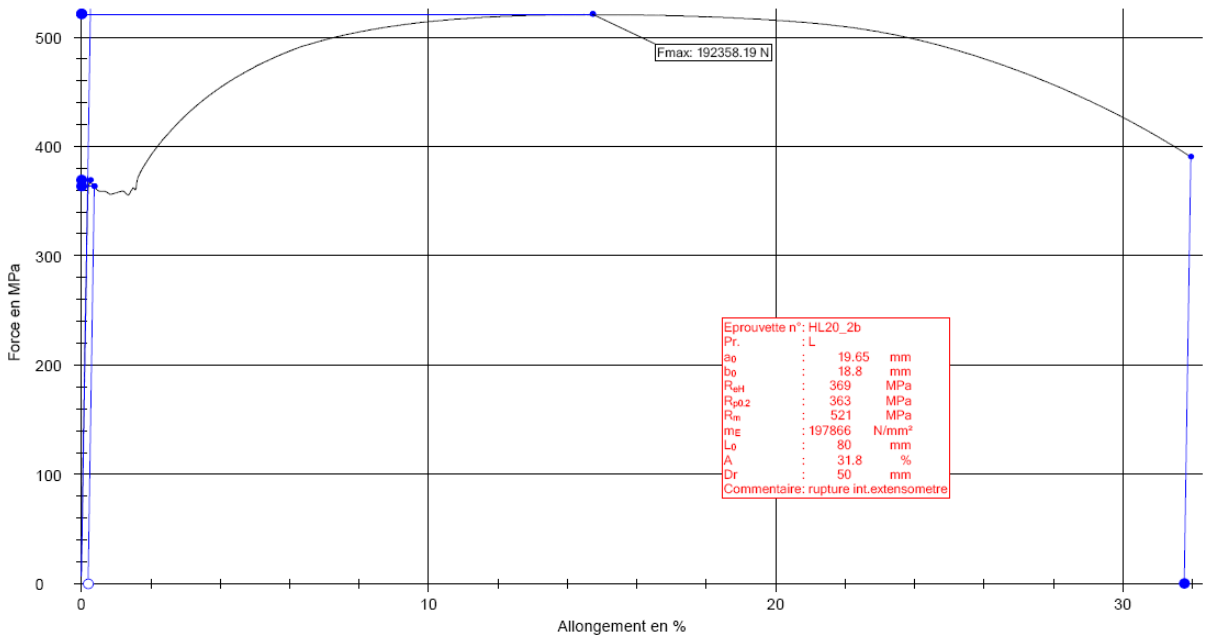

Figure 4.4.12

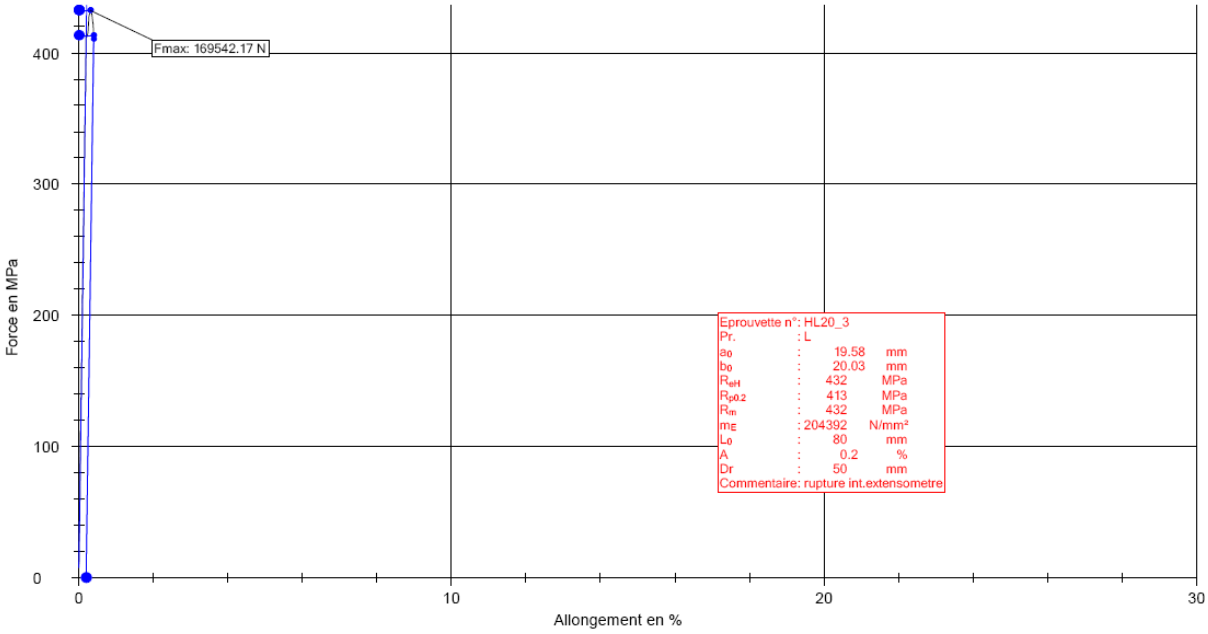

Figure 4.4.13

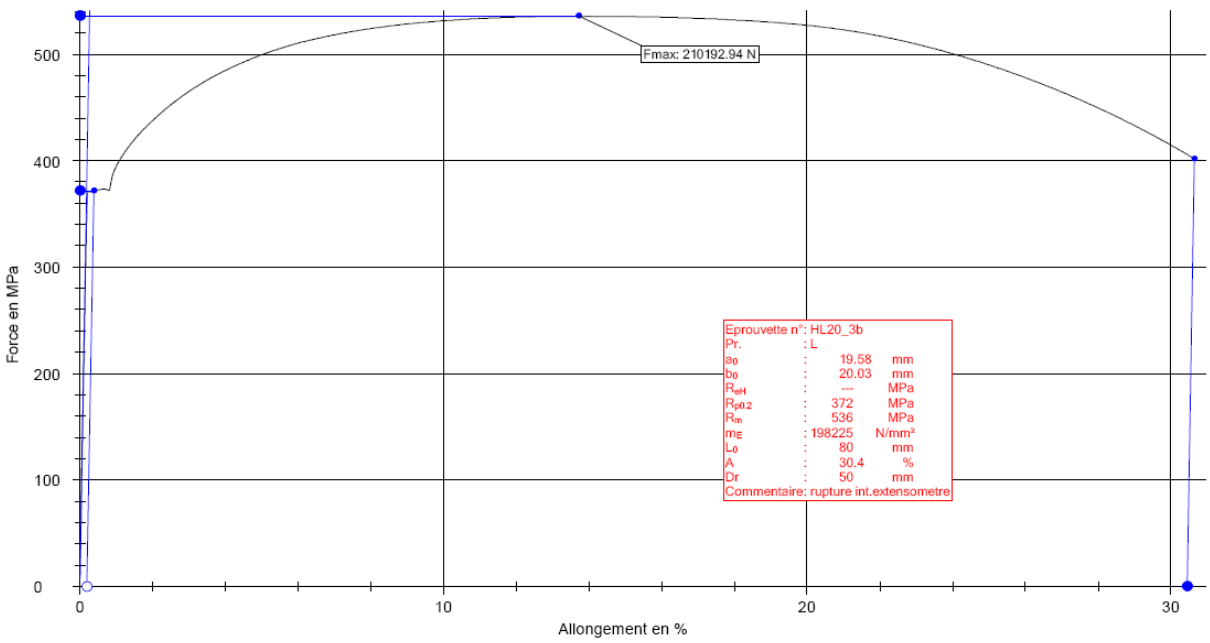

Figure 4.4.14

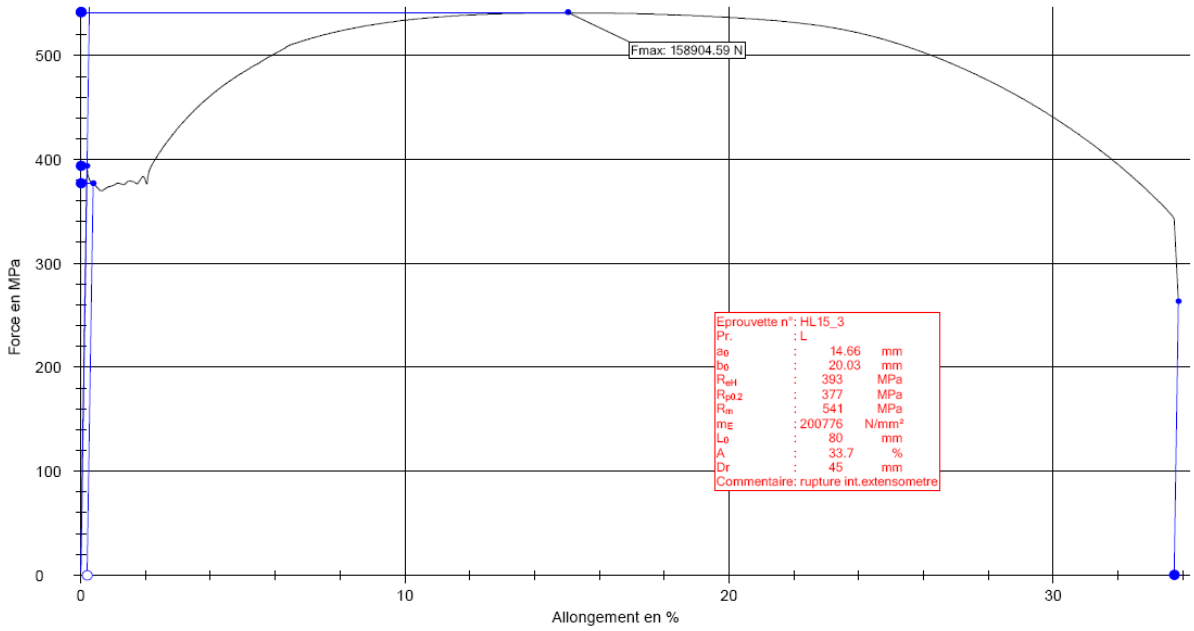

Figure 4.4.15

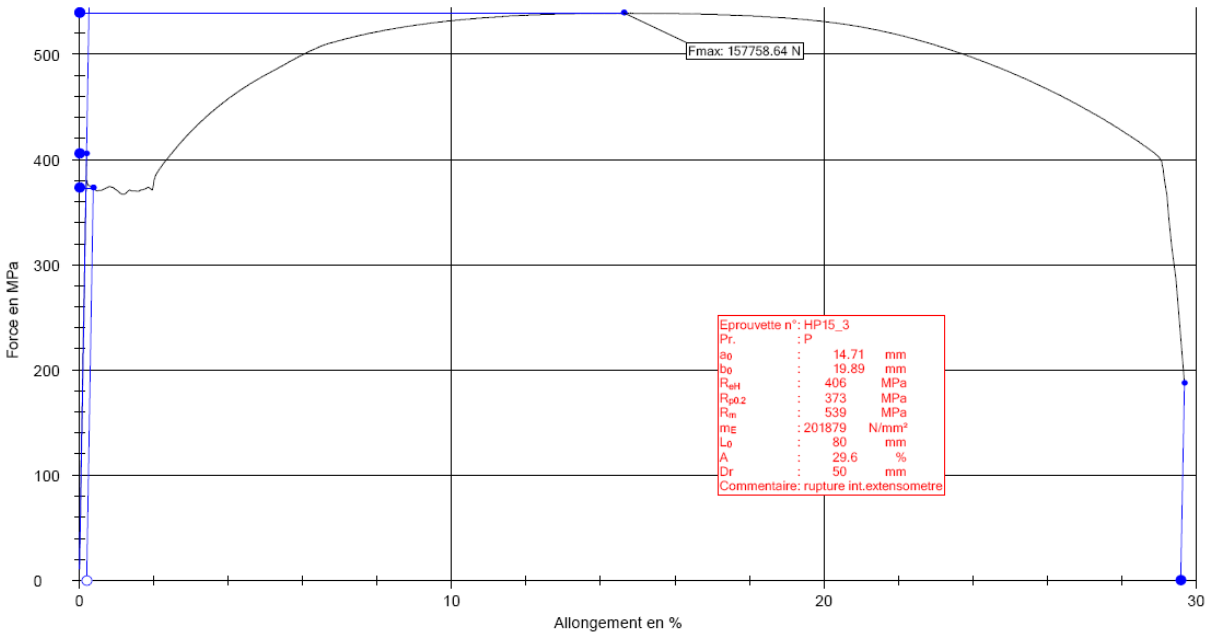

Figure 4.4.16

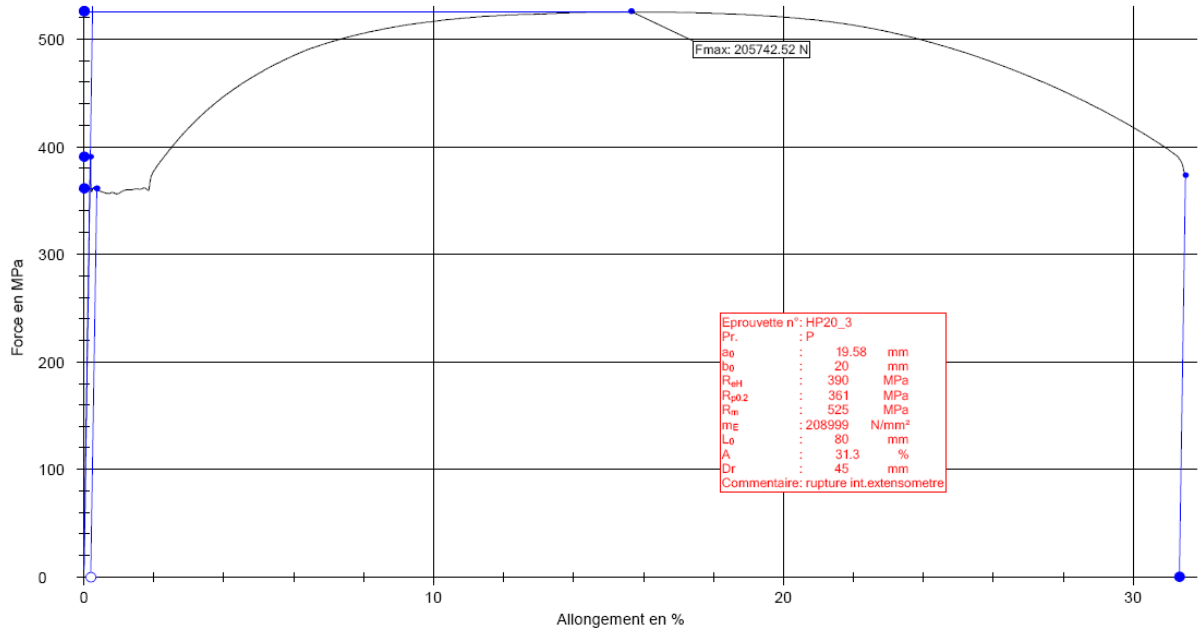

Figure 4.4.17

ANNEX 2: Data of the tests on bolts

Table 4.4.3

Tightening tests on bolts						
Specimen	M27_1Tig		M27_2Tig	M20_1Tig		M20_2Tig
Coefficient k	0,184		0,162	0,164		0,153
Tensile tests on bolts						
Specimen	M27_1	M27_2	M27_3	M20_1	M20_2	M20_3
Maximal load (kN)	425	397	419	231	234	230

Graphic of the tensile tests: In the title of the chart, “M27_1” indicates the specimen name, “D” indicates load-displacement curve, “BT” indicates the strain in the BT strain gauge inside the bolts.

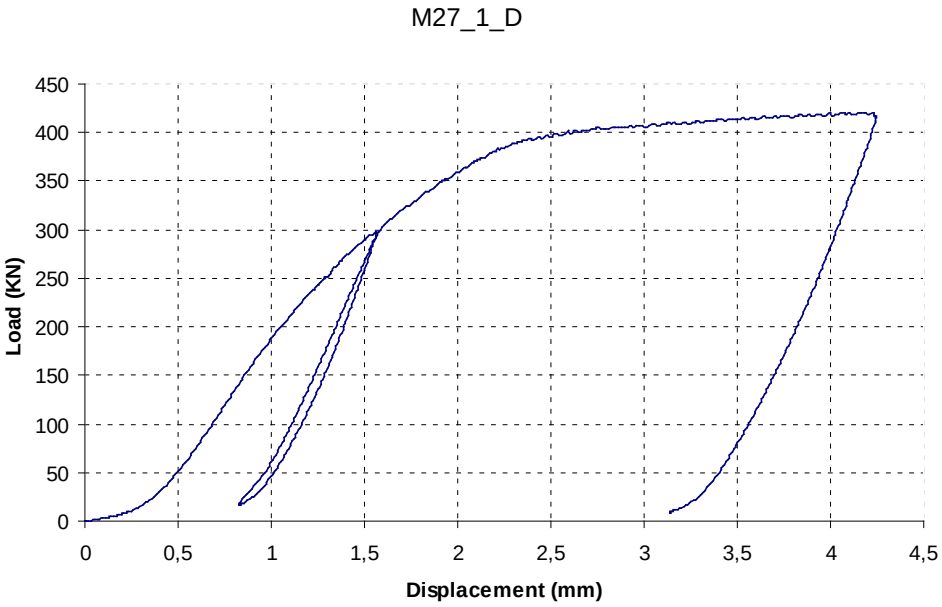

Figure 4.4.18

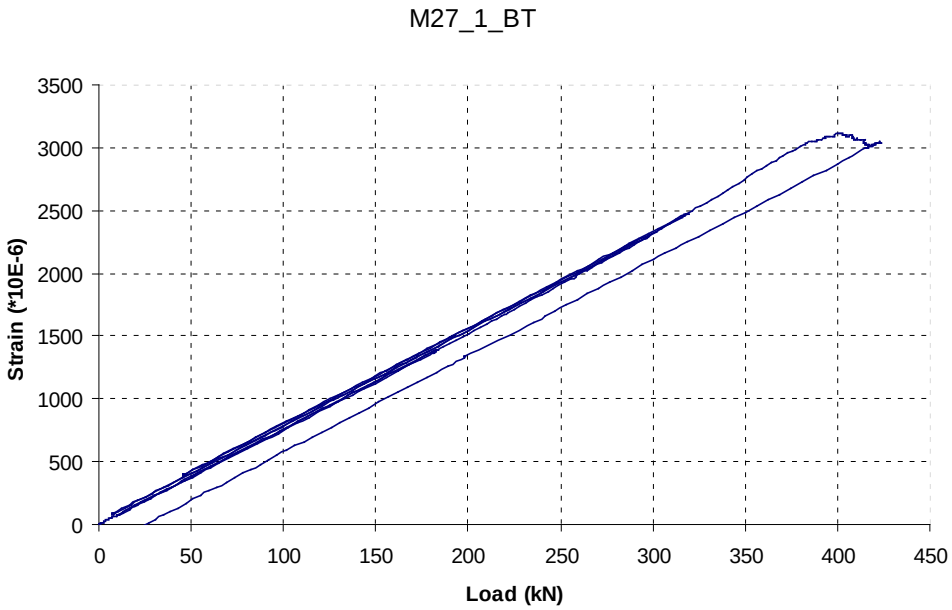

Figure 4.4.19

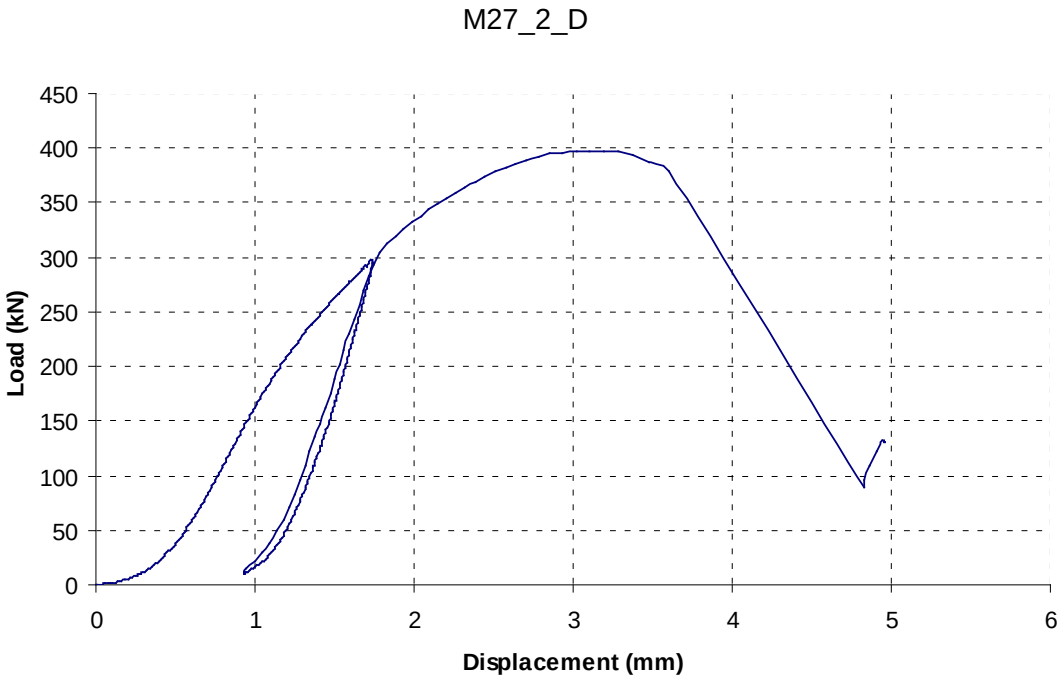

Figure 4.4.20

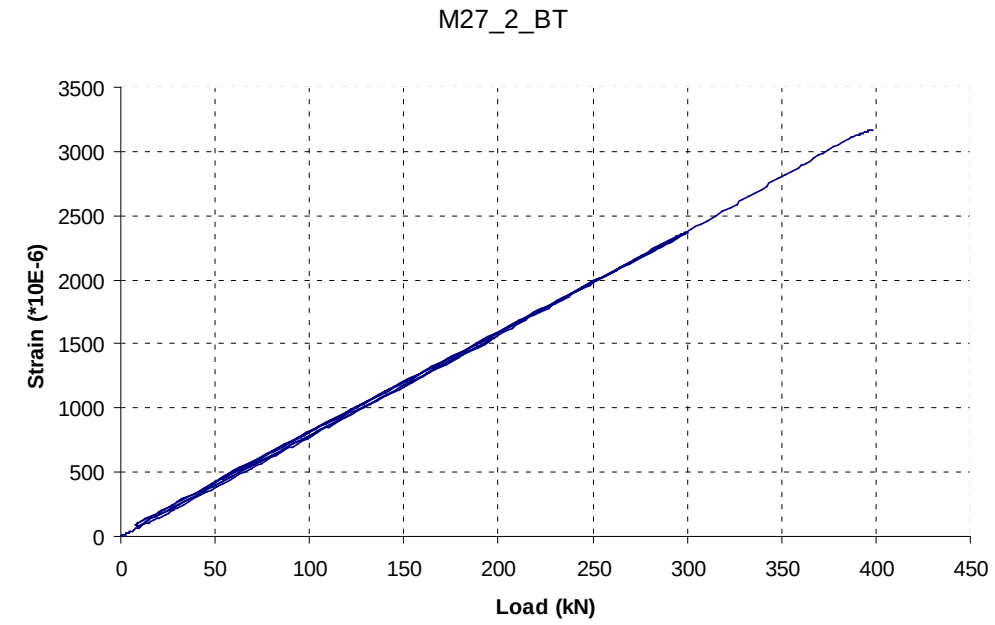

Figure 4.4.21

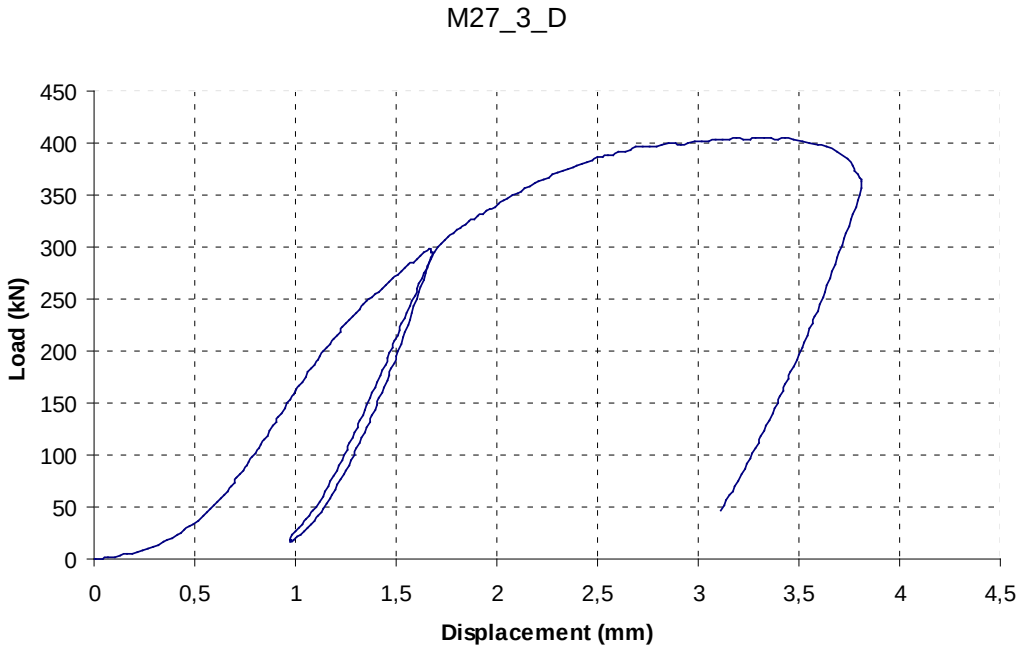

Figure 4.4.22

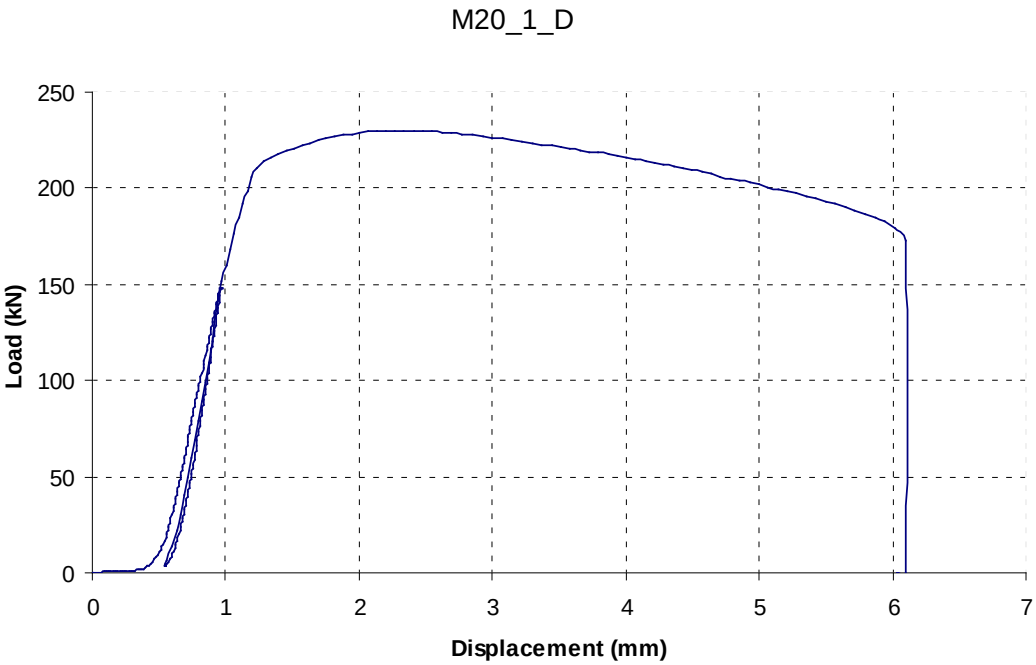

Figure 4.4.23

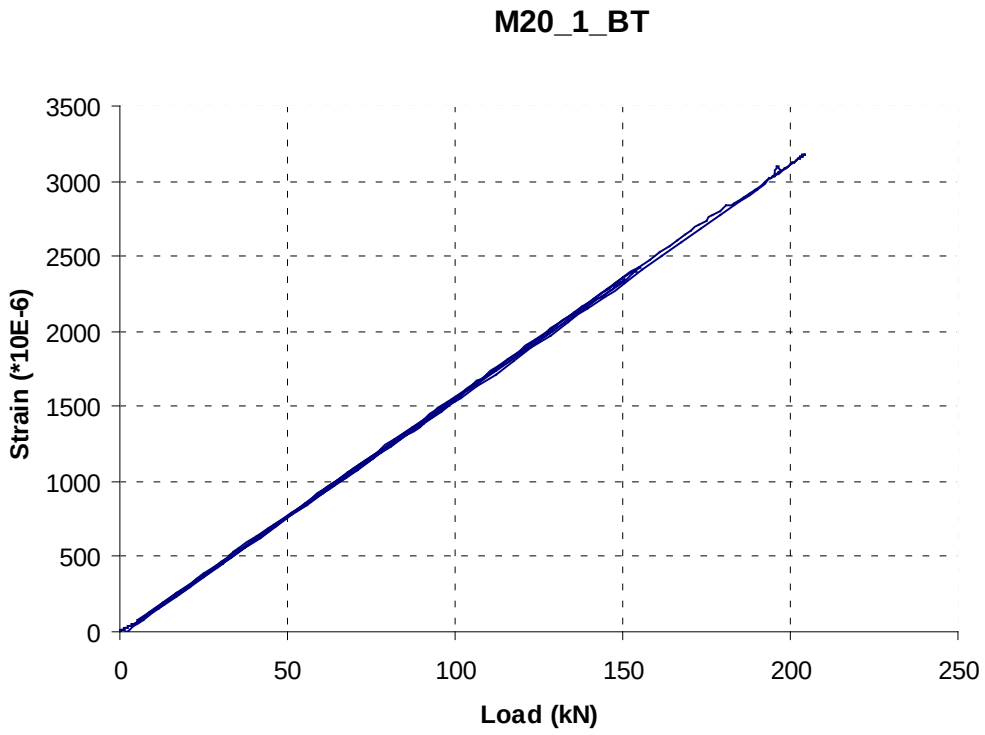

Figure 4.4.24

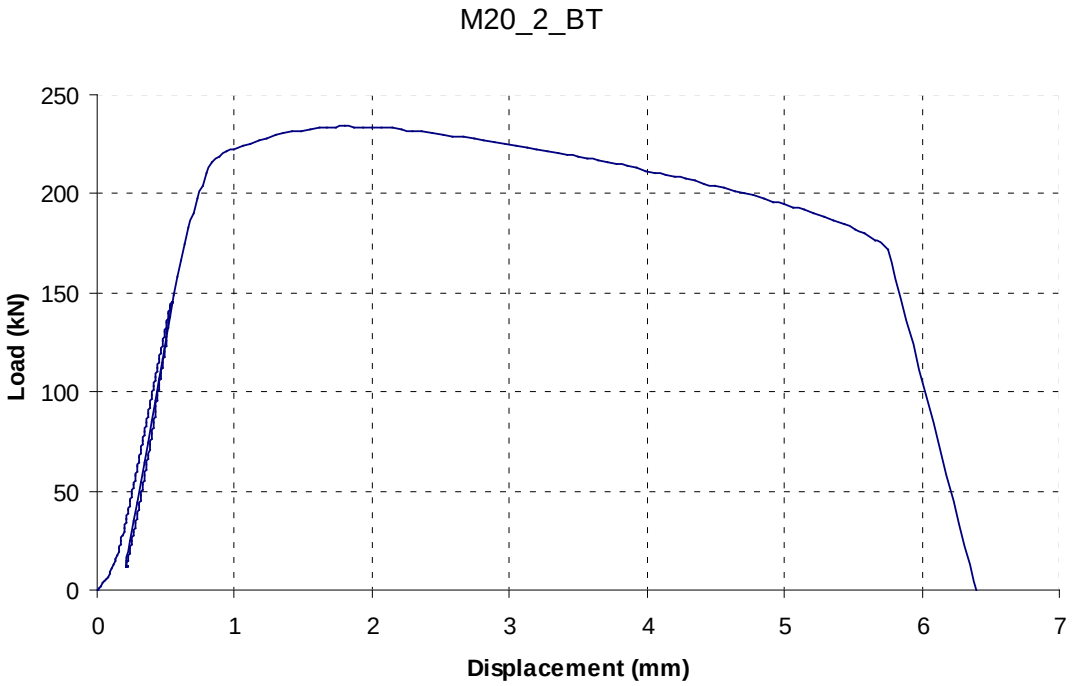

Figure 4.4.25

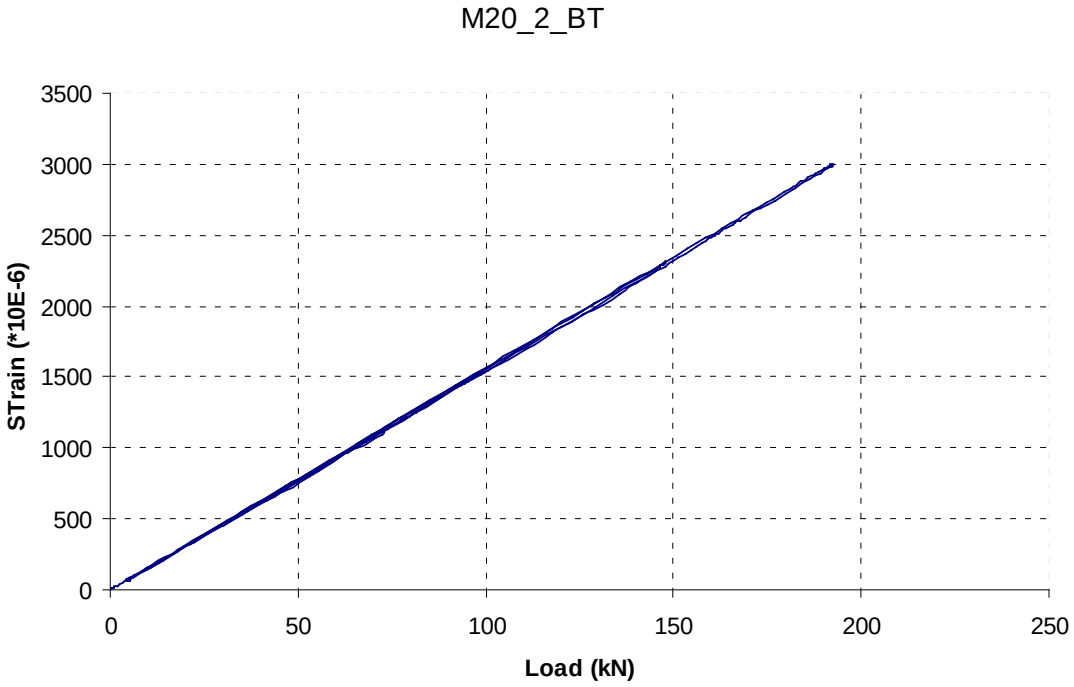

Figure 4.4.26

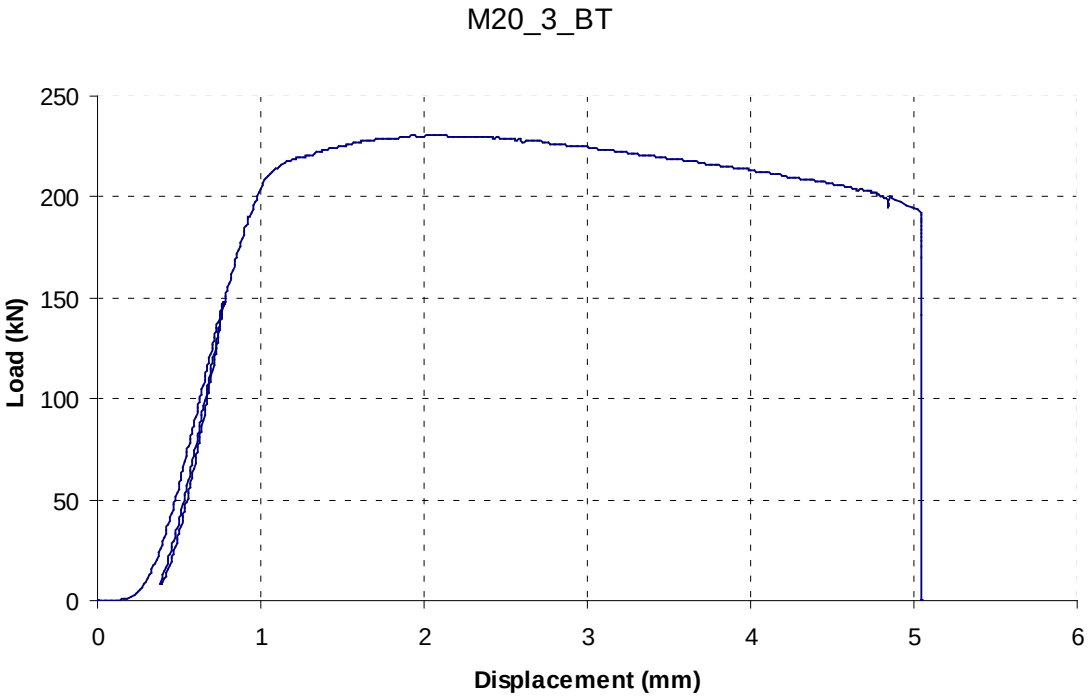

Figure 4.4.27

Graphic data of tightening tests:

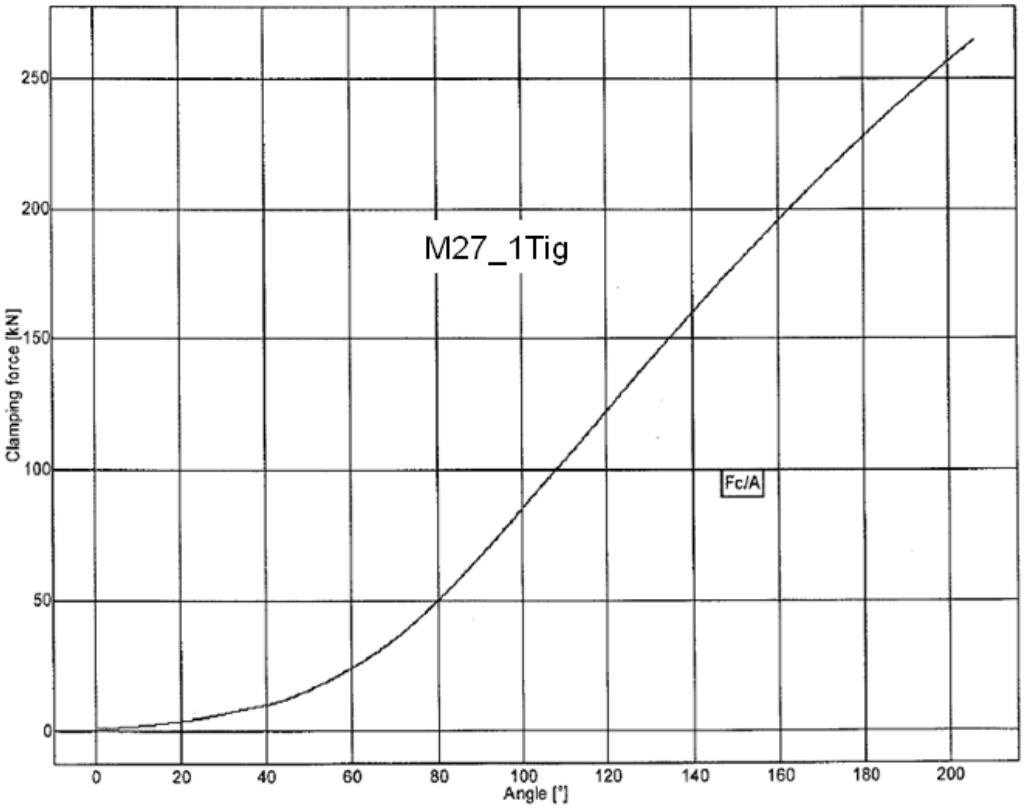

Figure 4.4.28

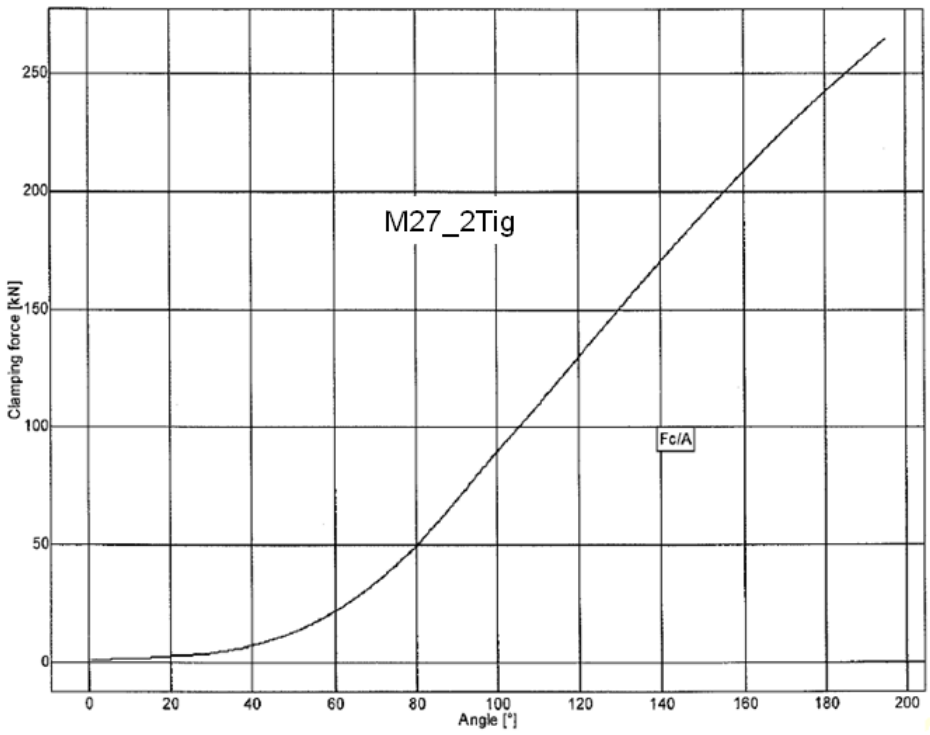

Figure 4.4.29

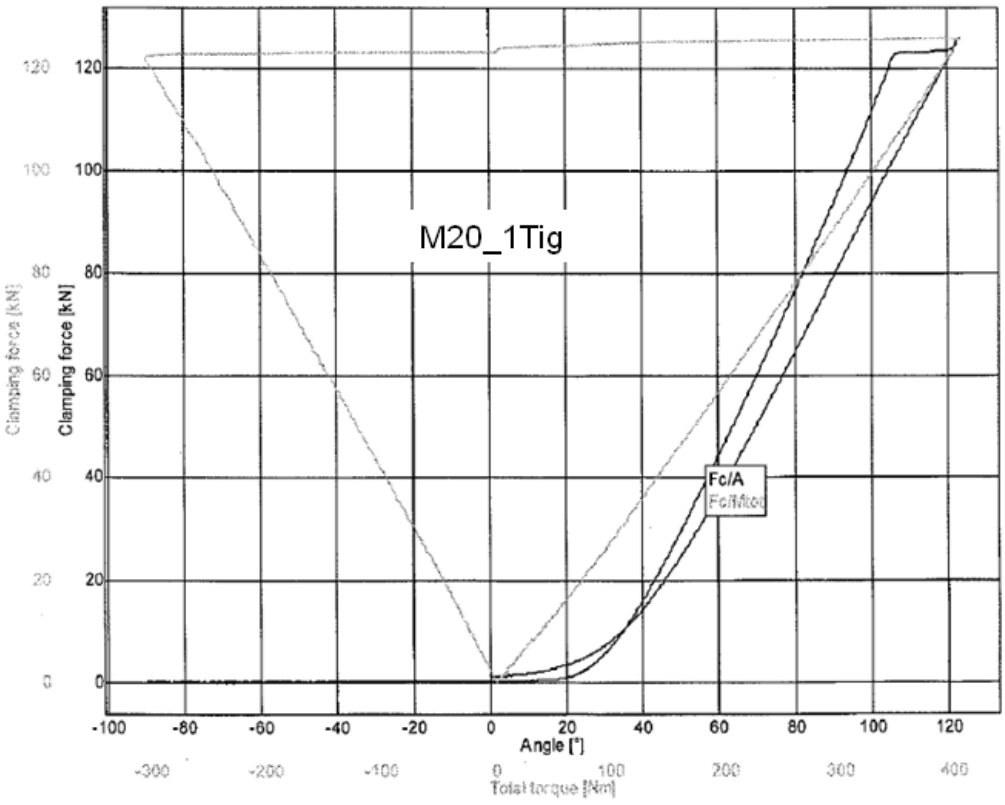

Figure 4.4.30

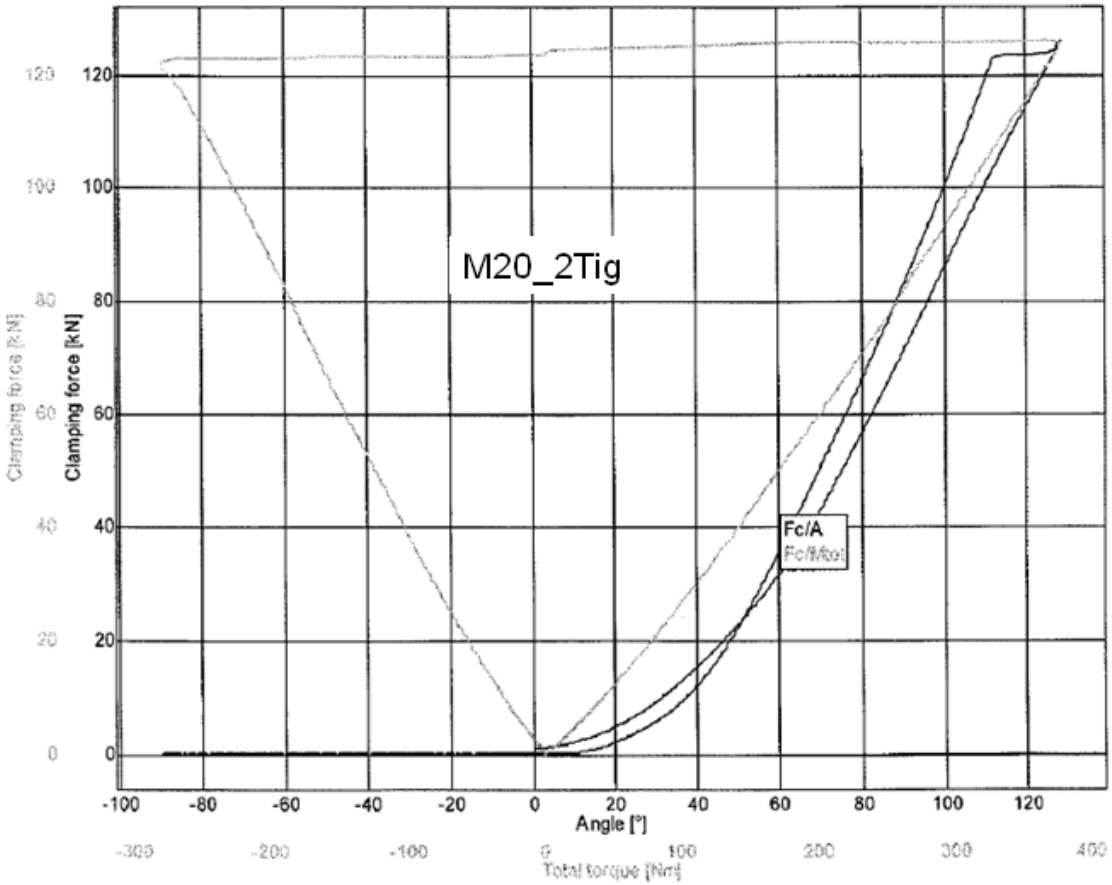

Figure 4.4.31

ANNEX 3: Graphic data of the tightening of the bolts

In the title of the charts, first term ("S1" for example) indicates the specimen name, the second term ("BT", "FL","FR","QF") indicates the strain gauge name (see Table 3 in Section 4.2.2.6 of the Six-monthly Report issued in September 2011).

Specimen S1:

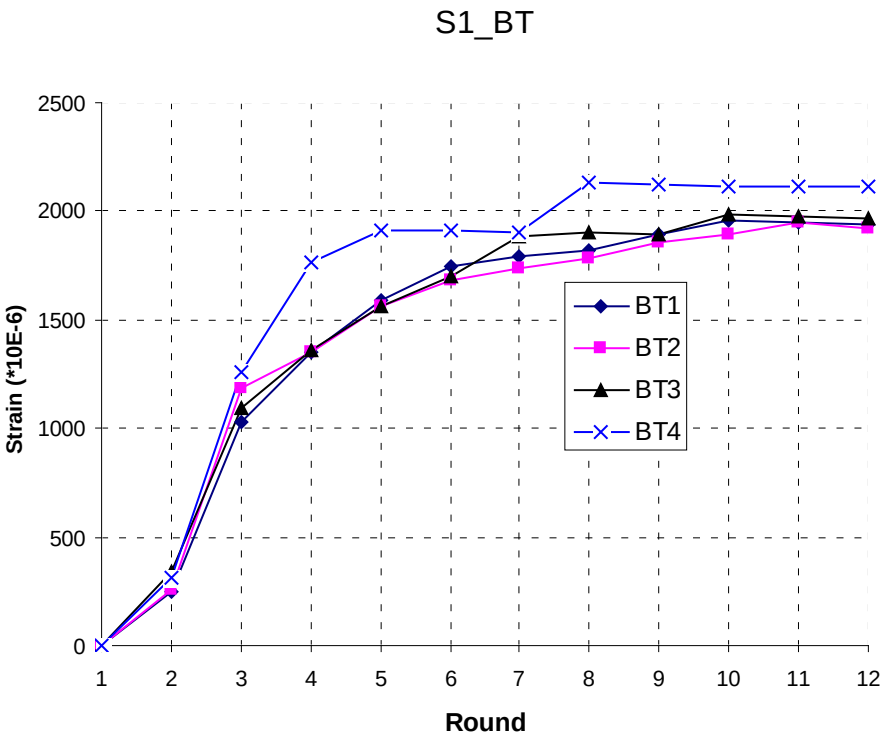

Figure 4.4.32

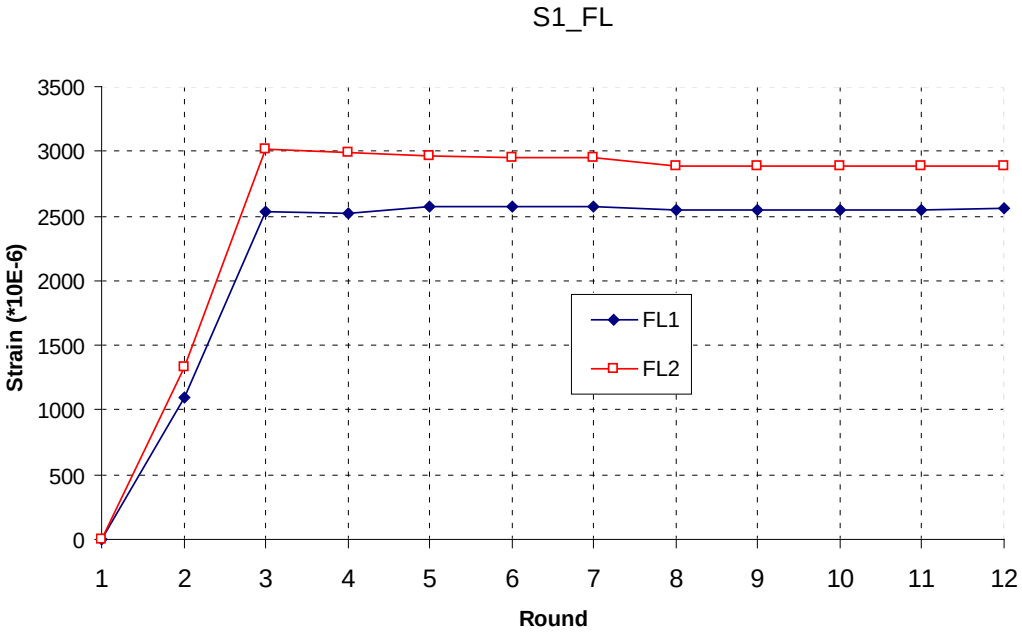

Figure 4.4.33

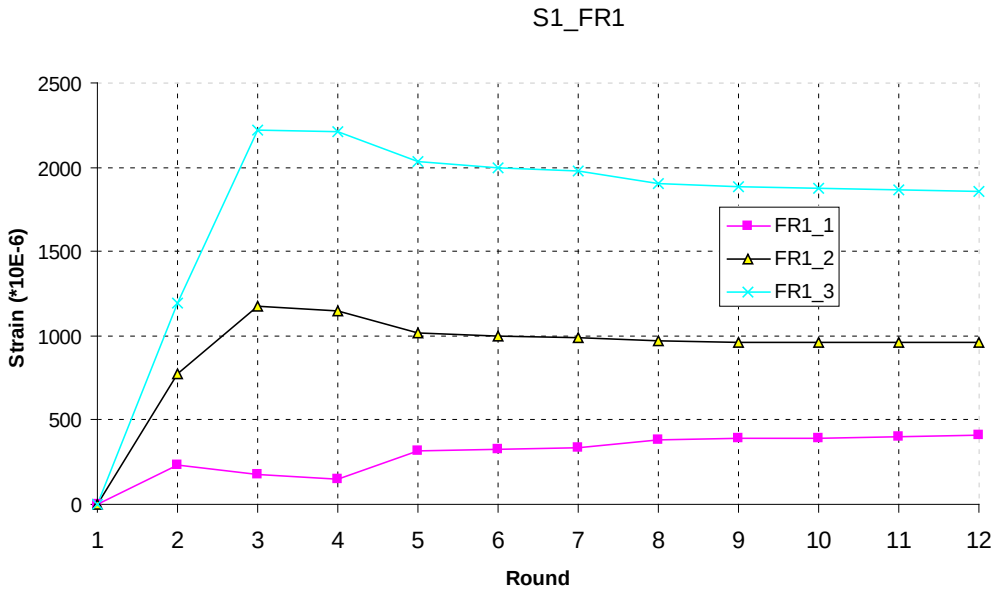

Figure 4.4.34

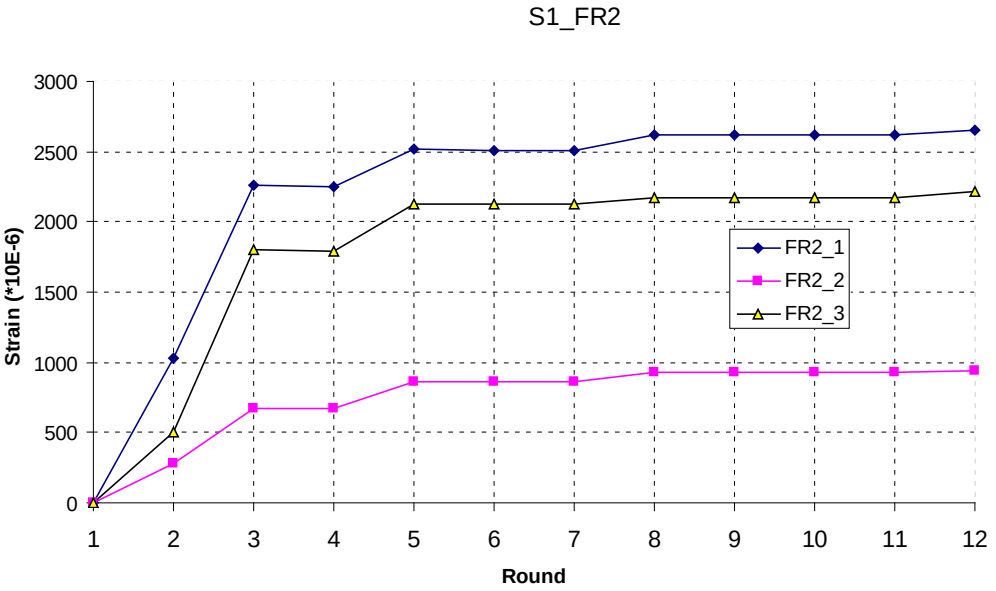

Figure 4.4.35

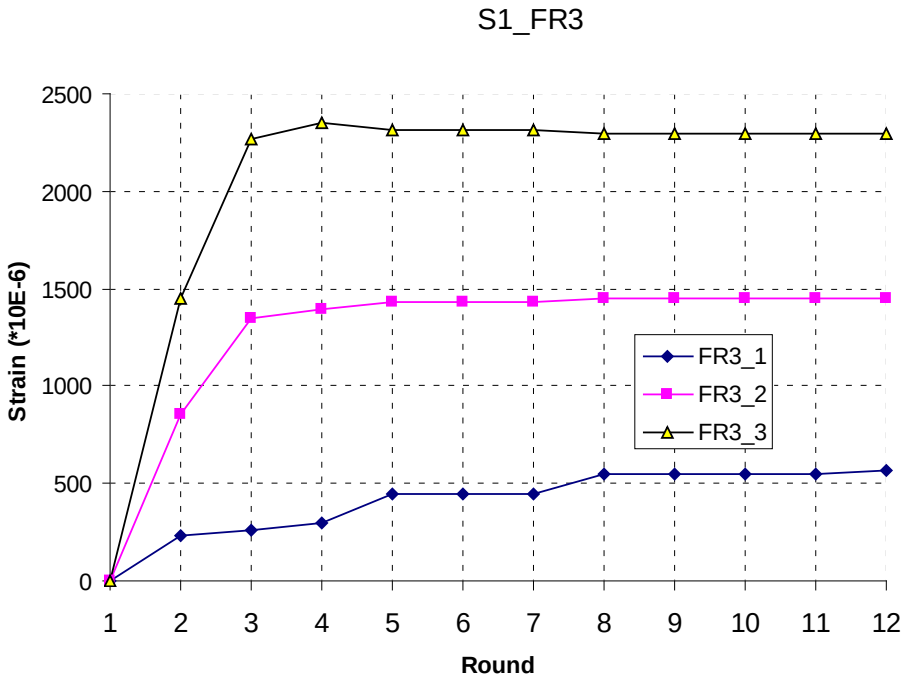

Figure 4.4.36

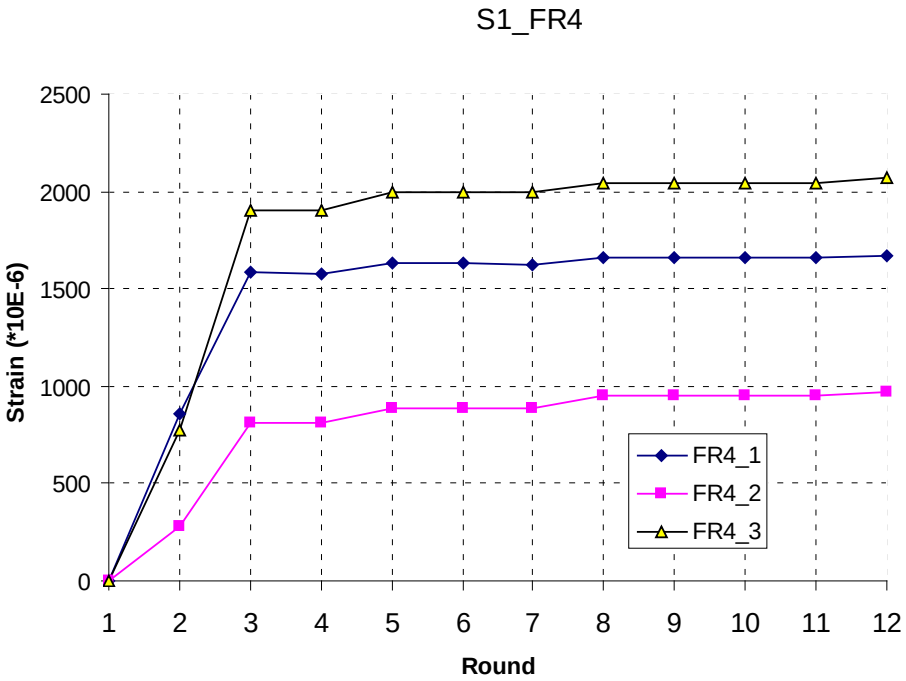

Figure 4.4.37

Specimen S2:

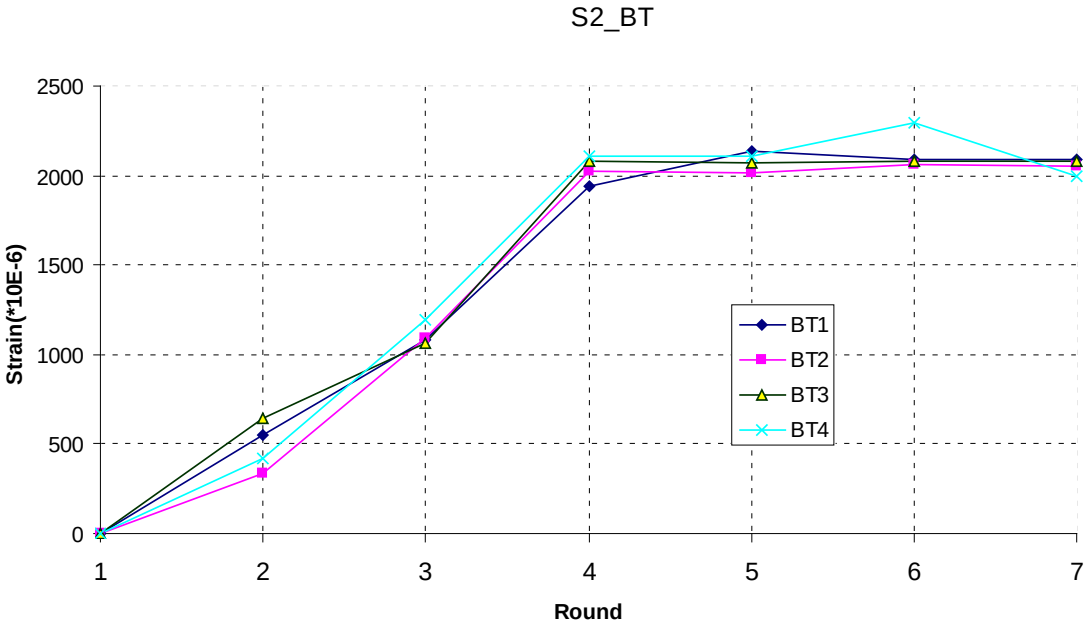

Figure 4.4.38

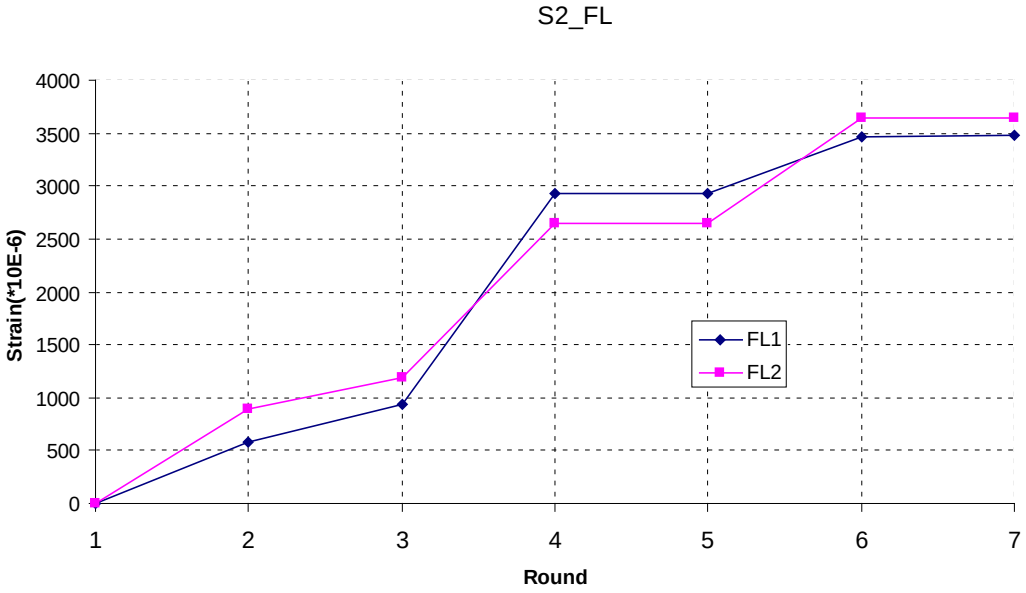

Figure 4.4.39

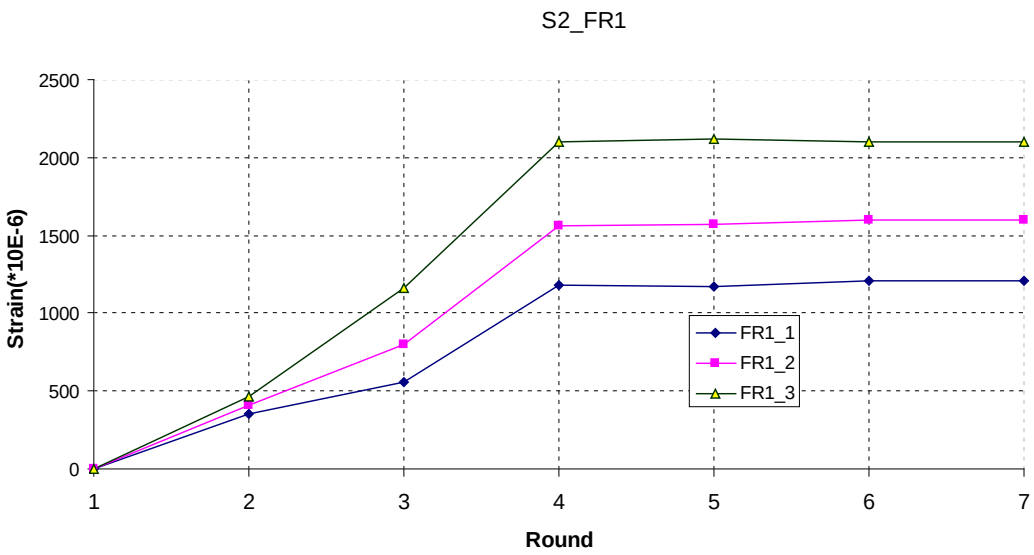

Figure 4.4.40

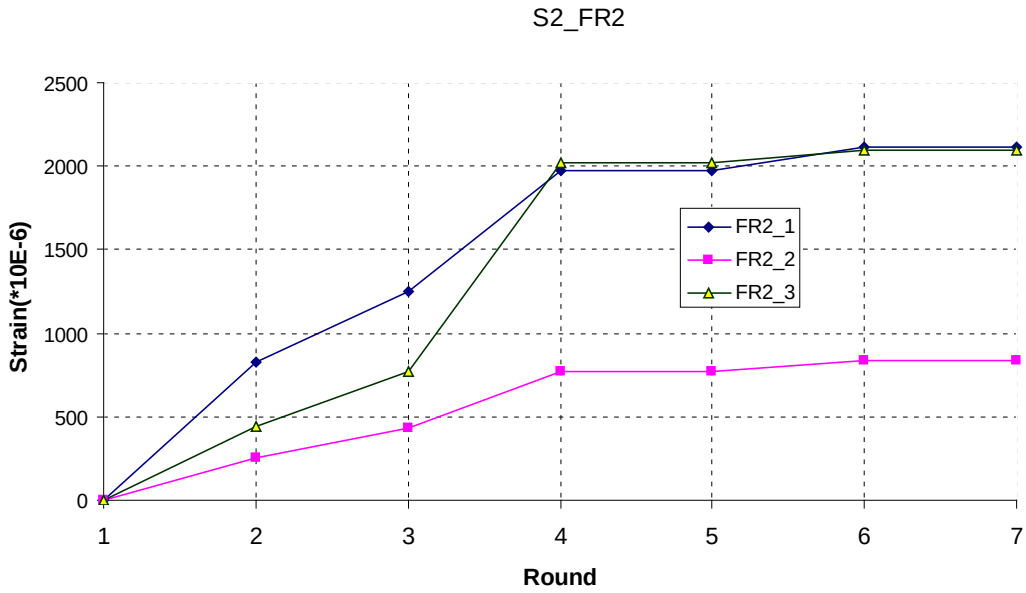

Figure 4.4.41

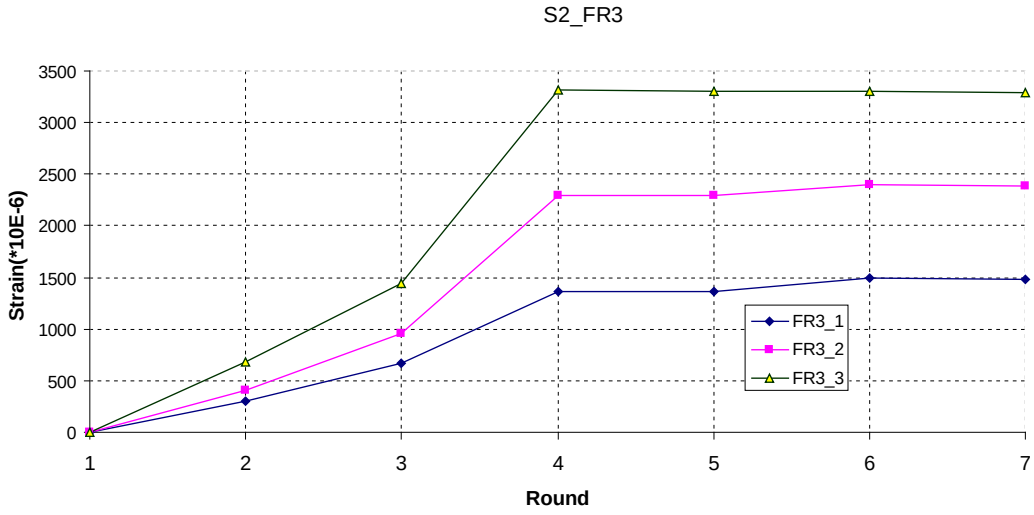

Figure 4.4.42

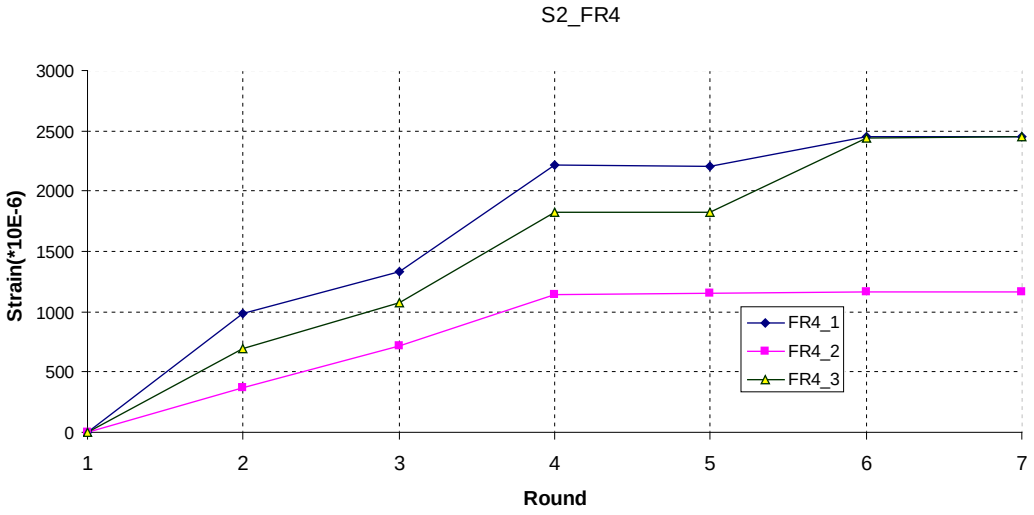

Figure 4.4.43

Specimen S3:

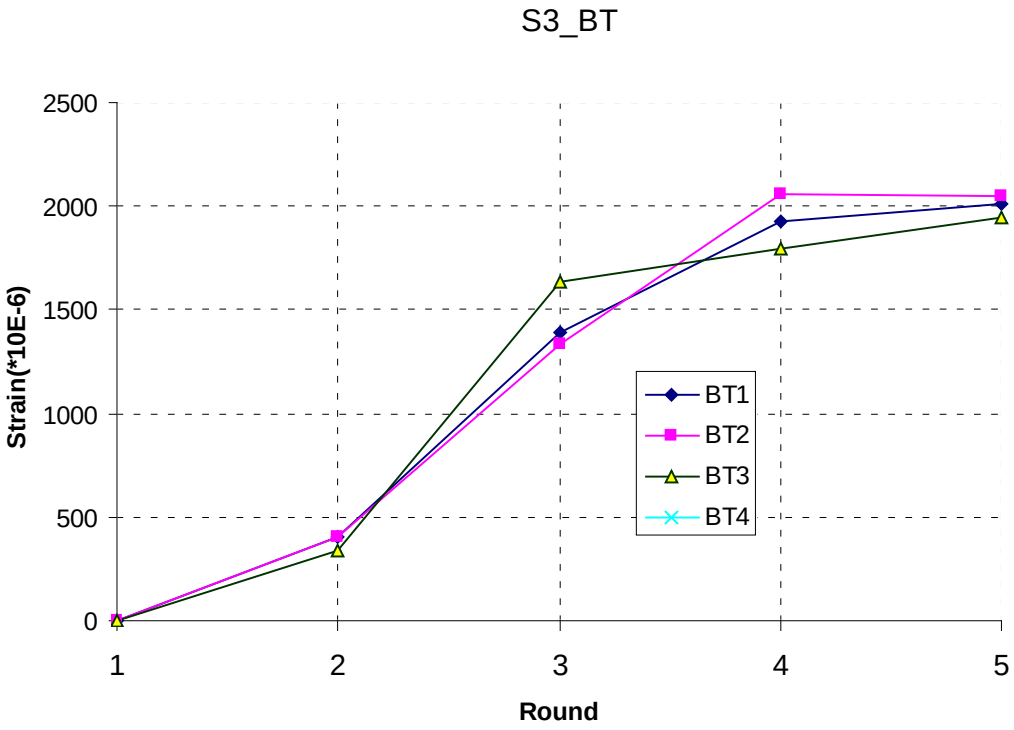

Figure 4.4.44

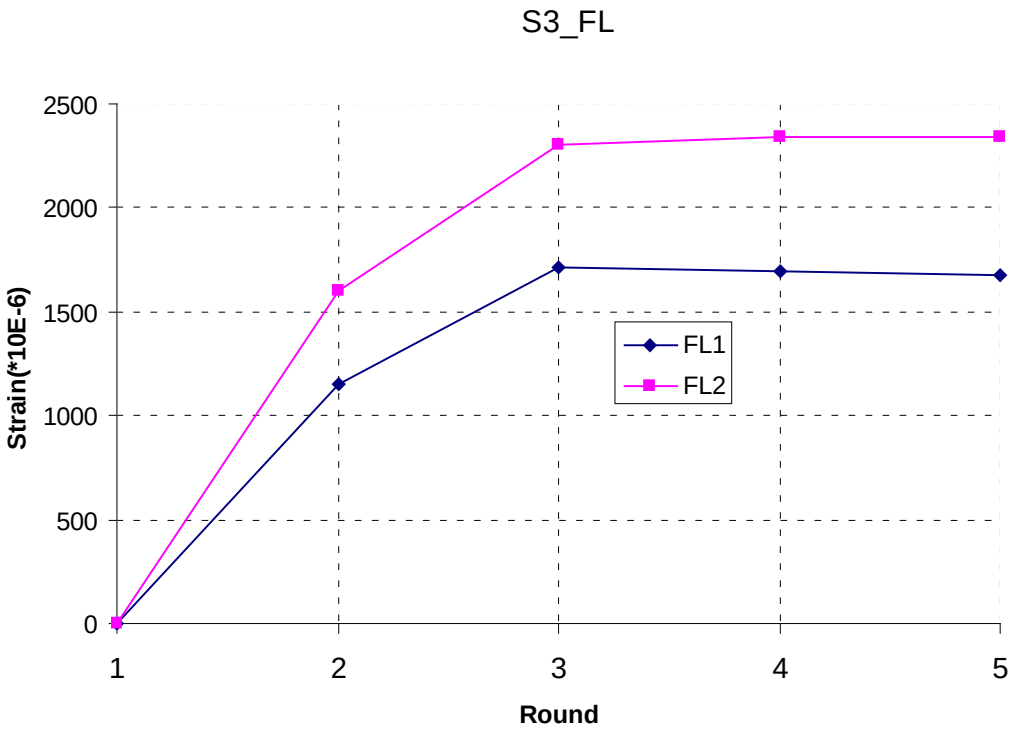

Figure 4.4.45

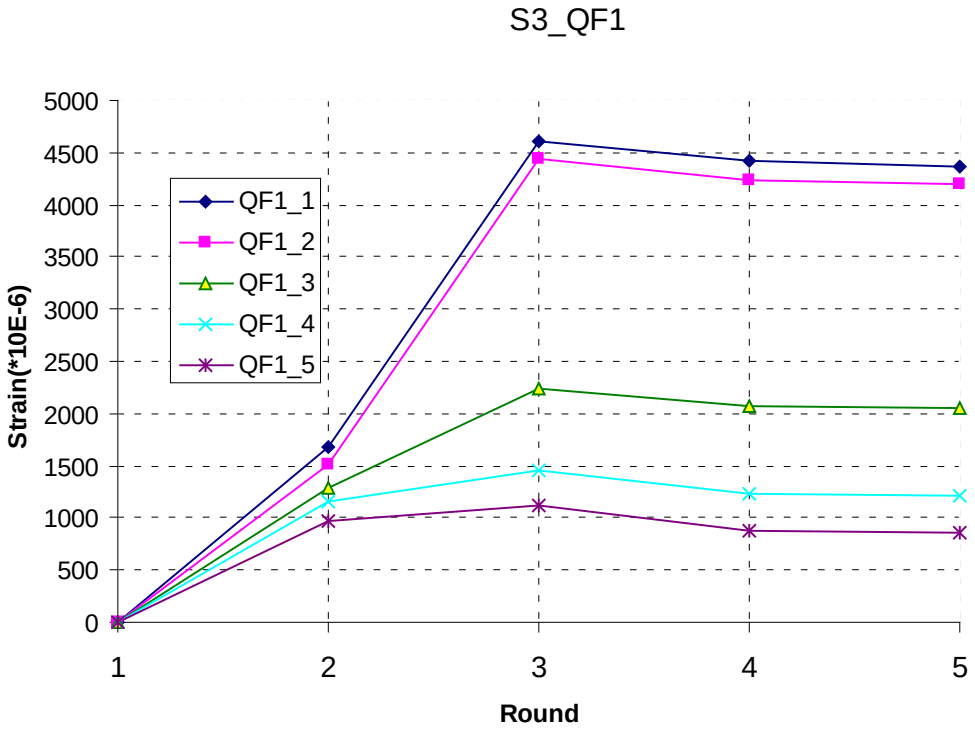

Figure 4.4.46

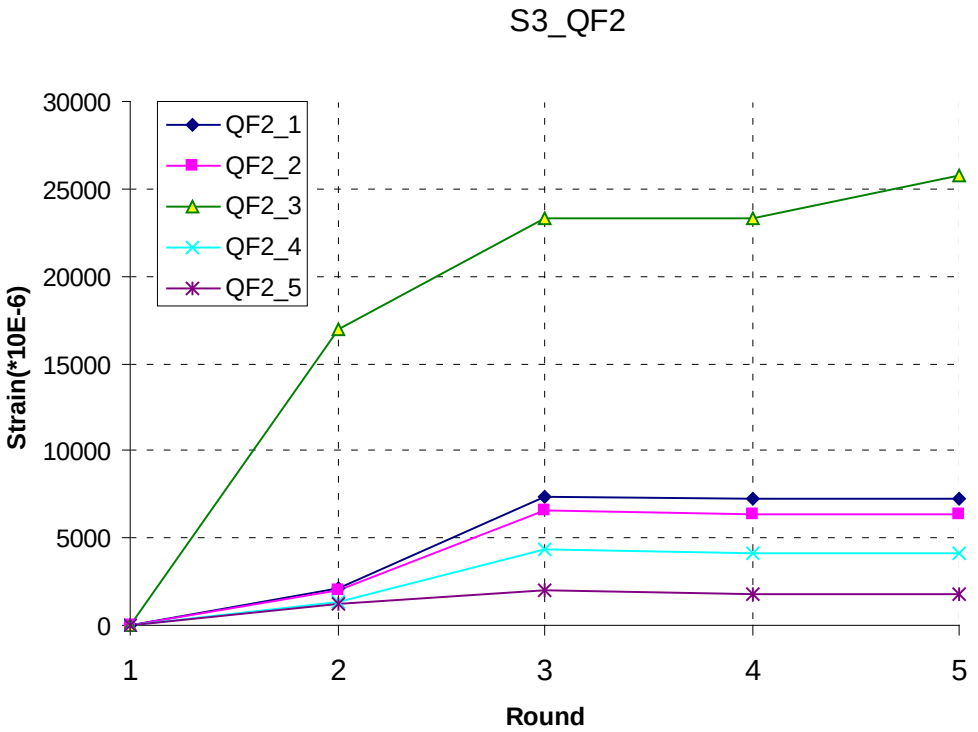

Figure 4.4.47

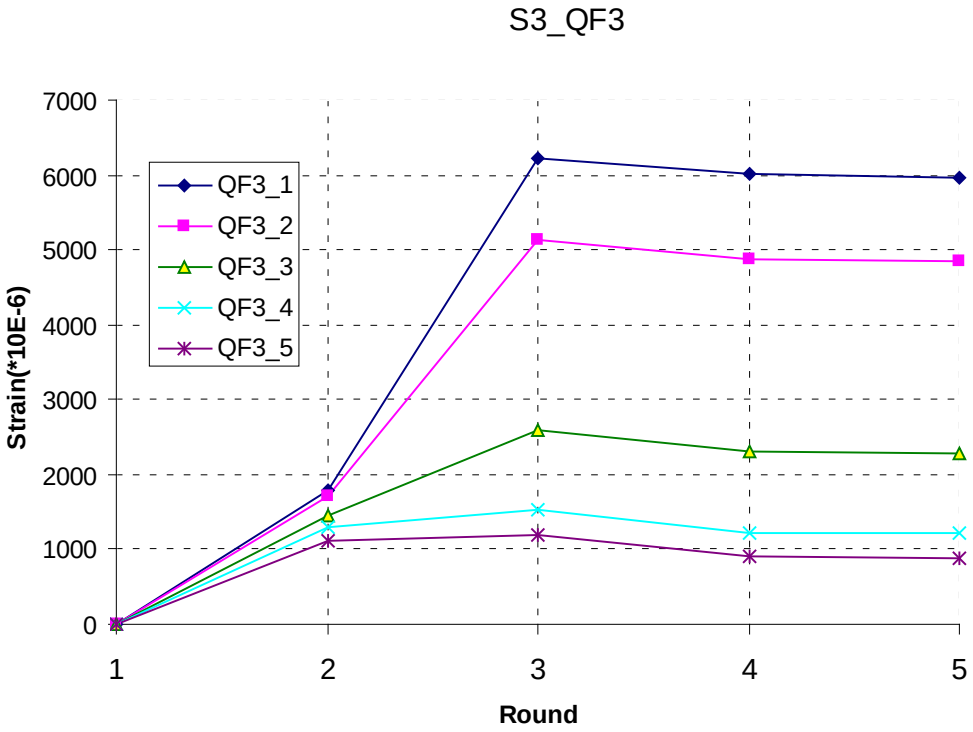

Figure 4.4.48

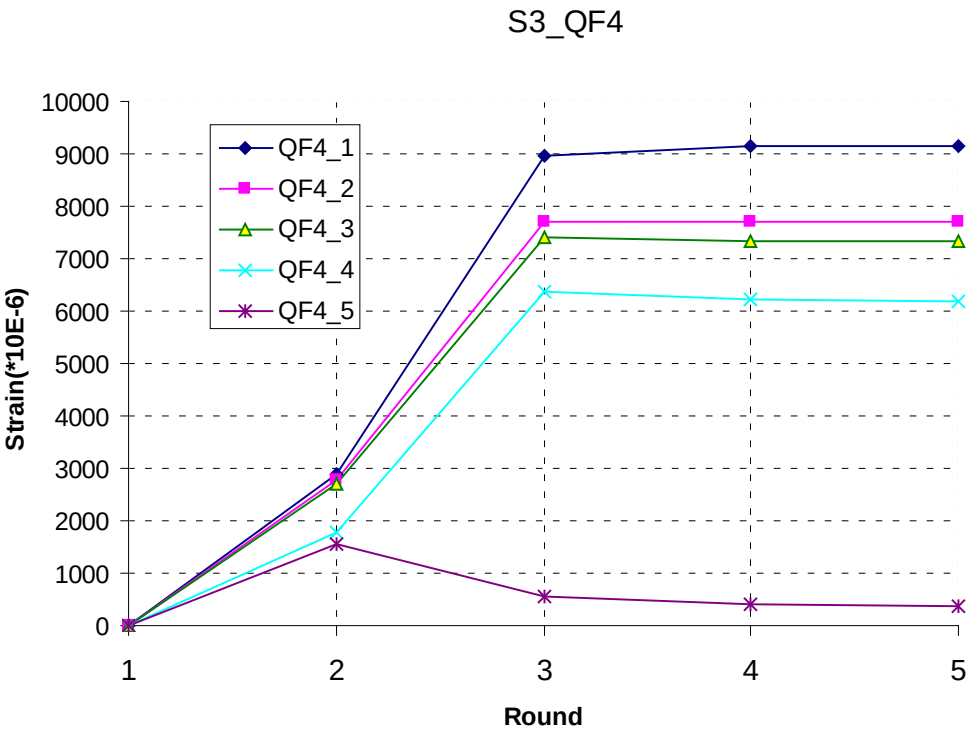

Figure 4.4.49

Specimen S4:

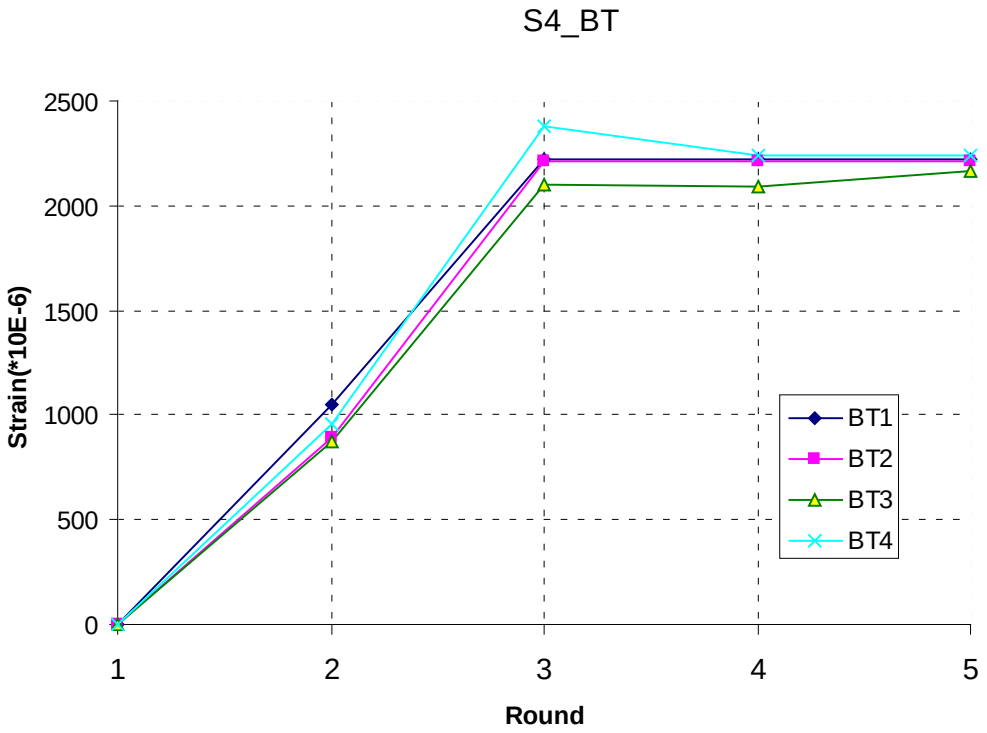

Figure 4.4.50

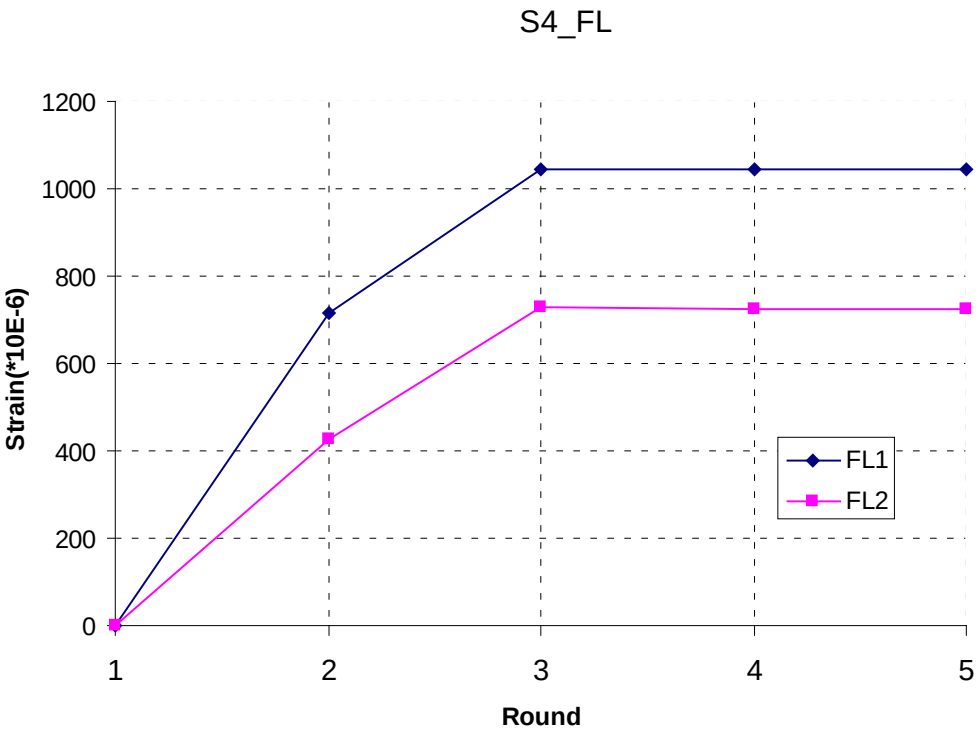

Figure 4.4.51

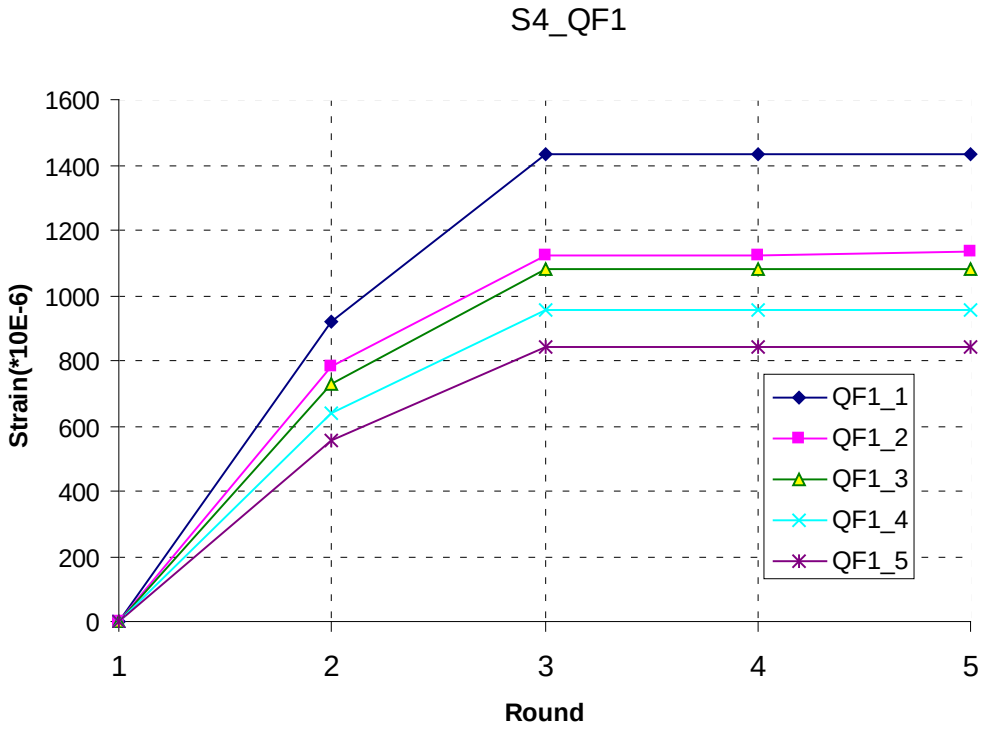

Figure 4.4.52

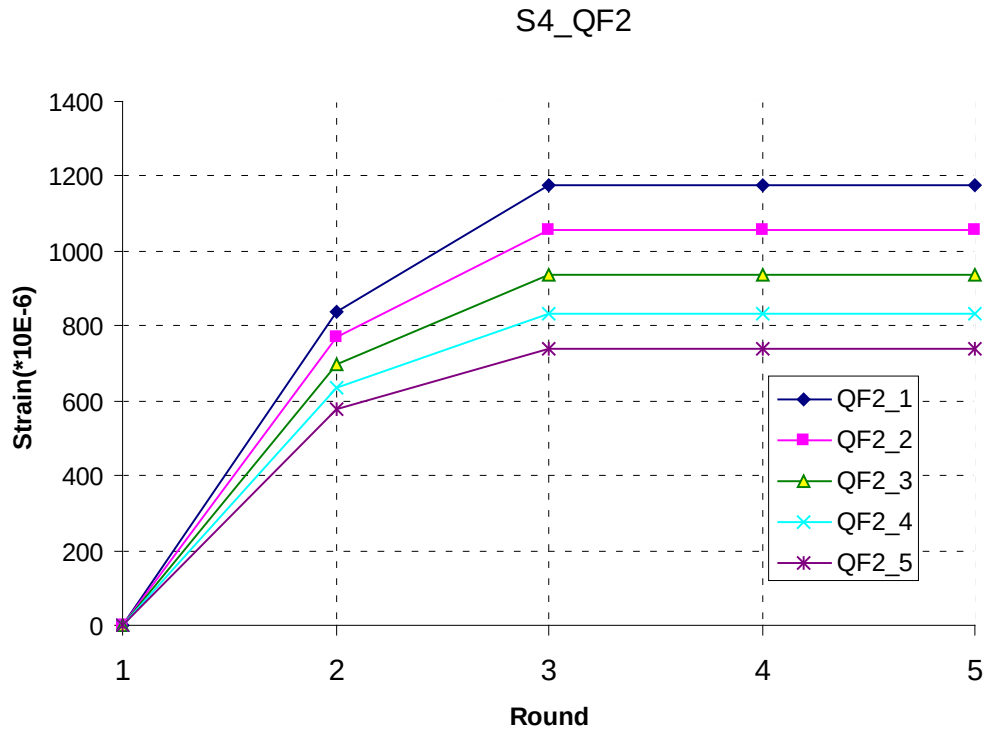

Figure 4.4.53

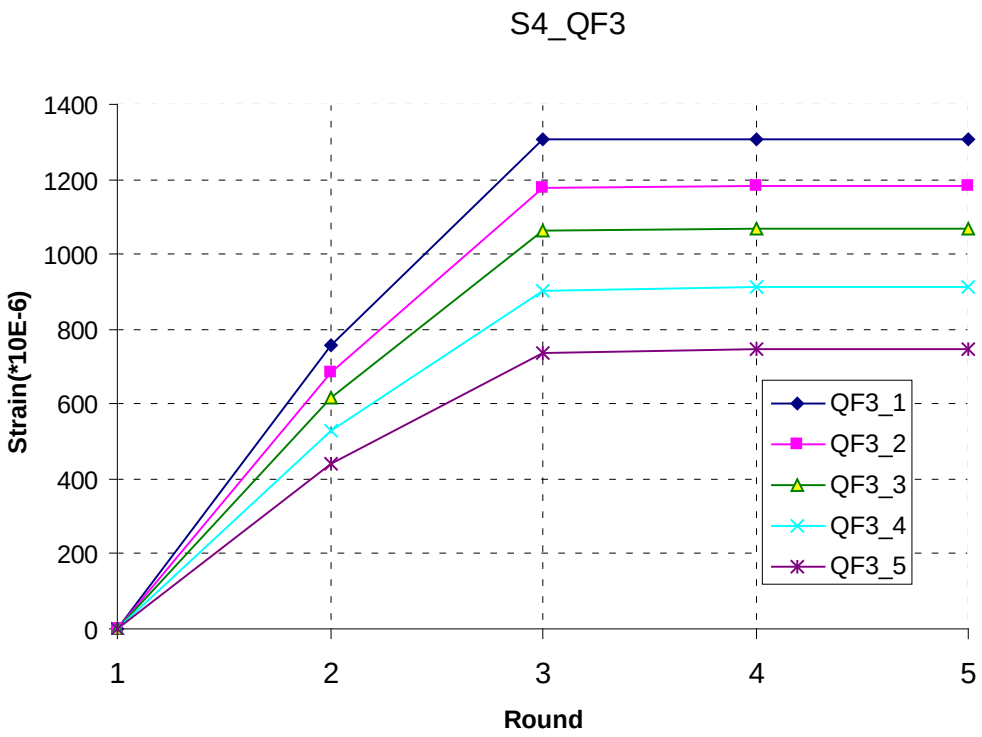

Figure 4.4.54

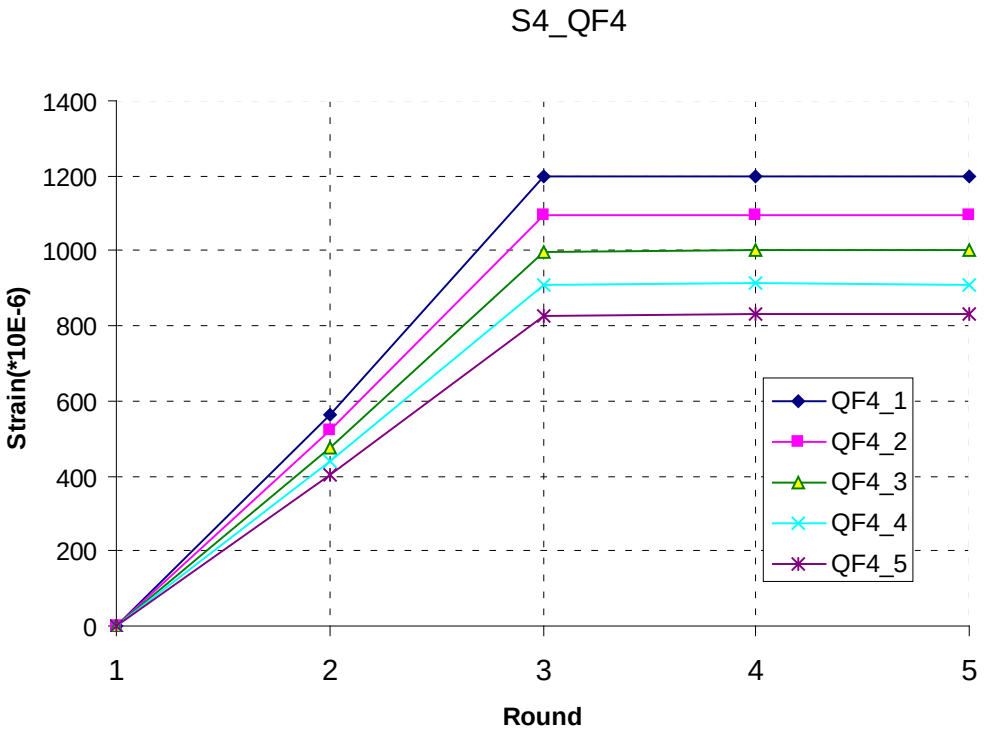

Figure 4.4.55

Specimen S5:

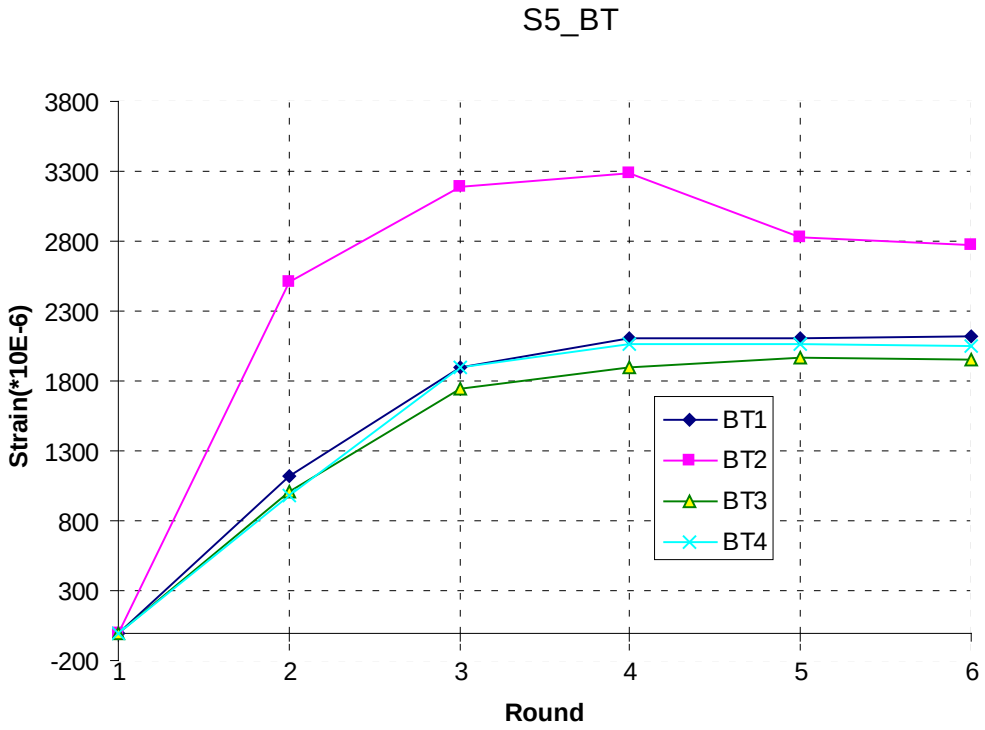

Figure 4.4.56

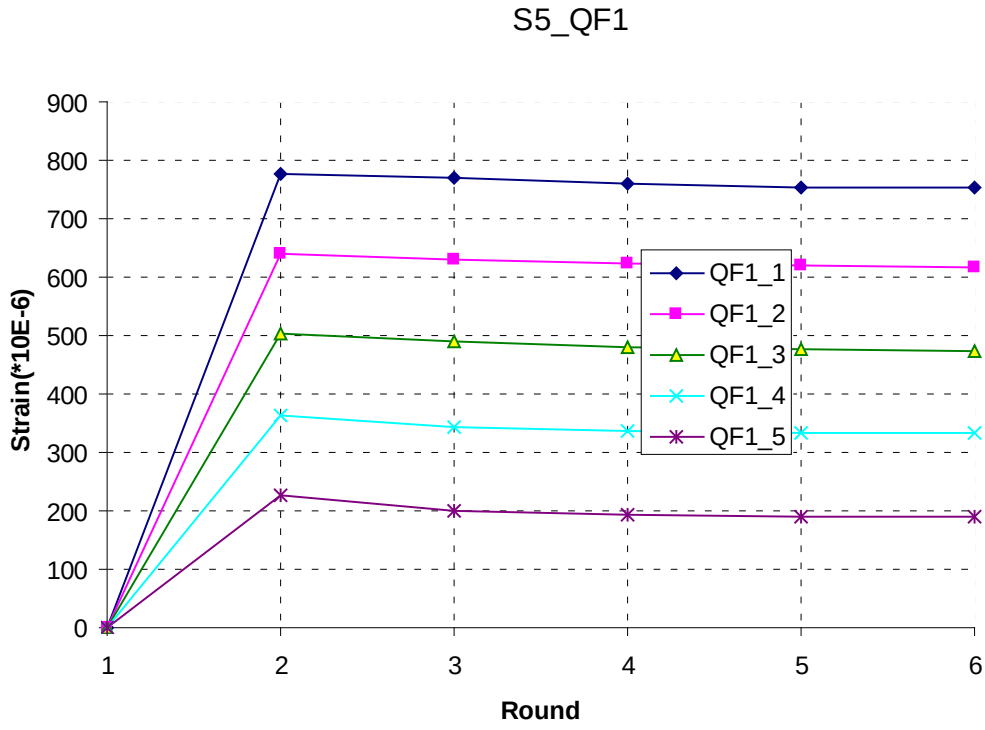

Figure 4.4.57

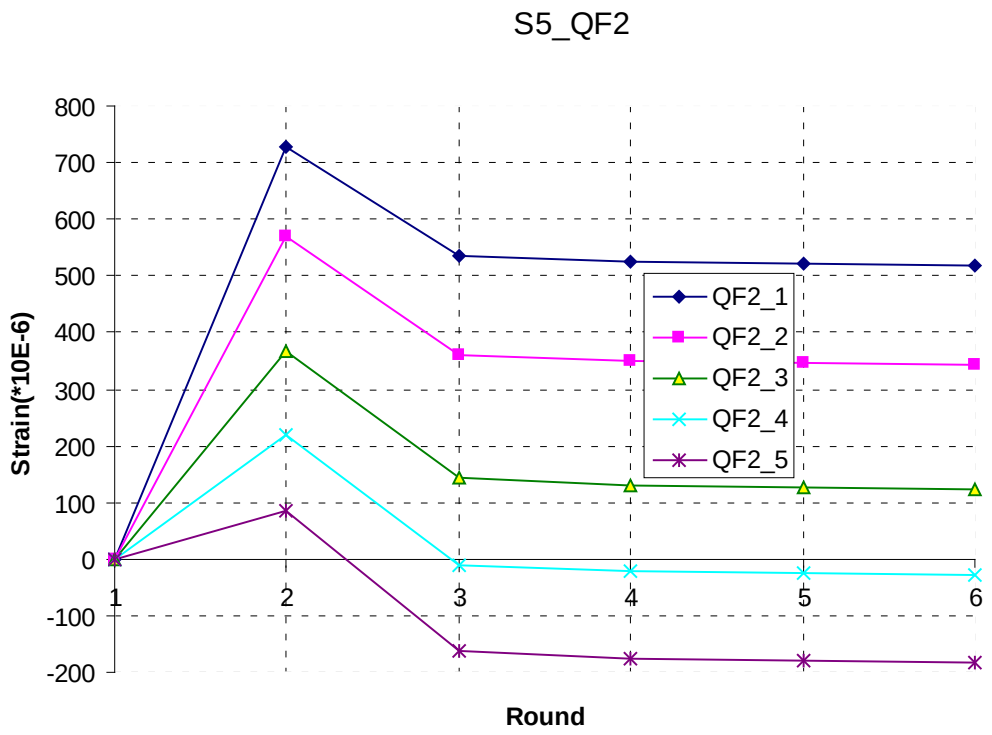

Figure 4.4.58

Specimen S6:

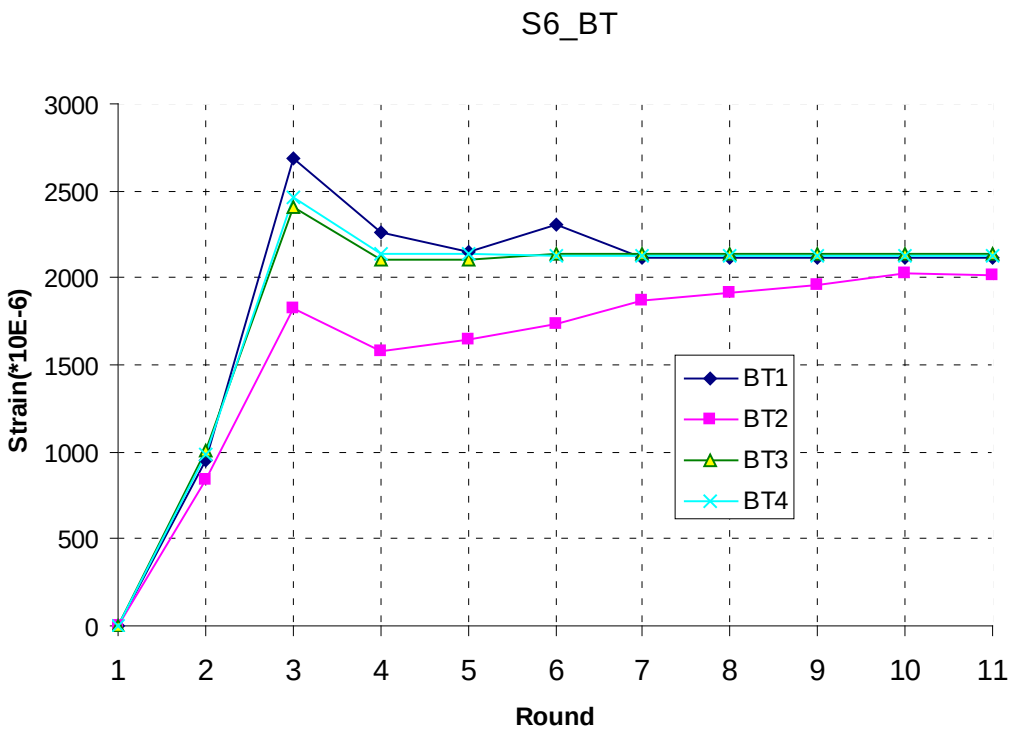

Figure 4.4.59

ANNEX 4: Graphic data of the T1 test

In the title of the charts, first term ("T1") indicates the test name, the second term:

"BT", "FL","FR" indicates the strain gauge name (see Table 3 in Section 4.2.2.6 of the Six-monthly Report issued in September 2011);

"D" indicates the absolute displacement in each displacement transducer (see Fig.13 in Section 4.2.2.6 of the Six-monthly Report issued in September 2011);

"DR" indicate the displacement relative of the joint: ((D1-D4)+D2-D3))/2, (see Fig.13 in Section 4.2.2.6 of the Six-monthly Report issued in September 2011).

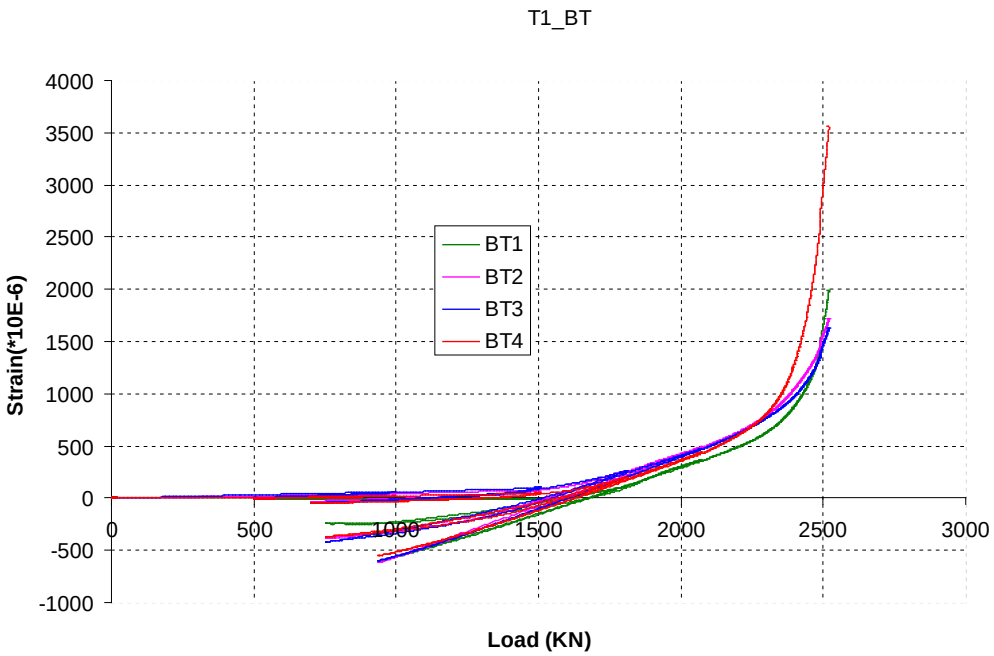

Figure 4.4.60

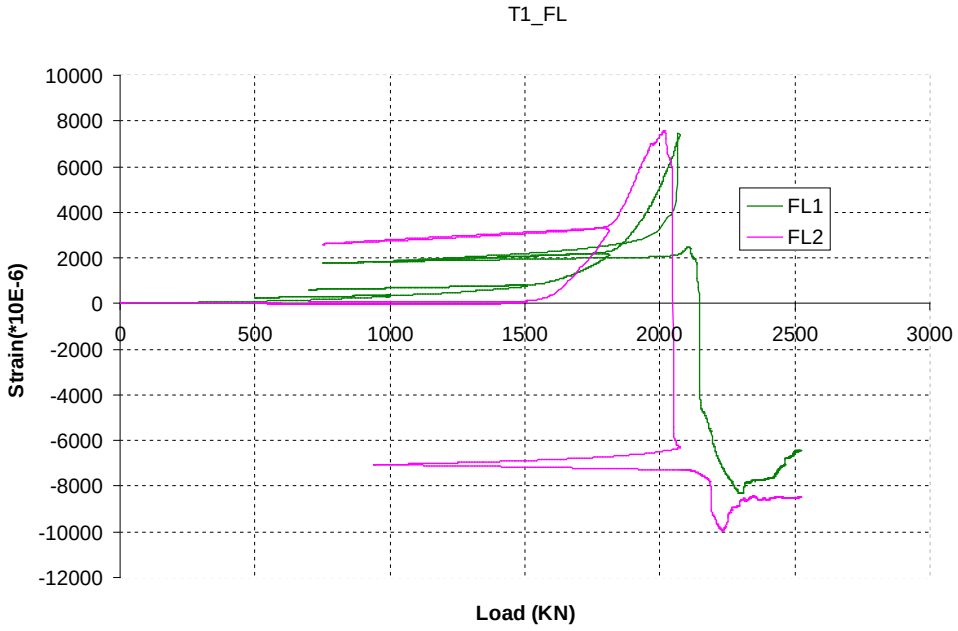

Figure 4.4.61

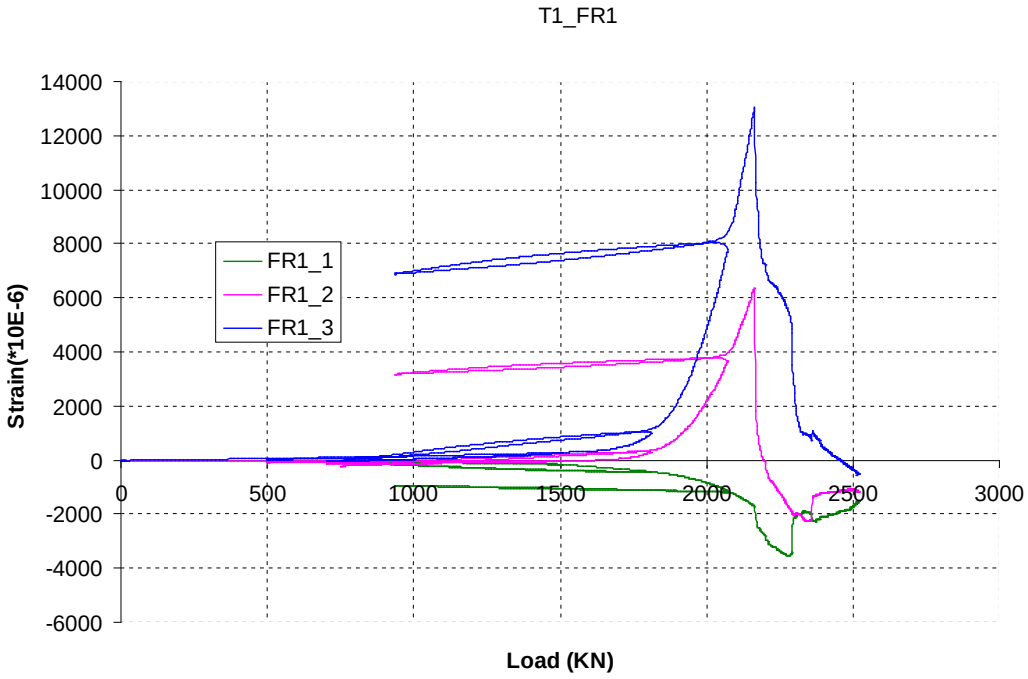

Figure 4.4.62

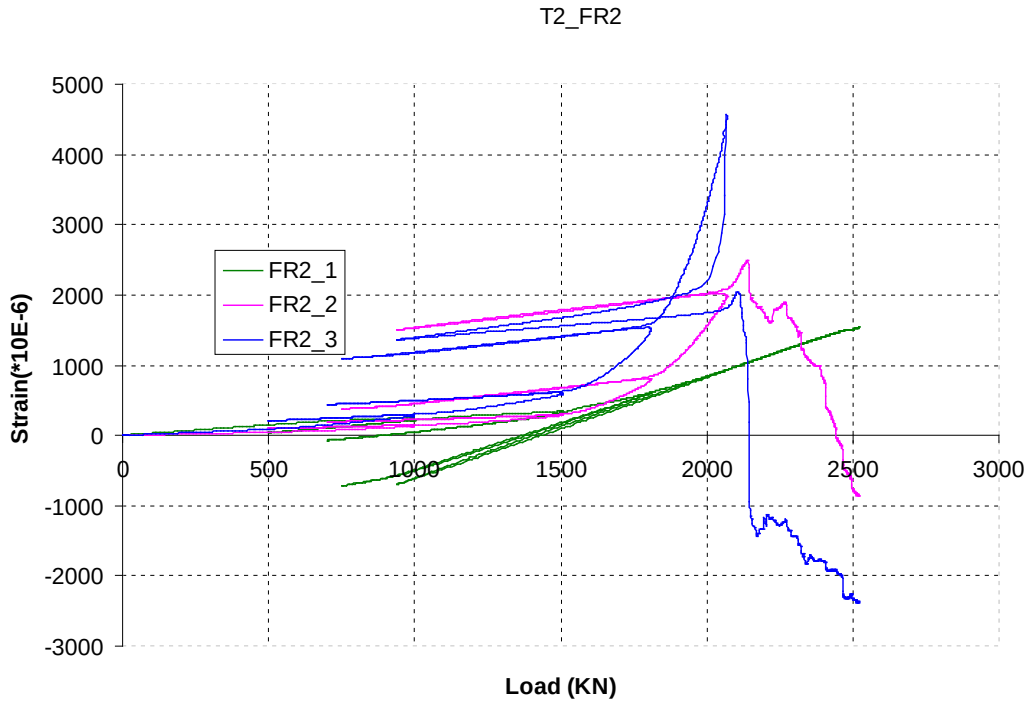

Figure 4.4.63

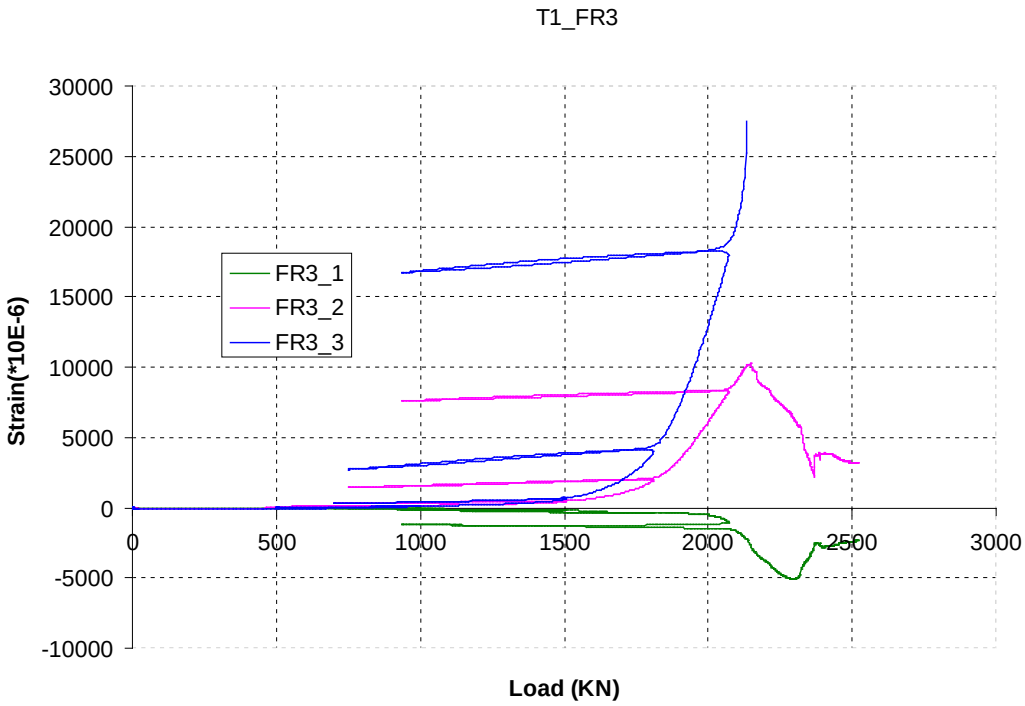

Figure 4.4.64

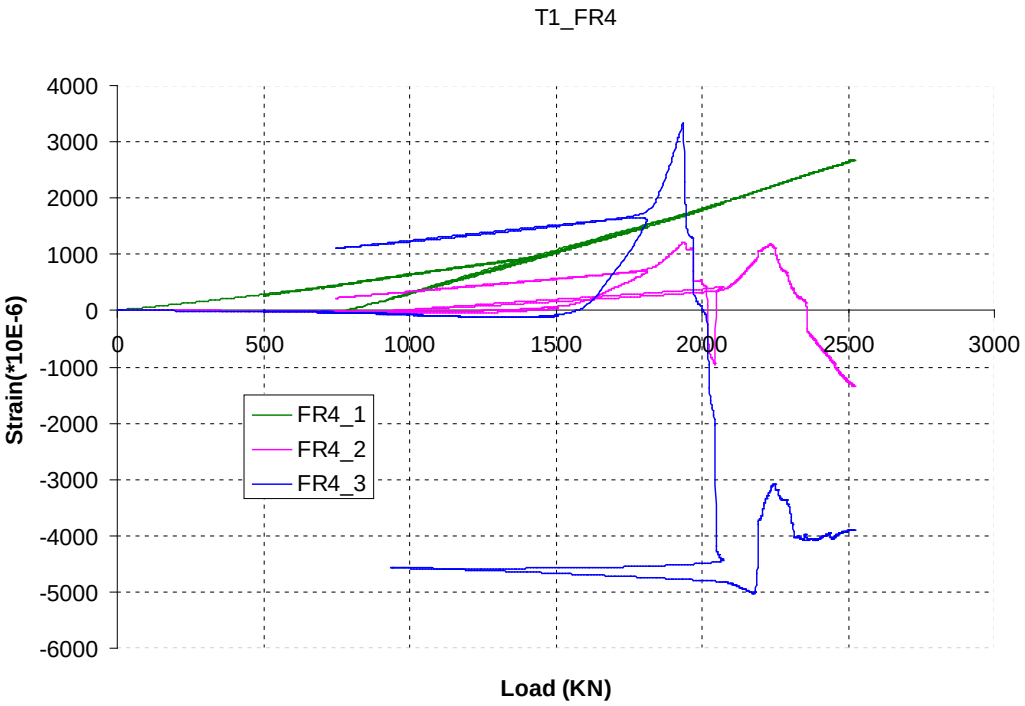

Figure 4.4.65

T1_D

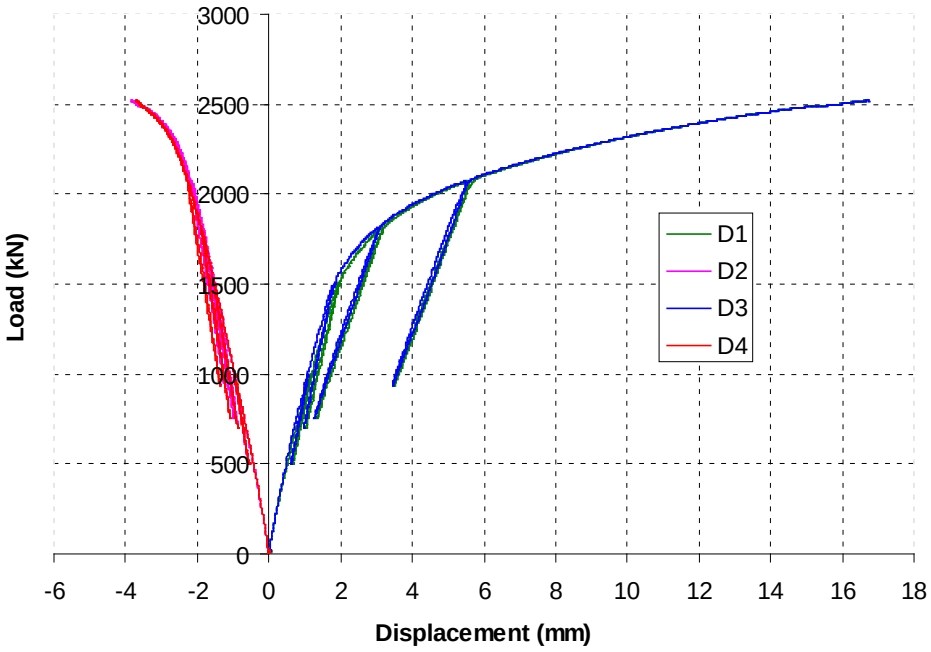

Figure 4.4.66

T1_DR

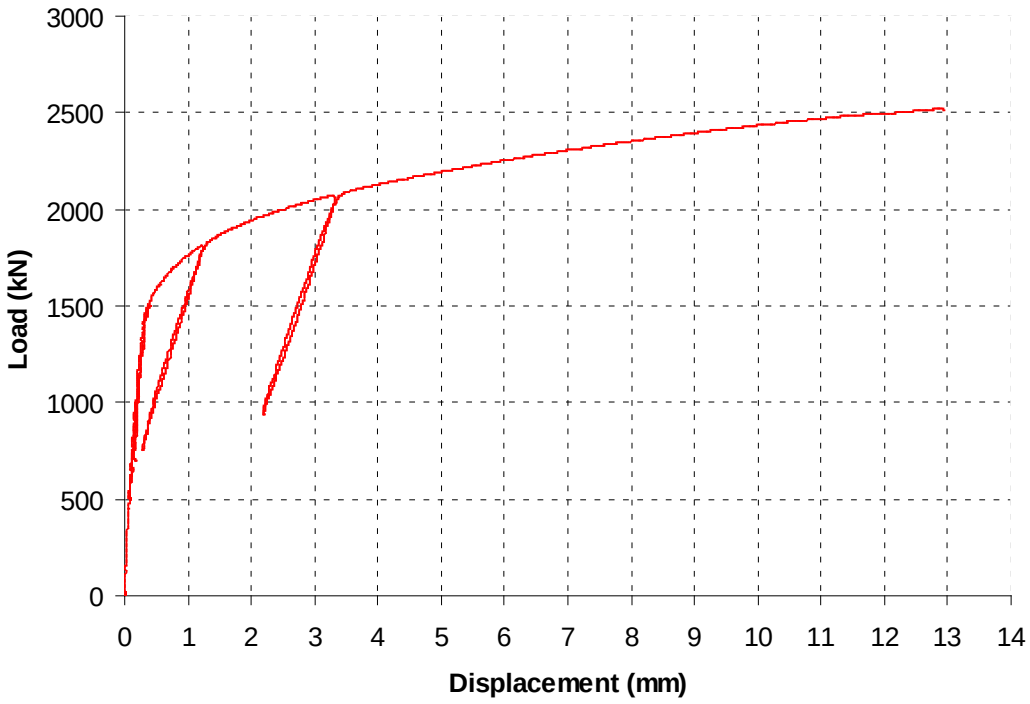

Figure 4.4.67

ANNEX 5: Graphic data of the T2 test

In the title of the charts, first term (“T2”) indicates the test name, the second term:

“BT”, “FL”,”FR” indicates the strain gauge name;

“D” indicates the absolute displacement in each displacement transducer;

“DR” indicate the displacement relative of the joint: ((D1-D4)+D2-D3))/2.

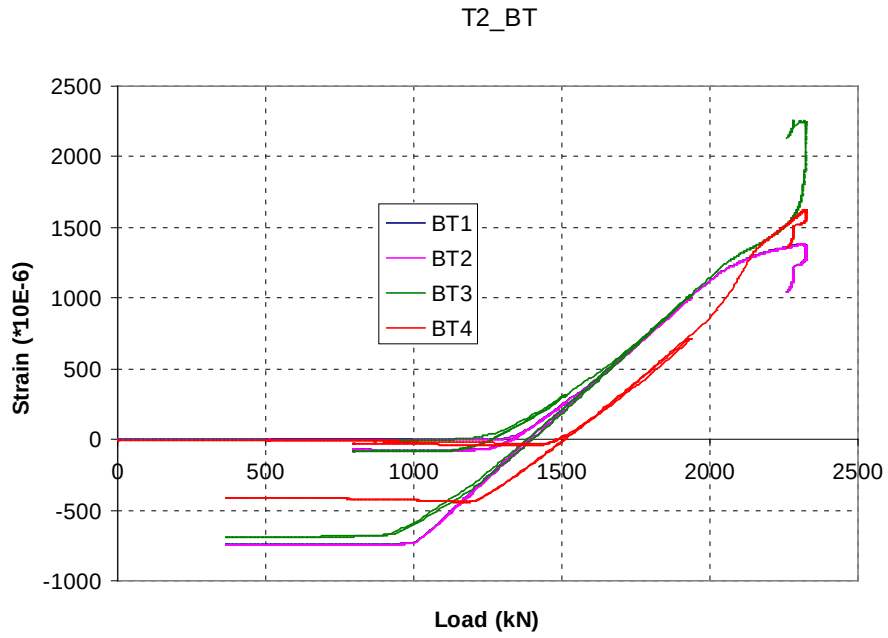

Figure 4.4.68

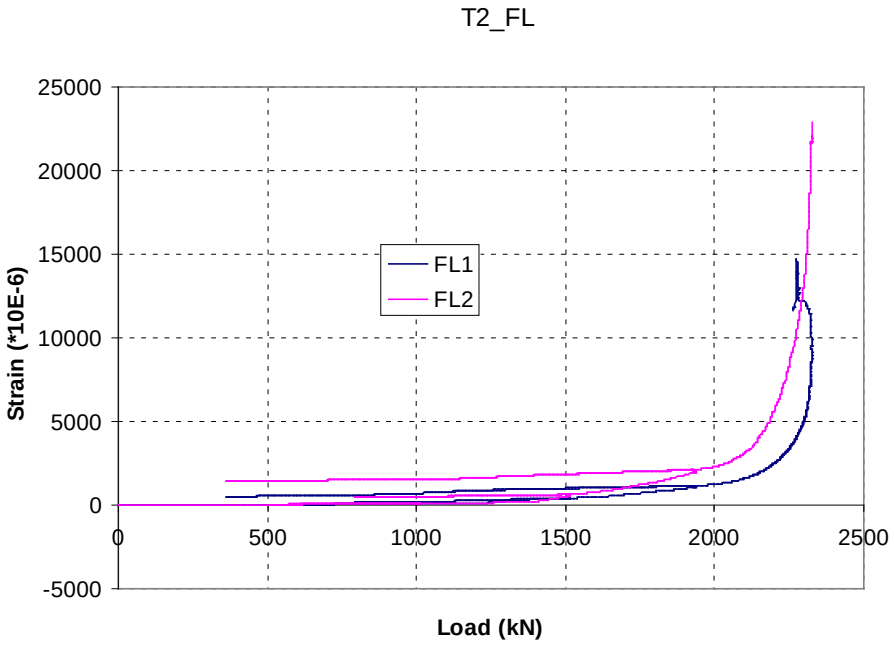

Figure 4.4.69

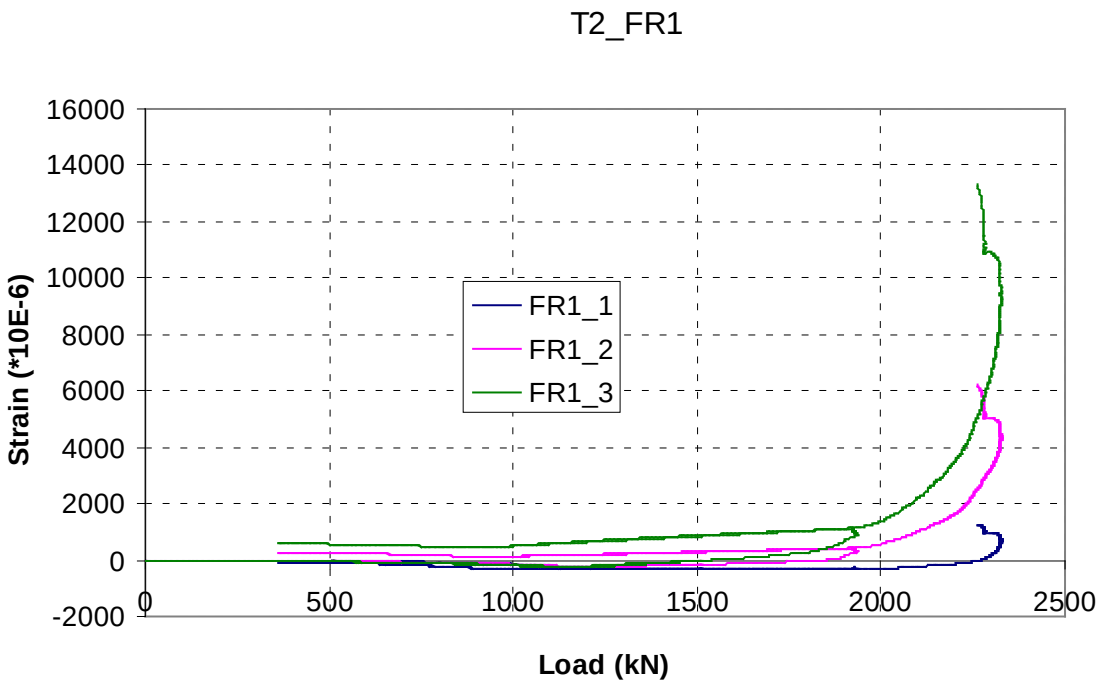

Figure 4.4.70

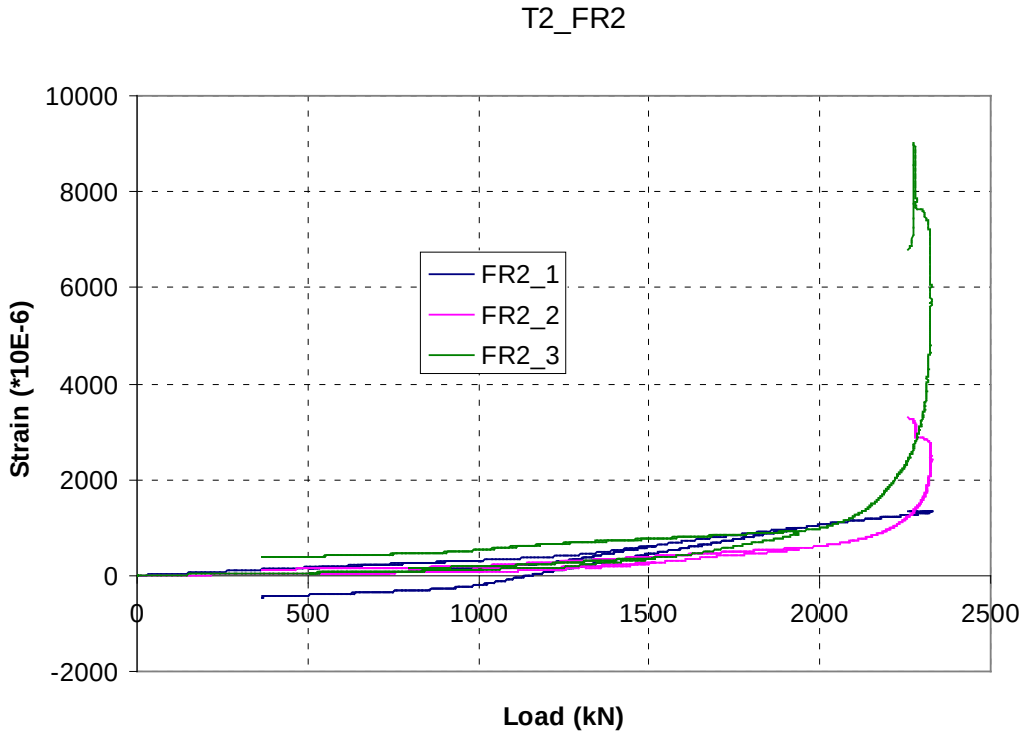

Figure 4.4.71

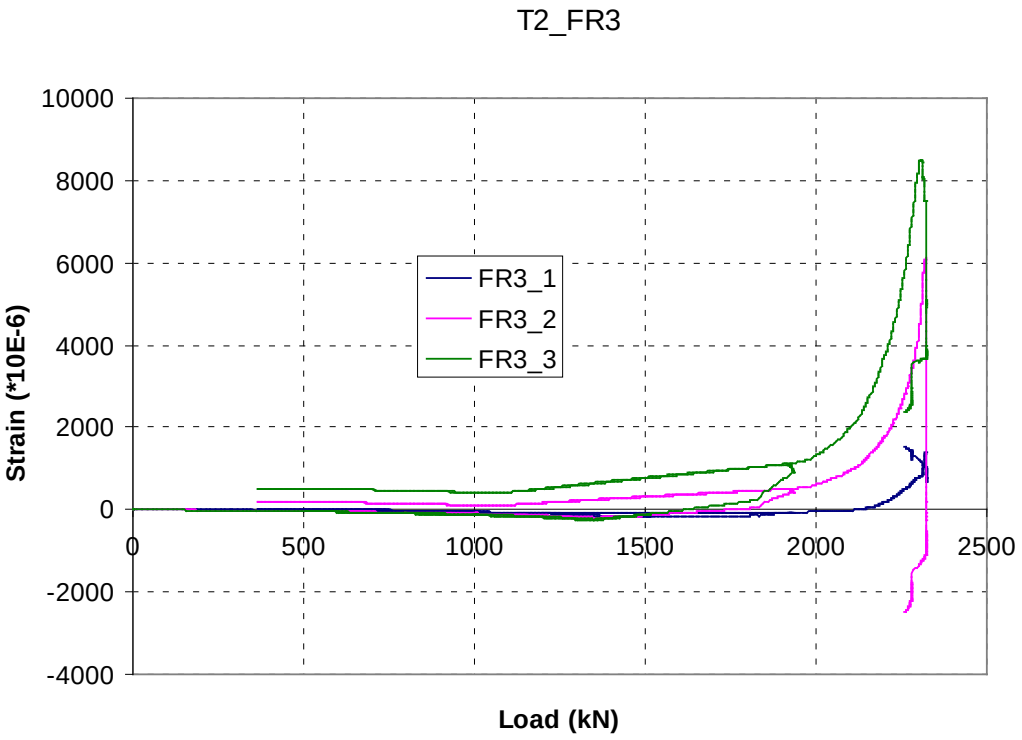

Figure 4.4.72

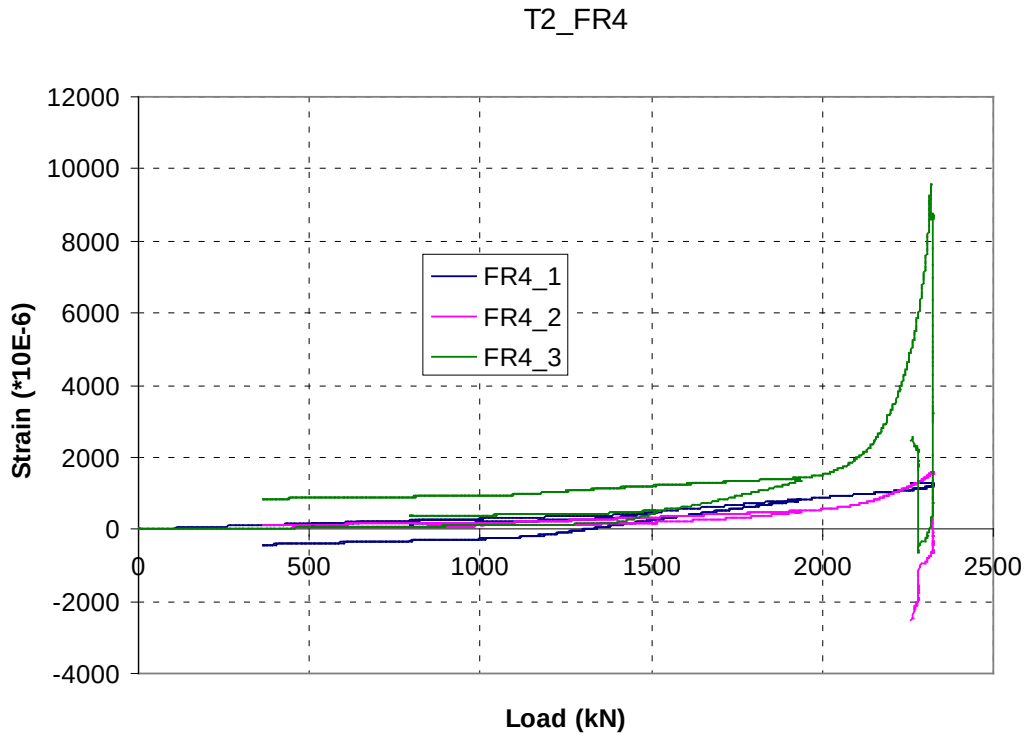

Figure 4.4.73

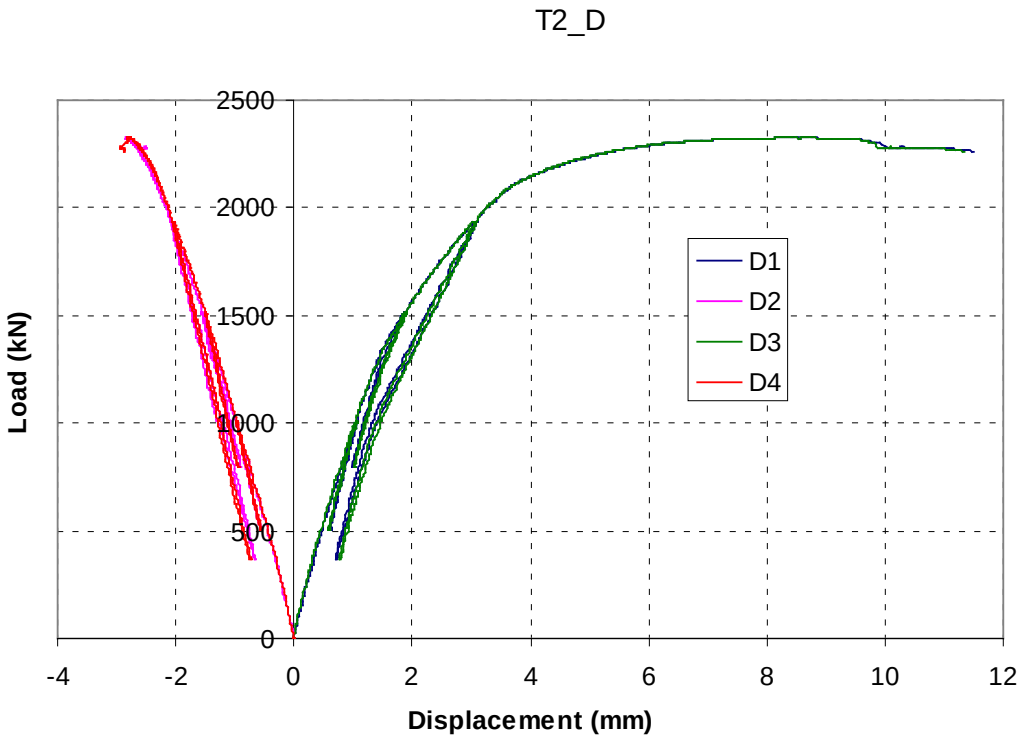

Figure 4.4.74

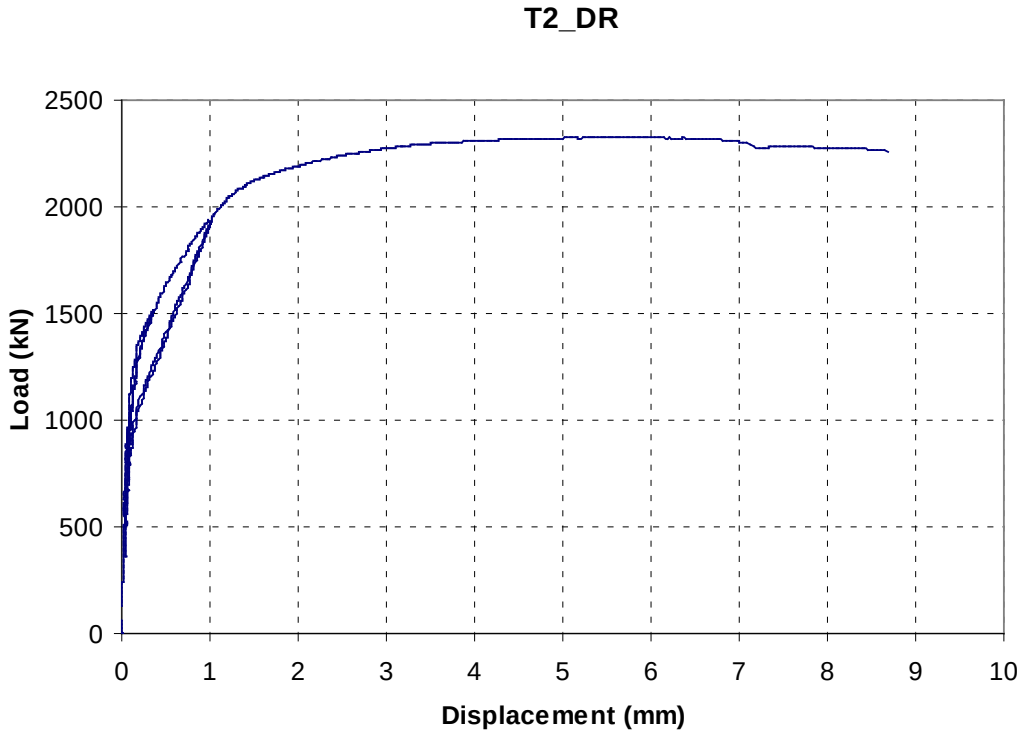

Figure 4.4.75

ANNEX 6: Graphic data of the T3a test

In the title of the charts, first term (“T3a”) indicates the test name, the second term:

“BT”, “FL”,”QF” indicates the strain gauge name;

“D” indicates the absolute displacement in each displacement transducer;

“DR” indicate the displacement relative of the joint: ((D1-D4)+D2-D3))/2.

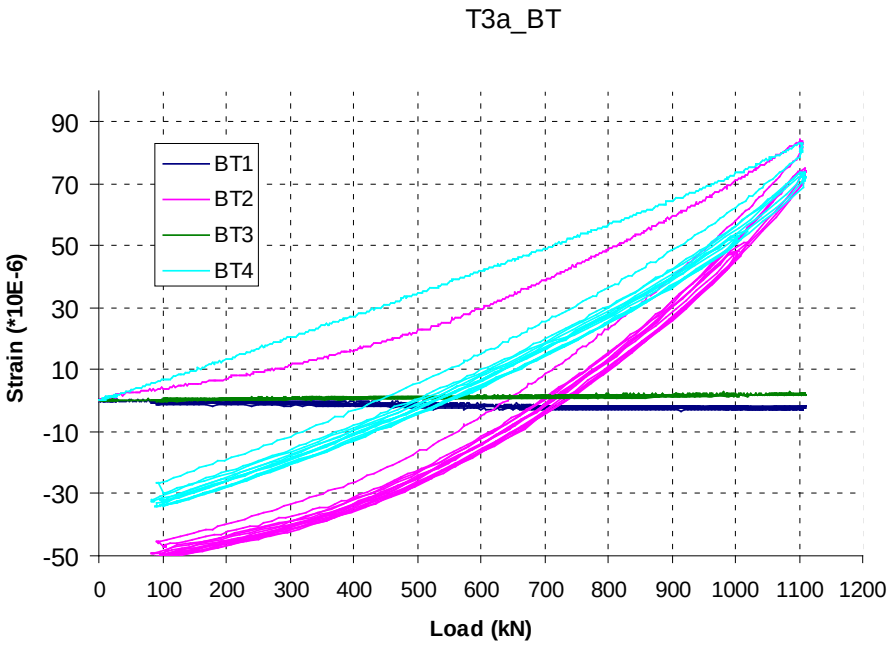

Figure 4.4.76

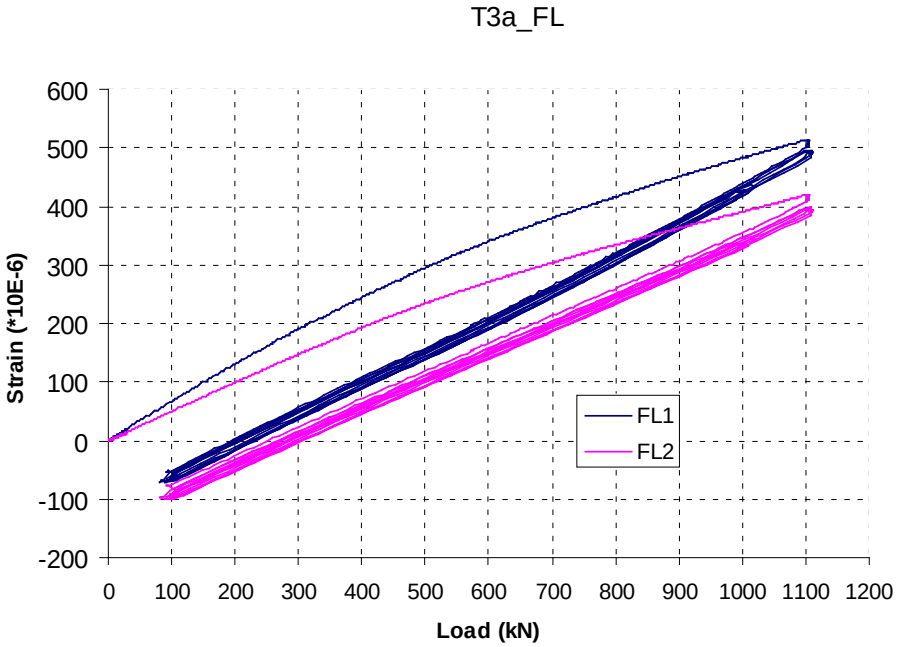

Figure 4.4.77

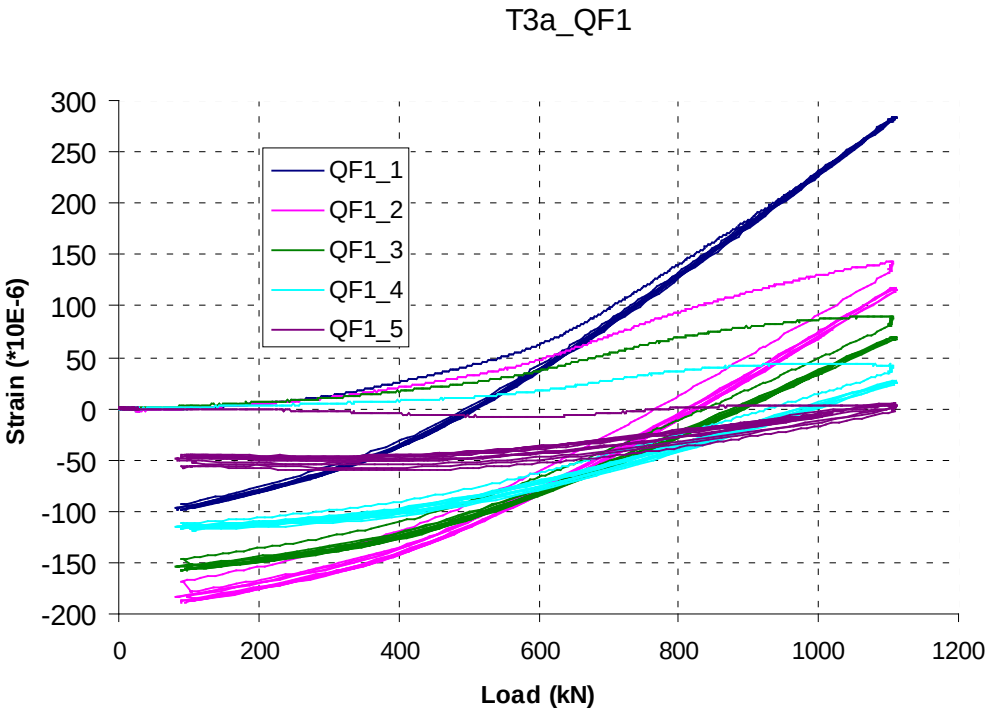

Figure 4.4.78

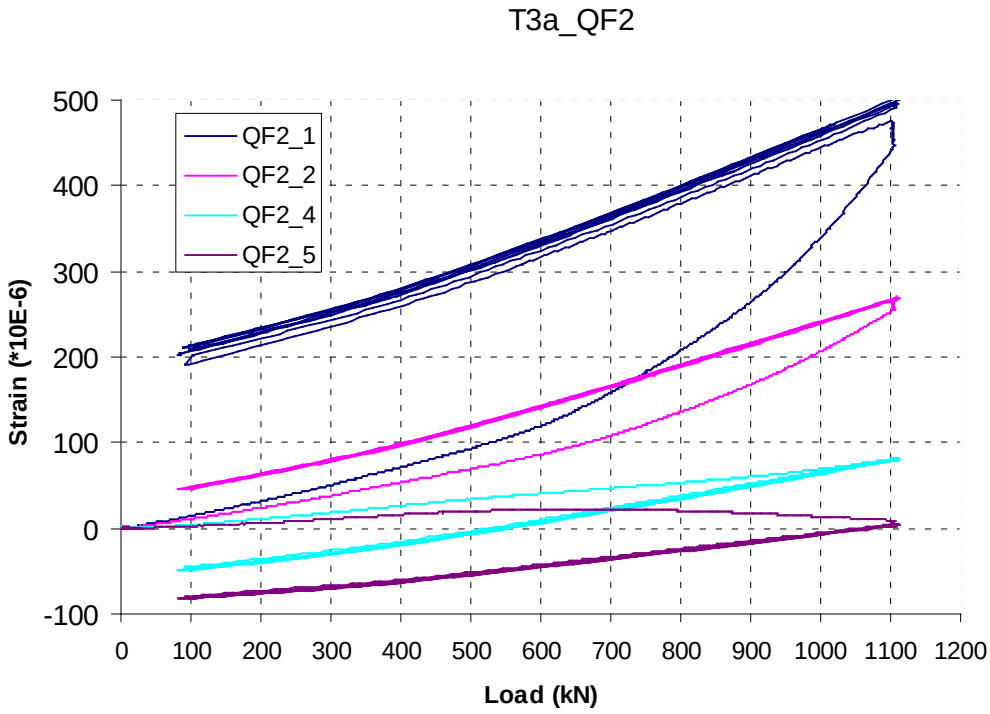

Figure 4.4.79

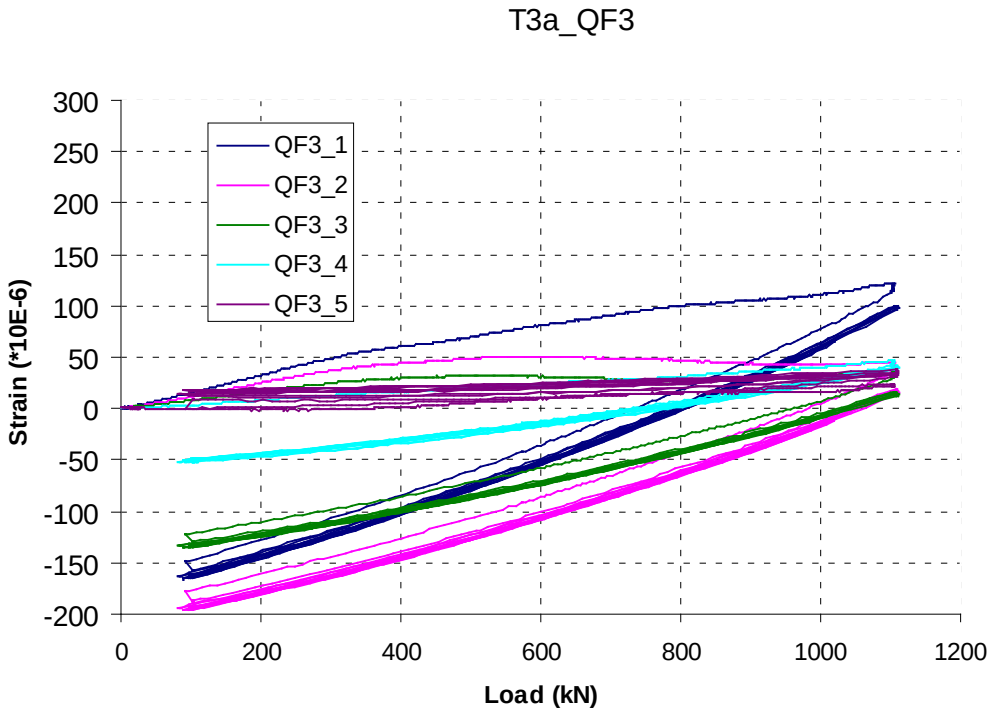

Figure 4.4.80

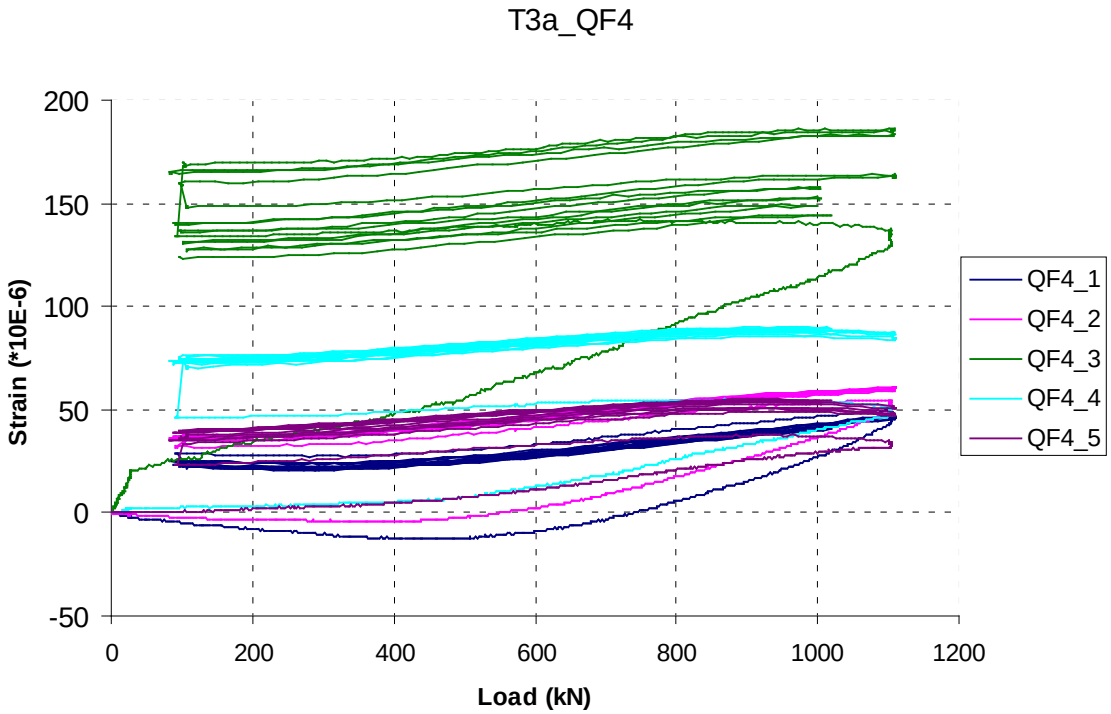

Figure 4.4.81

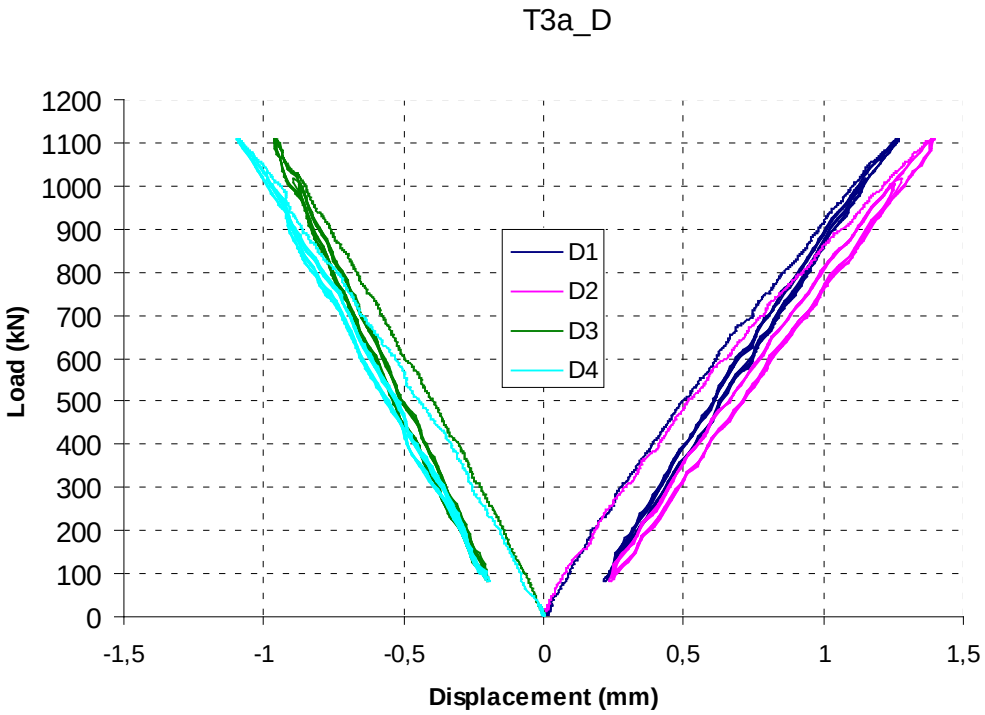

Figure 4.4.82

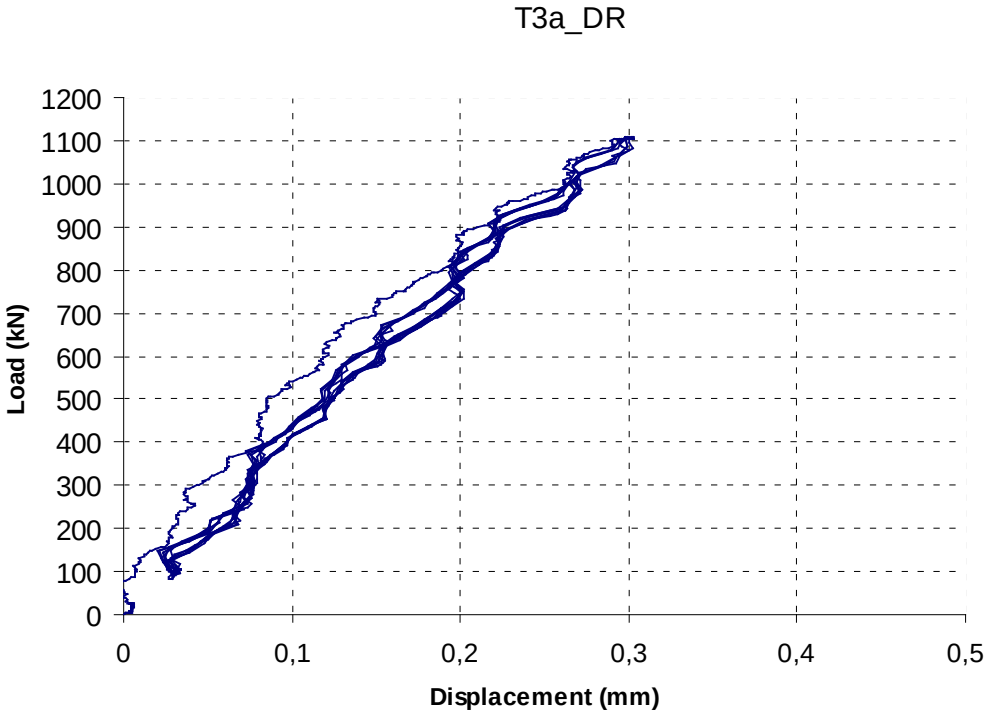

Figure 4.4.83

ANNEX 7: Graphic data of the T4a test

In the title of the charts, first term (“T4a”) indicates the test name, the second term:

“BT”, “FL”,”QF” indicates the strain gauge name ;

“D” indicates the absolute displacement in each displacement transducer;

“DR” indicate the displacement relative of the joint: ((D1-D4)+D2-D3))/2.

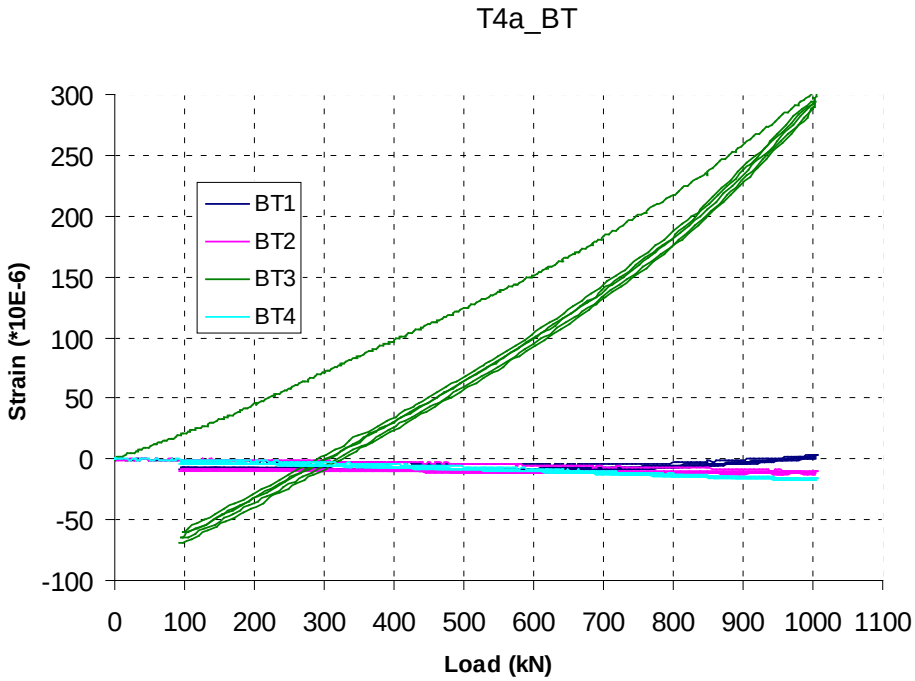

Figure 4.4.84

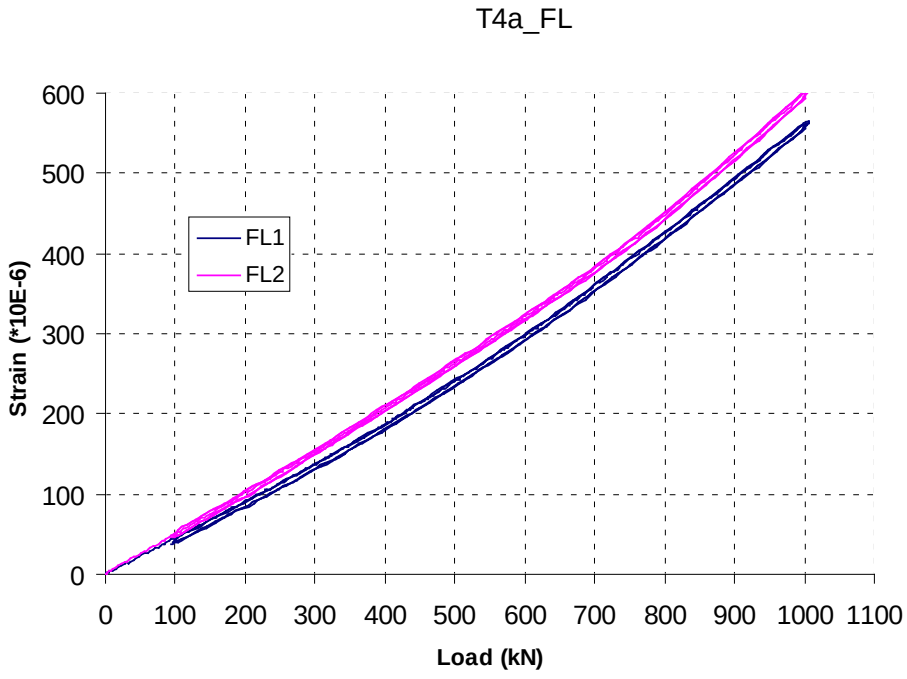

Figure 4.4.85

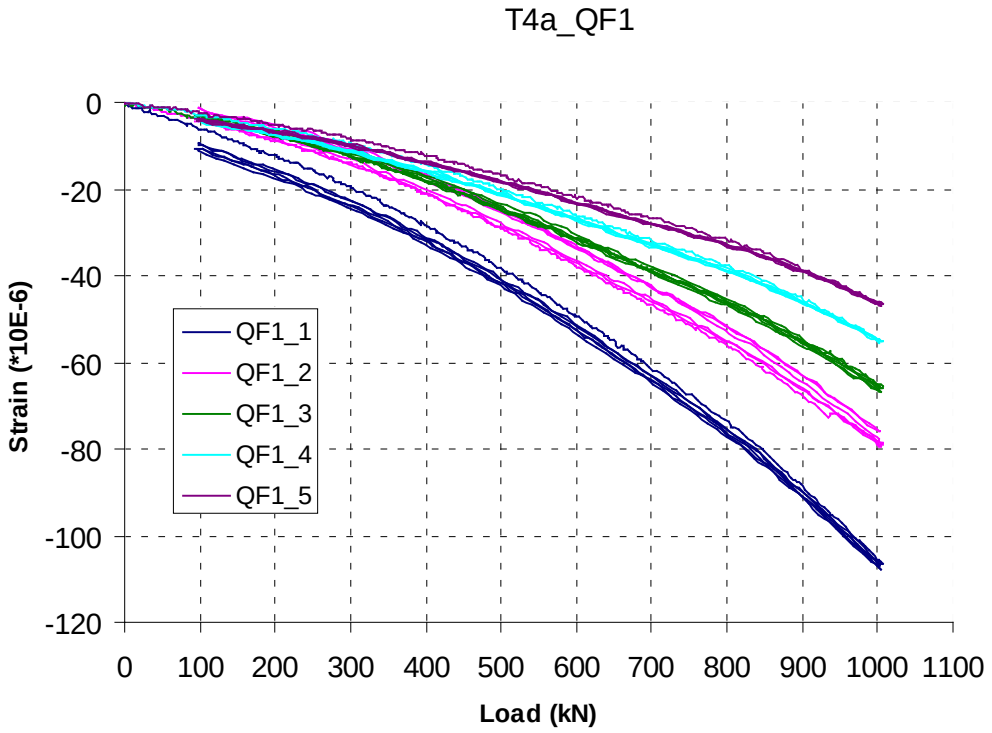

Figure 4.4.86

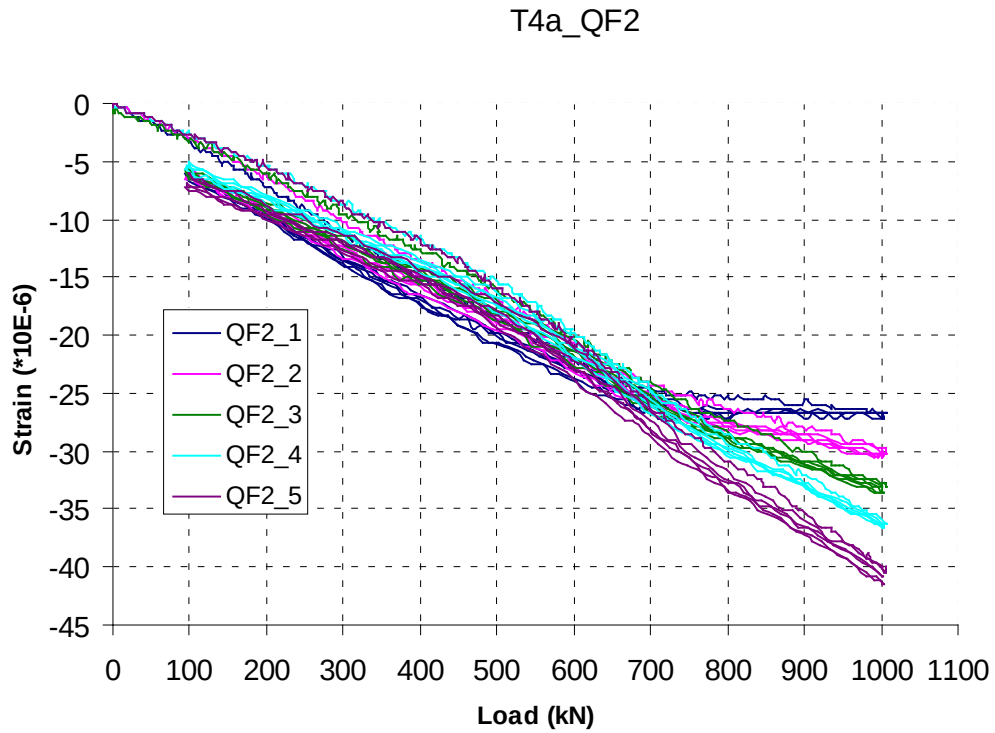

Figure 4.4.87

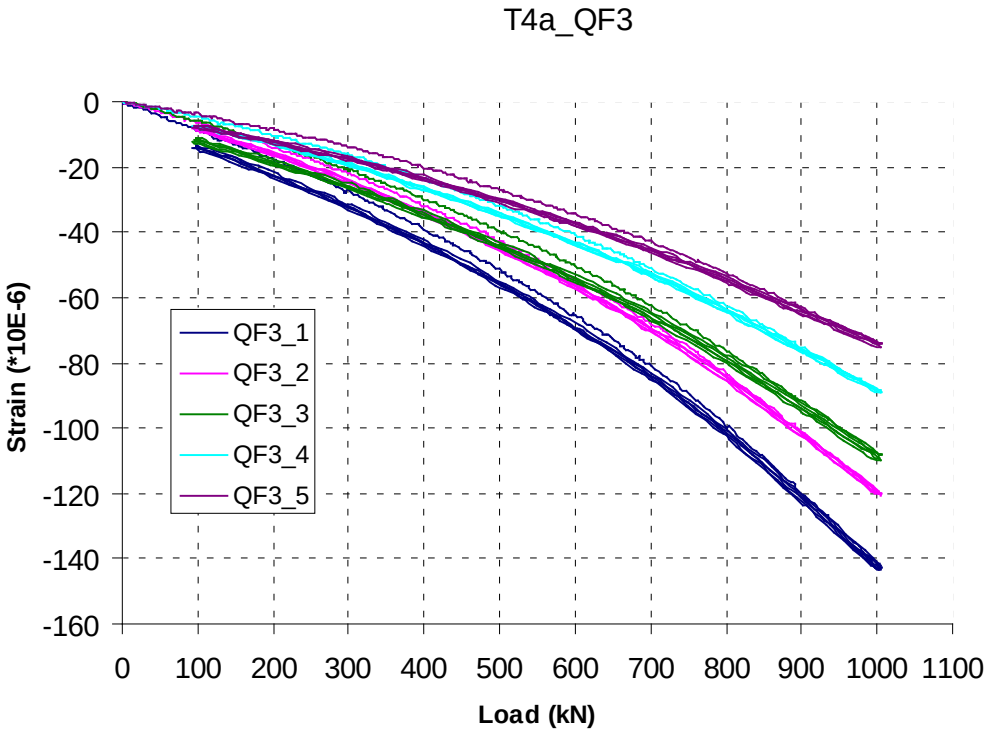

Figure 4.4.88

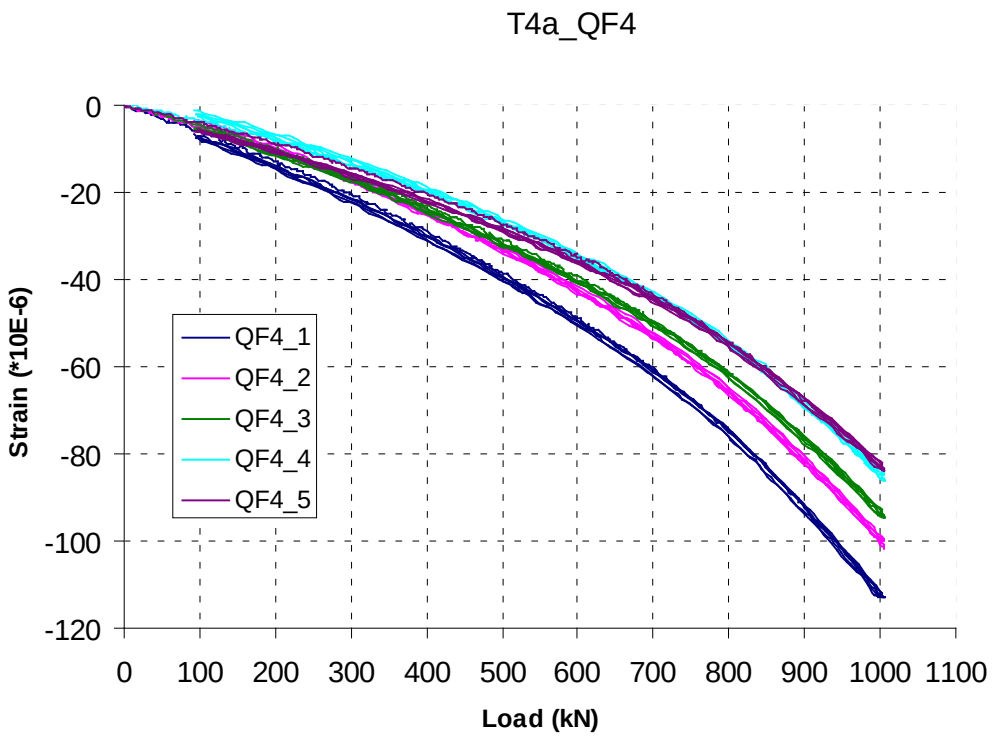

Figure 4.4.89

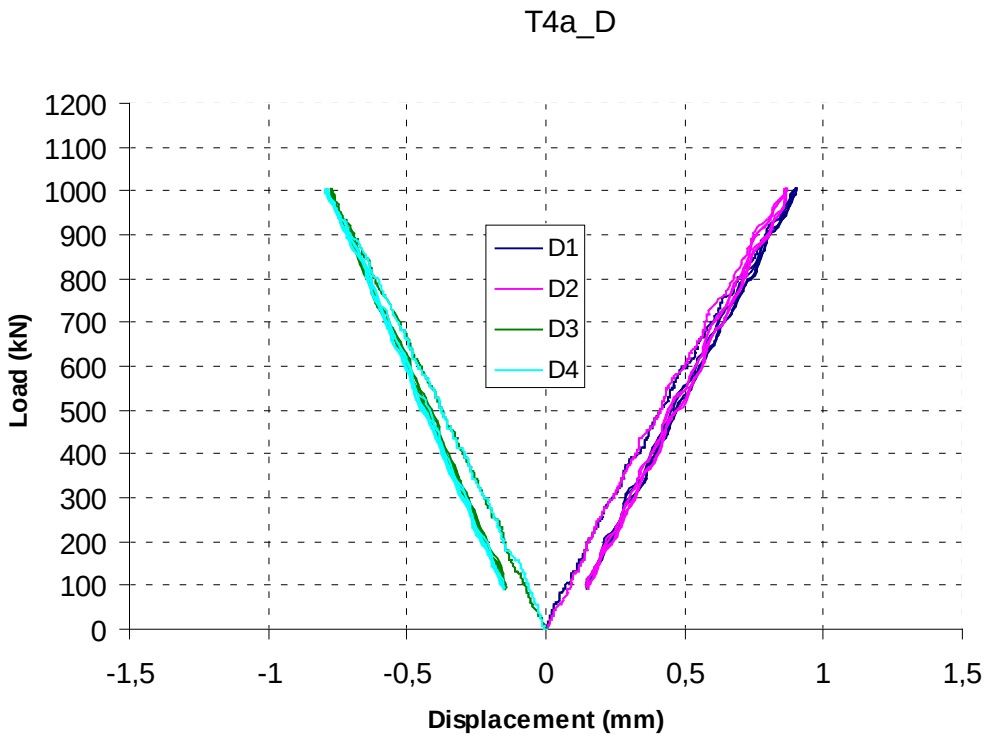

Figure 4.4.90

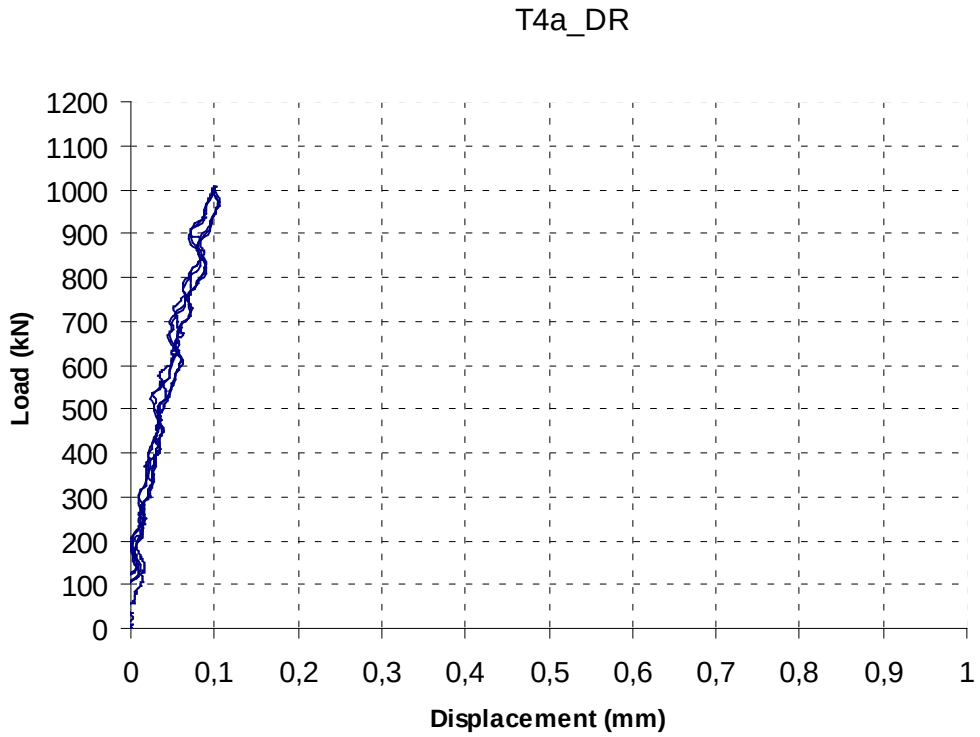

Figure 4.4.91

ANNEX 8: Graphic data of the T4c test

In the title of the charts, first term ("T4c") indicates the test name, the second term:

"BT", "FL","QF" indicates the strain gauge name;

"D" indicates the absolute displacement in each displacement transducer;

"DR" indicate the displacement relative of the joint: ((D1-D4)+D2-D3))/2.

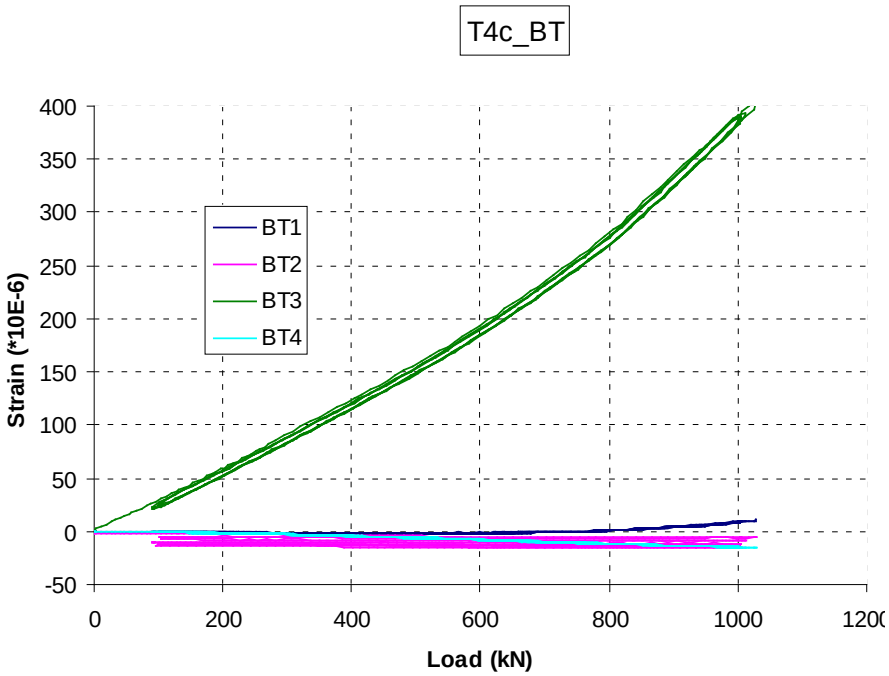

Figure 4.4.92

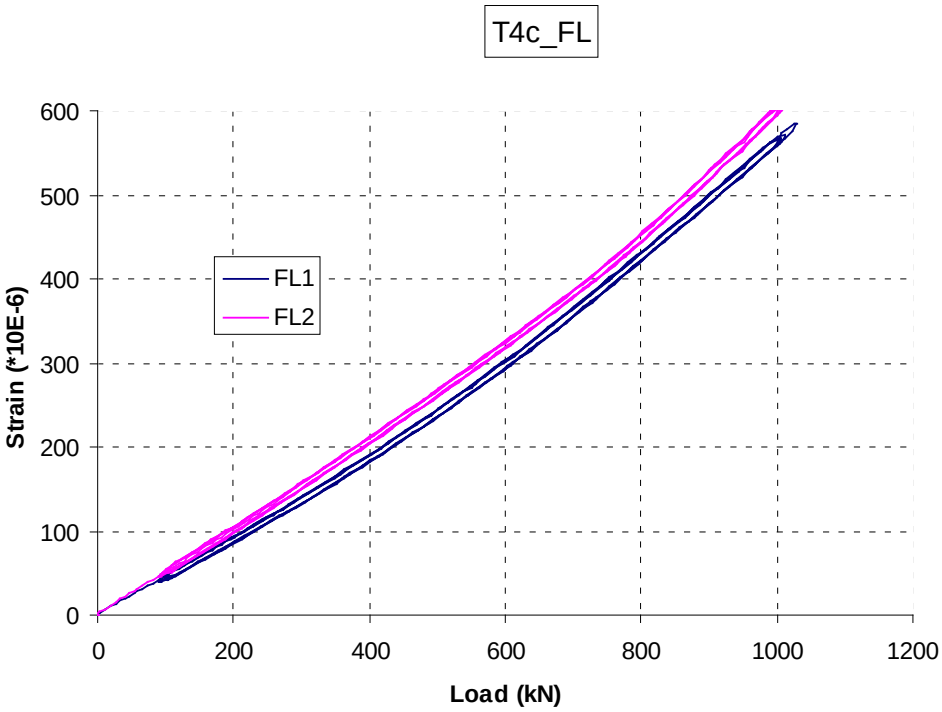

Figure 4.4.93

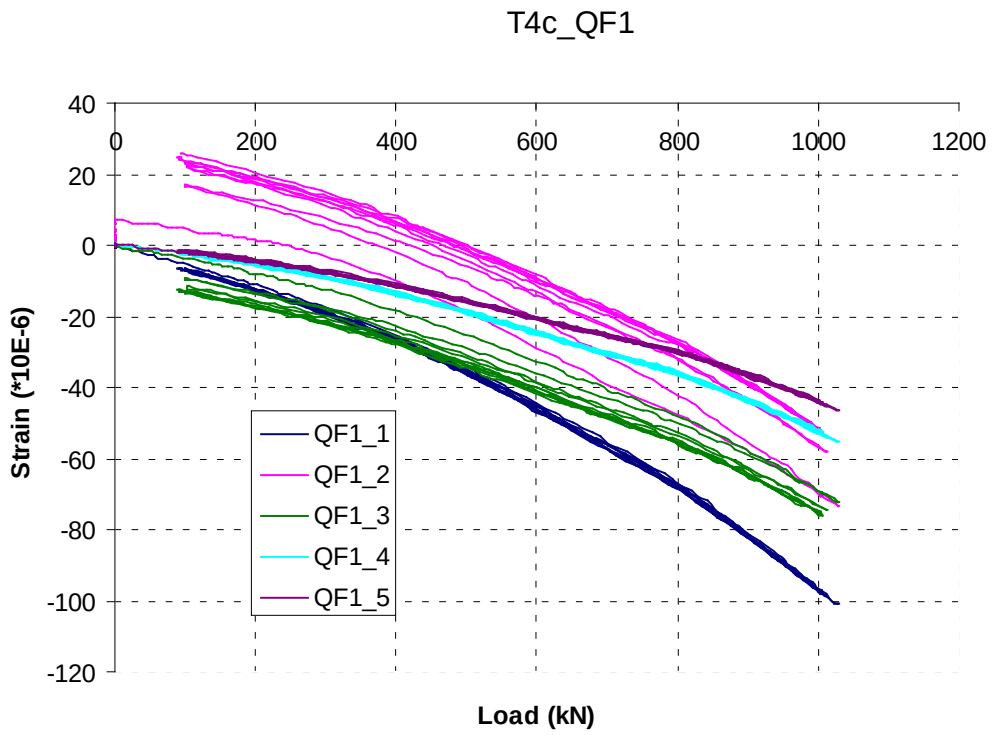

Figure 4.4.94

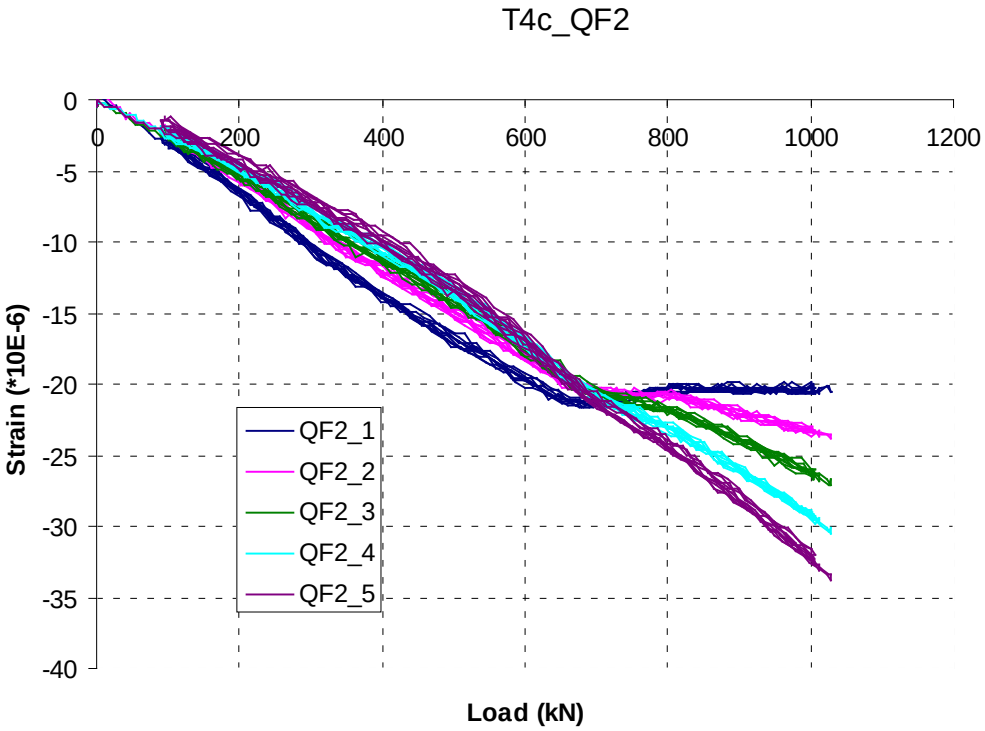

Figure 4.4.95

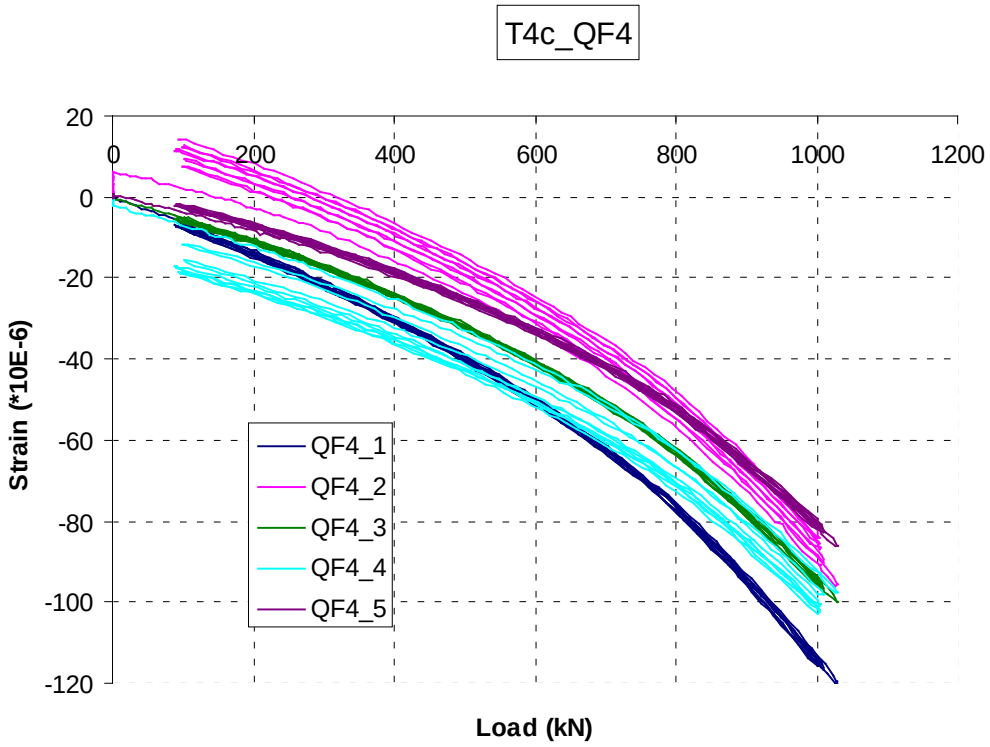

Figure 4.4.96

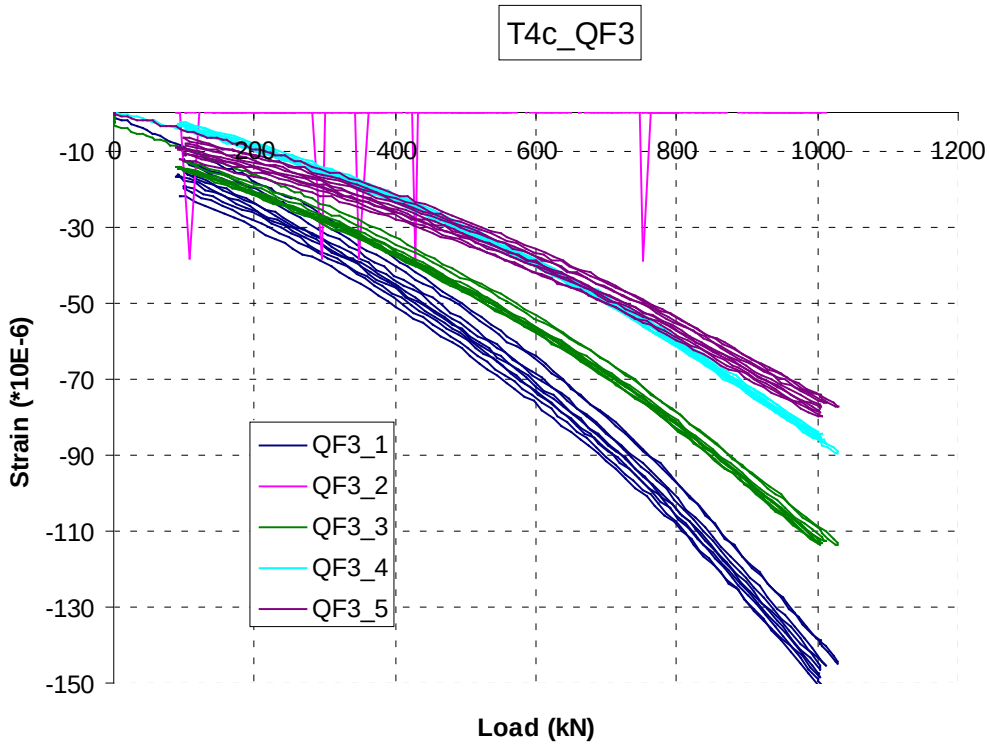

Figure 4.4.97

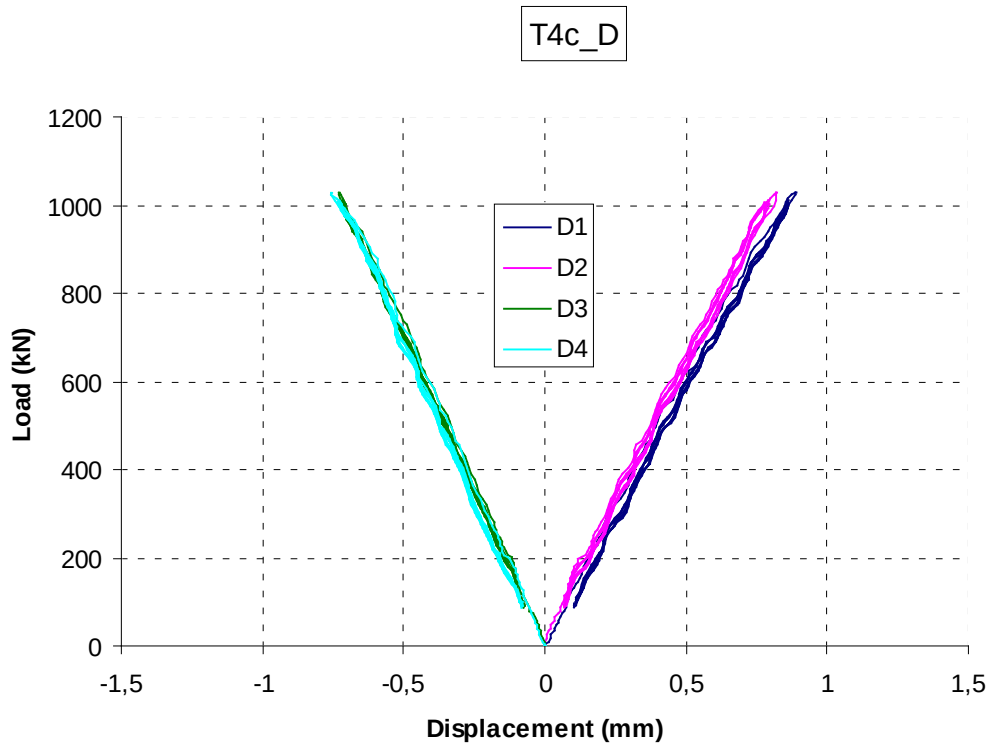

Figure 4.4.98

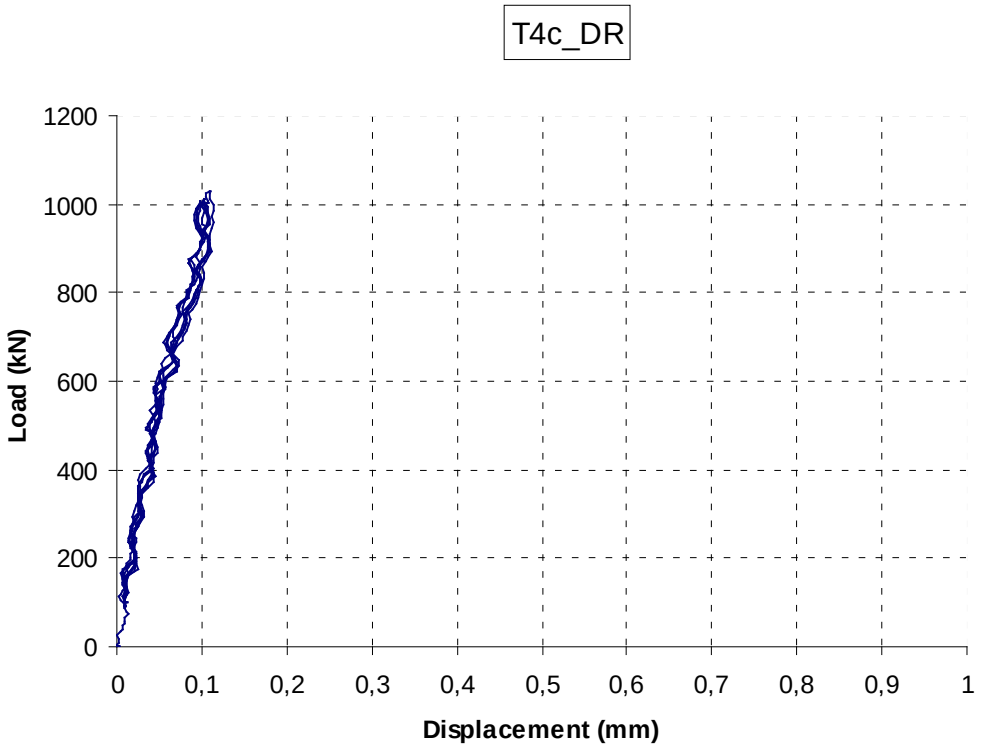

Figure 4.4.99

ANNEX 9: Graphic data of the T5a test

In the title of the charts, first term (“T5a”) indicates the test name, the second term:

“BT”, “QF” indicates the strain gauge name;

“D” indicates the absolute displacement in each displacement transducer;

“DR” indicate the displacement relative of the joint: ((D1-D4)+D2-D3))/2.

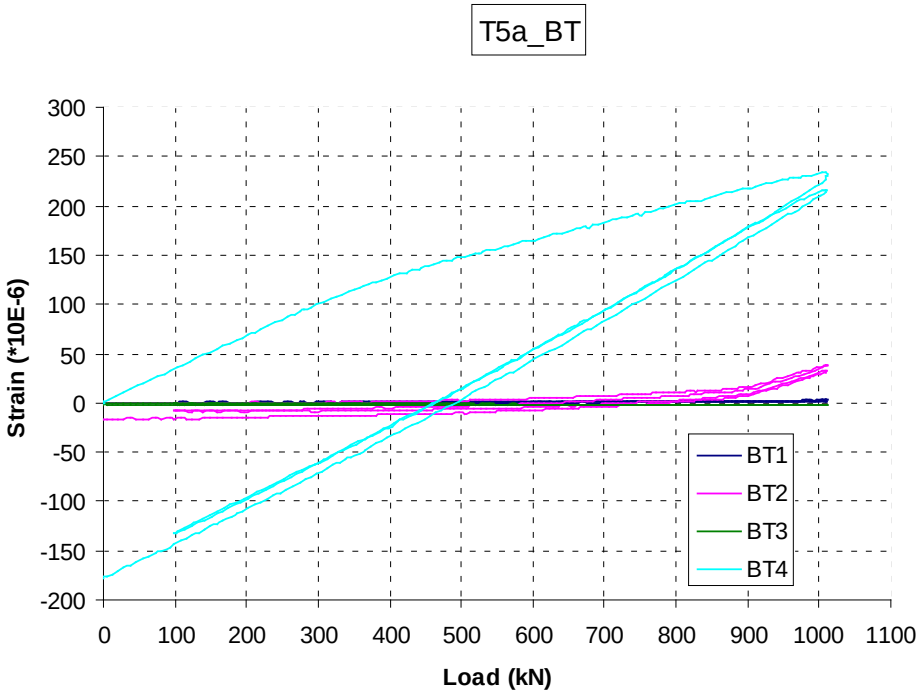

Figure 4.4.100

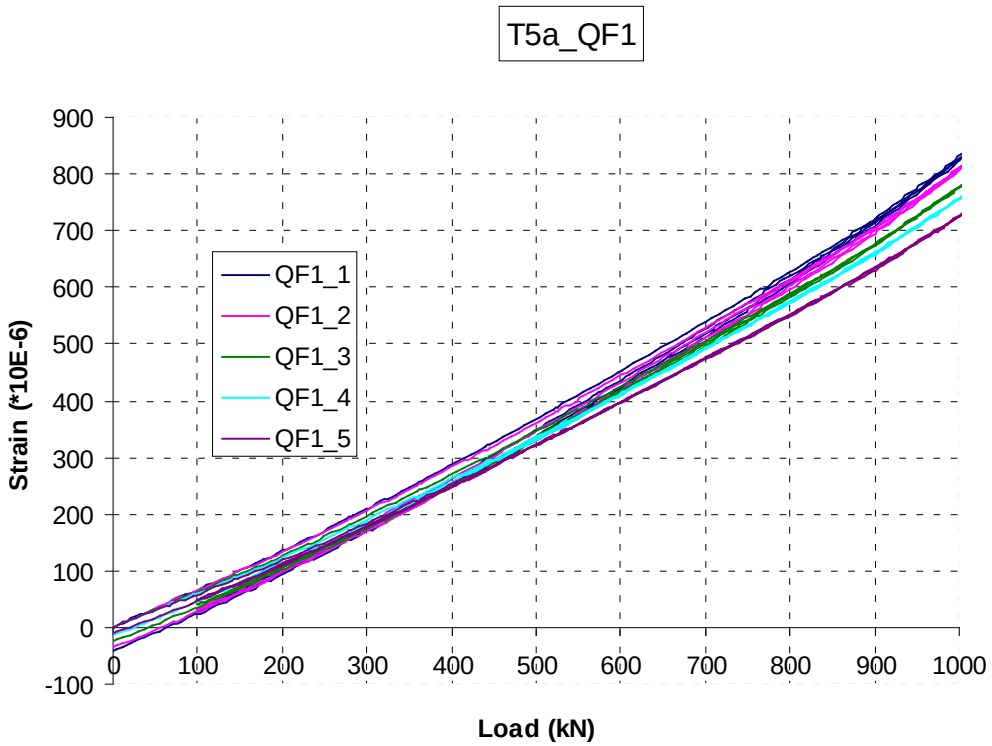

Figure 4.4.101

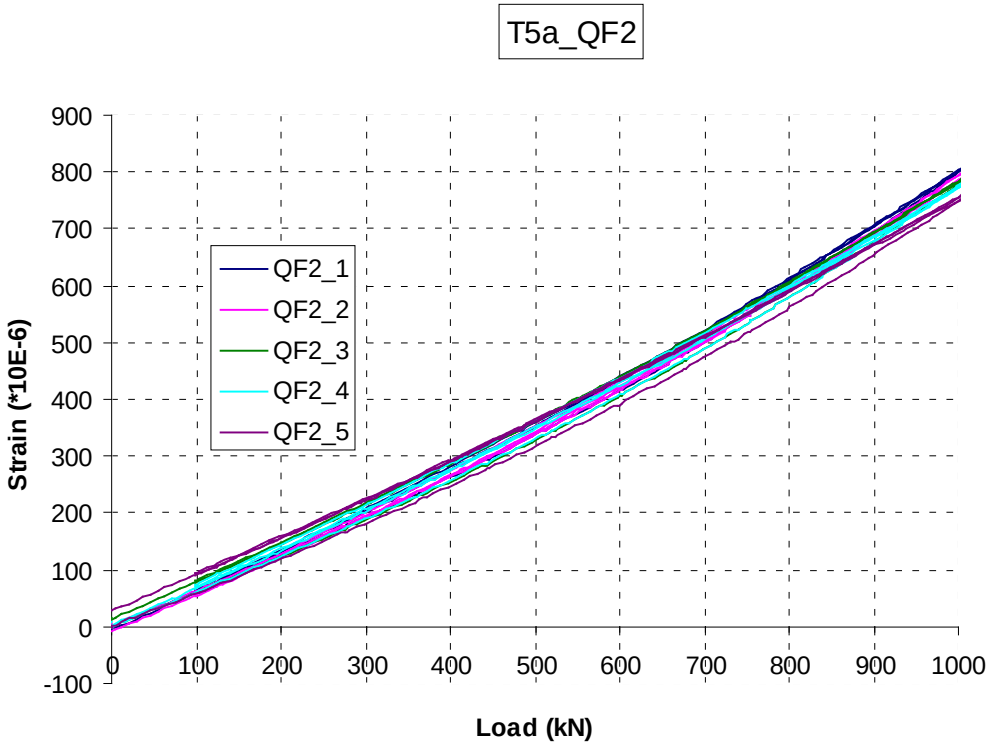

Figure 4.4.102

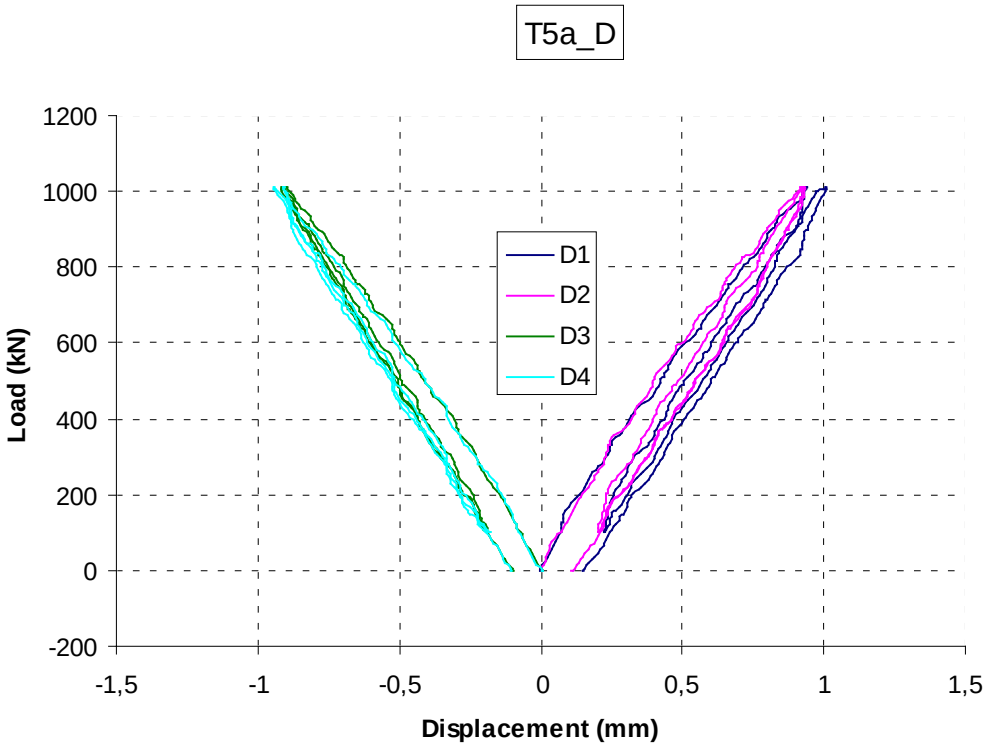

Figure 4.4.103

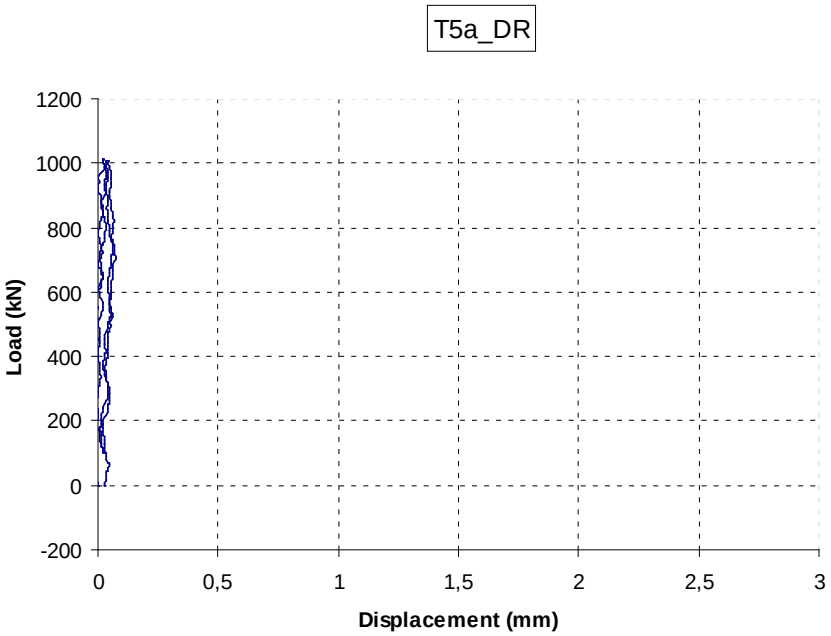

Figure 4.4.104

ANNEX 10: Graphic data of the T5b test

In the title of the charts, first term (“T5b”) indicates the test name, the second term:

“BT”, “QF” indicates the strain gauge name;

“DR” indicate the displacement relative of the joint: ((D1-D4)+D2-D3))/2.

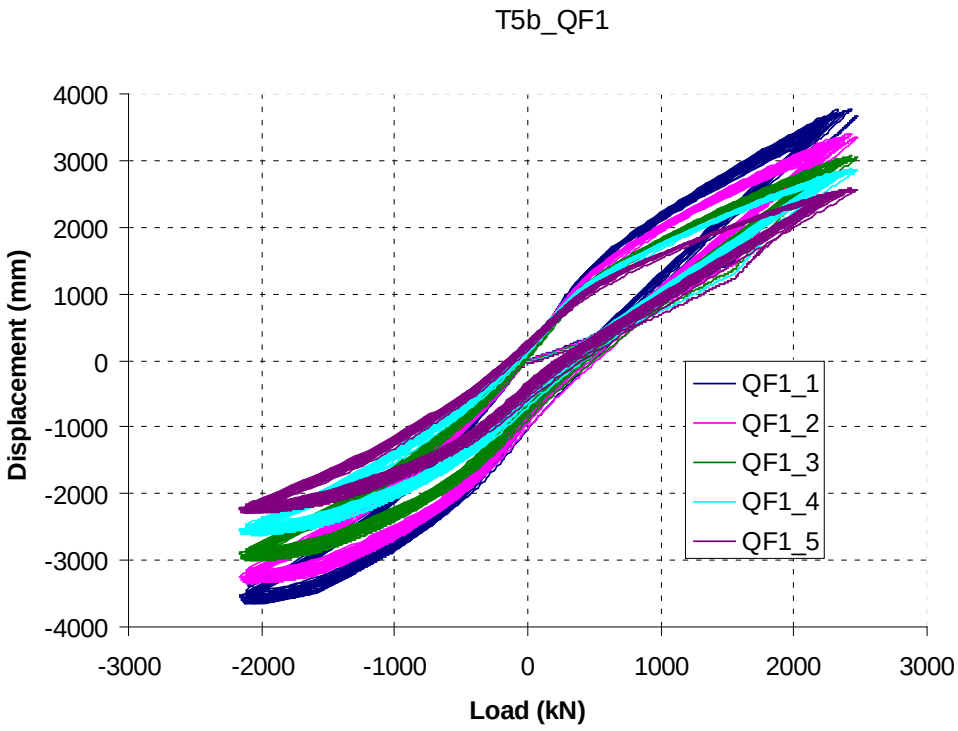

Figure 4.4.105

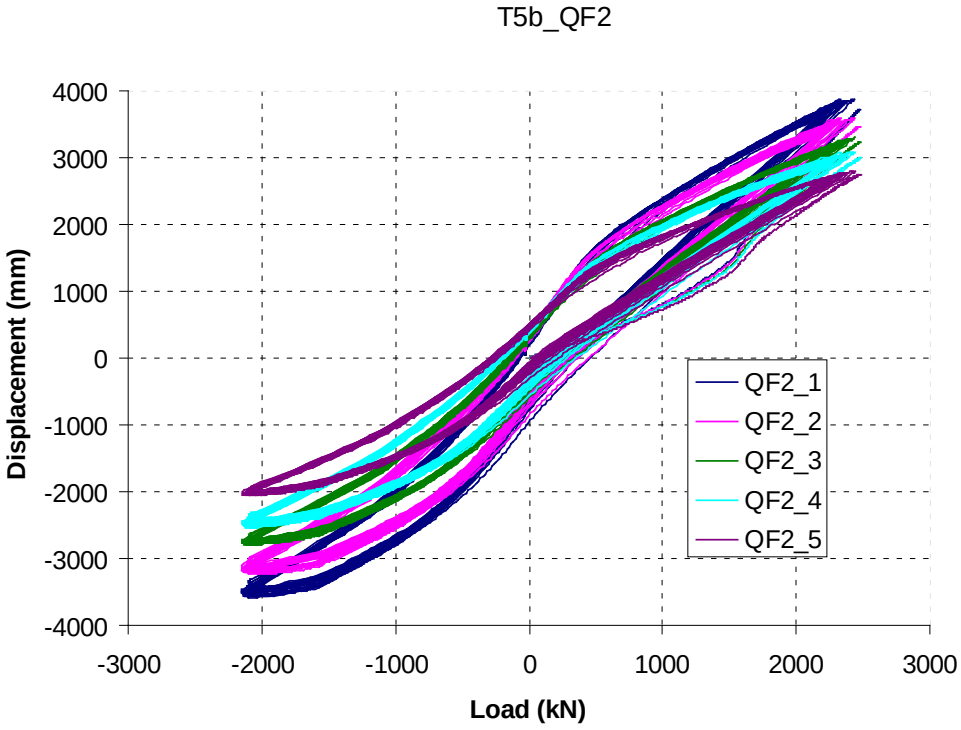

Figure 4.4.106

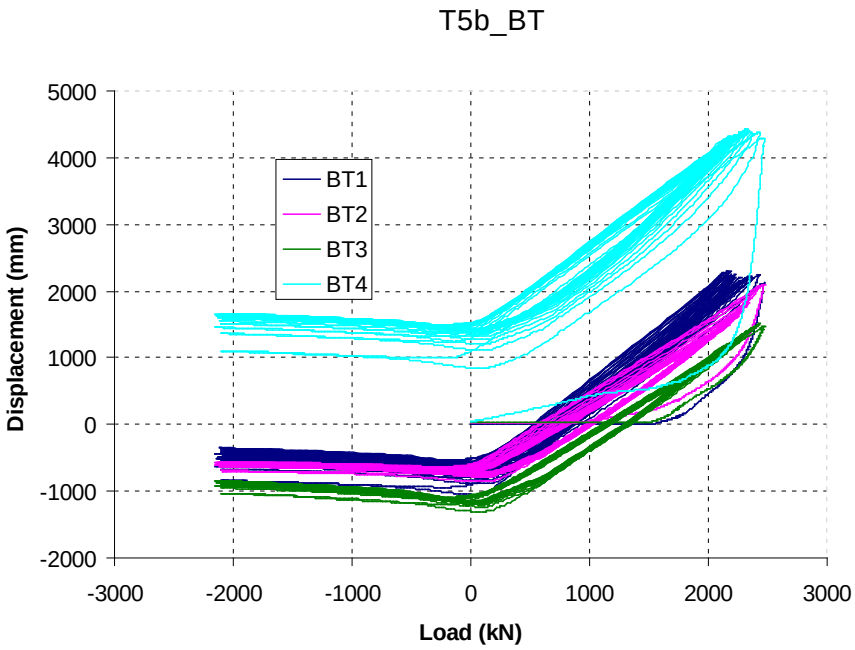

Figure 4.4.107

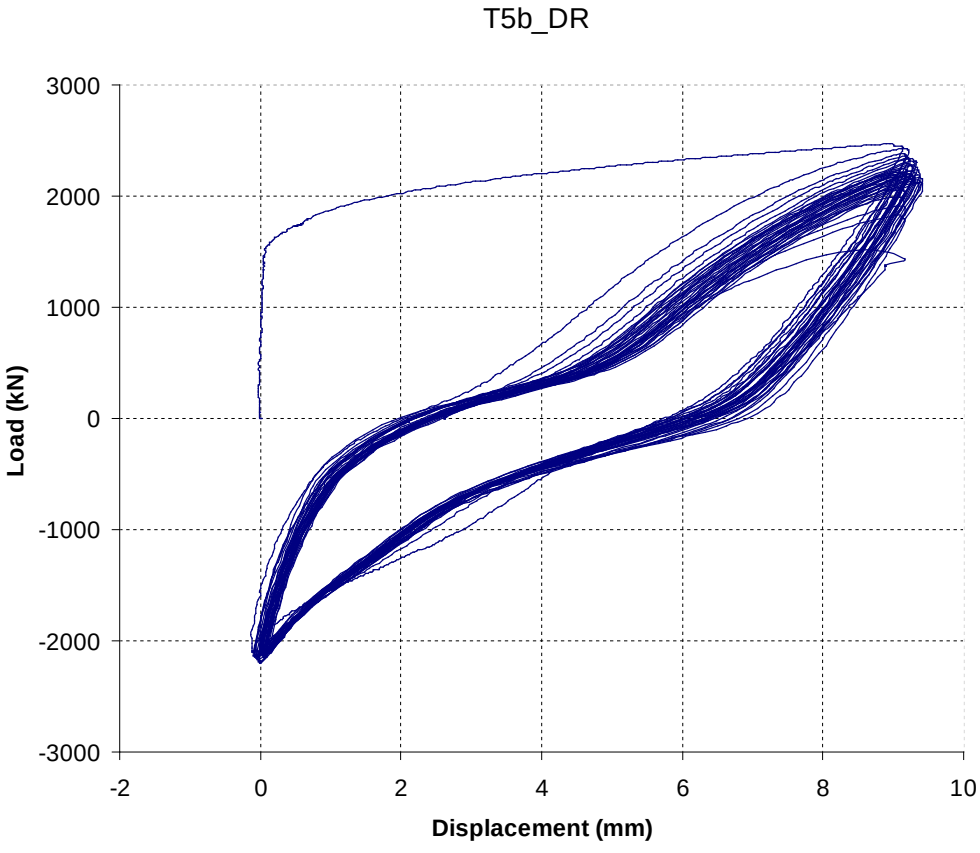

Figure 4.4.108

ANNEX 11: Graphic data of the T6 test

In the title of the charts, first term (“T6”) indicates the test name, the second term:

“BT” indicates the strain gauge name;

“DR” indicate the displacement relative of the joint: ((D1-D4)+D2_D3))/2.

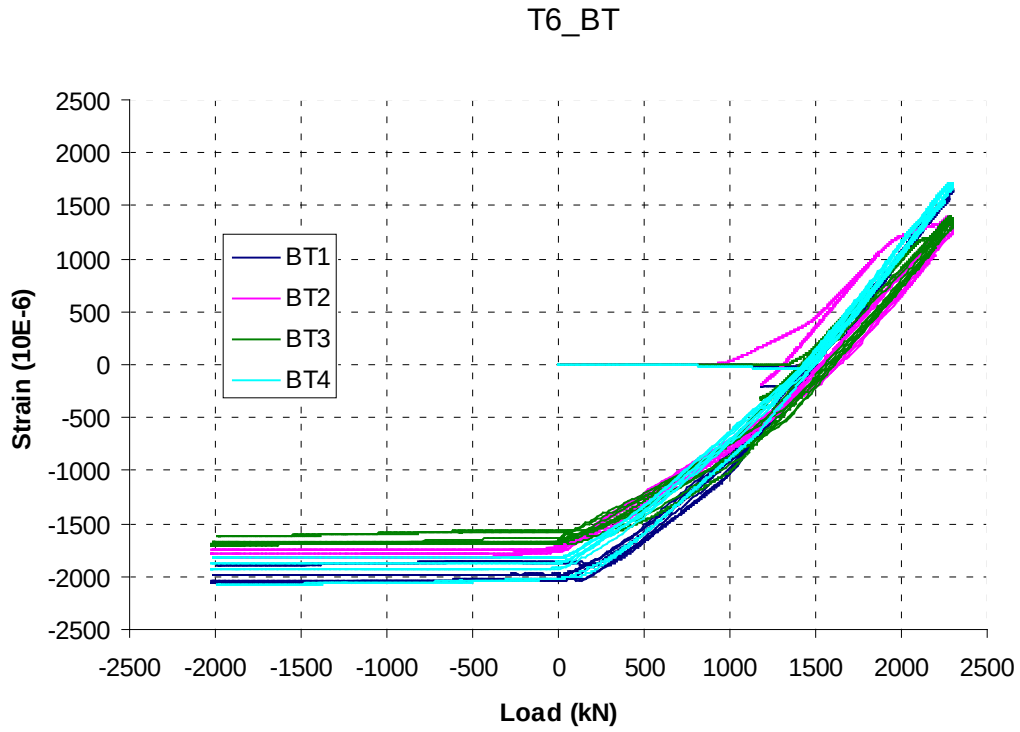

Figure 4.4.109

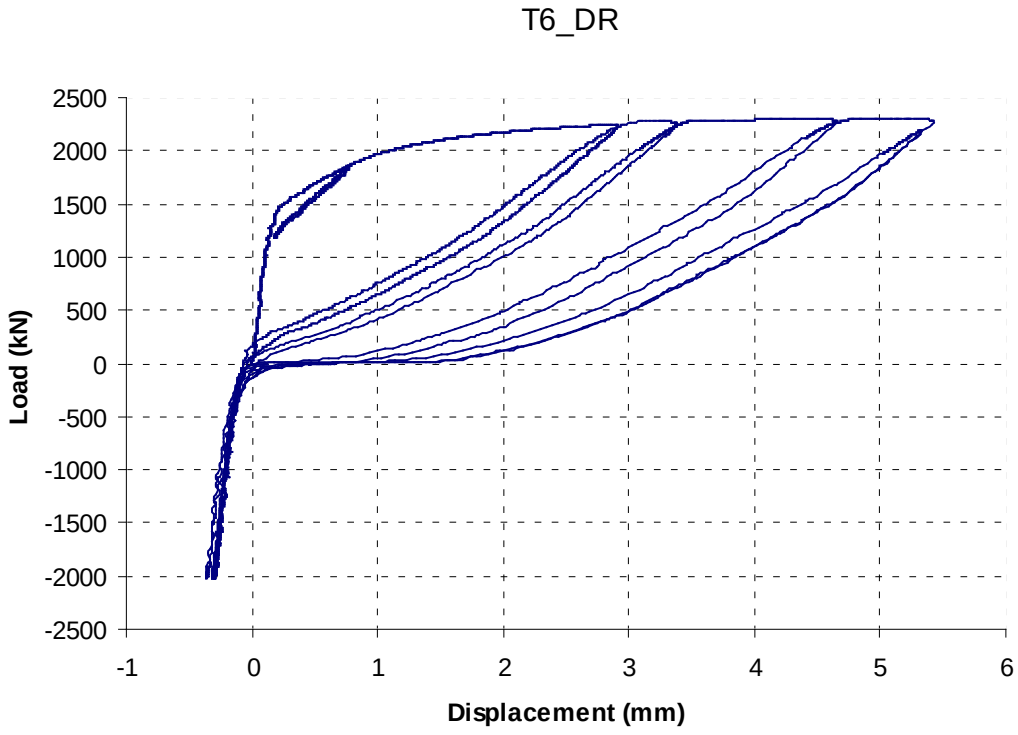

Figure 4.4.110